

THE DEVELOPMENT OF NOVEL THERAPEUTICS IN PANCREATIC AND
BREAST CANCERS: POTENTIAL ROLE OF MUC1

by

Dahlia M. Besmer

A dissertation submitted to the faculty of
The University of North Carolina at Charlotte
in partial fulfillment of the requirements
for the degree of Doctor of Philosophy in
Biology

Charlotte

2013

Approved by:

Dr. Pinku Mukherjee

Dr. Valery Grdzlishvili

Dr. Mark Clemens

Dr. Didier Dréau

Dr. Craig Ogle

ABSTRACT

DAHLIA MARIE BESMER. Development of novel therapeutics in pancreatic and breast cancers: potential role of MUC1. (Under the direction of DR. PINKU MUKHERJEE)

Pancreatic ductal adenocarcinoma (PDA) is the 4th leading cause of cancer-related deaths in the US, and breast cancer (BC) contributes to ~40,000 deaths annually. The development of novel therapeutic agents for improving patient outcome is of paramount importance. Importantly, MUC1 is a mucin glycoprotein expressed on the apical surface of normal glandular epithelia but is over expressed and aberrantly glycosylated in >80% of human PDA and in >90% of BC. In the present study, we first utilize a model of PDA that is Muc1-null in order to elucidate the oncogenic role of MUC1. We show that lack of Muc1 significantly decreased proliferation, invasion, and mitotic rates both *in vivo* and *in vitro*. Next, we evaluated the anticancer efficacy of oncolytic virus (OV) therapy that utilizes viruses to kill tumor cells. The oncolytic potential of vesicular stomatitis virus (VSV) was analyzed in a panel of human PDA cell lines *in vitro* and *in vivo* in immune compromised mice. Our results demonstrate that VSV has potential as an OV against human PDA cells. Next, we tested oncolytic VSV in an immunocompetent mouse model. In agreement with our *in vitro* results, *in vivo* administration of live VSV resulted in the significant growth reduction of PDA tumors, with an enhanced efficacy when used in combination with a chemotherapeutic drug, gemcitabine. Finally, we tested a MUC1 specific tumor vaccine with targeted inhibition of immune suppression in a model of BC. Our results indicate that Indomethacin in combination with a MUC1 vaccine resulted in a significant reduction in tumor burden. These data, therefore, may have implications in the future design of MUC1-targeted therapies for BC and OV therapies for PDA.

ACKNOWLEDGEMENTS

I would like to thank my advisor, Dr. Pinku Mukherjee for her mentorship, guidance, and never-ending support. I would like to thank Dr. Valery Grdzlishvili, Dr. Mark Clemens, Dr. Didier Dréau, and Dr. Craig Ogle for serving on my committee and providing me with support and feedback along the way. I would like to thank members of the Mukherjee lab, Dr. Jorge Schettini, Dr. Lopamudra Das Roy, Dr. Jennifer Curry, Dr. Mahnaz Sahraei, Sritama Nath, and Amritha Kidiyoor for their support and friendship throughout my graduate career. I would also like to thank the members of the Grdzlishvili lab, Andrea Murphy, Megan Moerdyk-Shauwecker, Nirav Shah, and Eric Hastie for all of their assistance. I would like to thank the Department of Defense for awarding me a generous pre-doctoral fellowship, as well as the National Institutes of Health for providing the funding for this research. I would also like to thank the UNCC graduate school for the Graduate Assistant Support Plan for providing funding for my graduate education. Lastly, I would like to thank my family and friends whom have always been there to support and encourage me along the way.

TABLE OF CONTENTS

LIST OF FIGURES	vii
LIST OF TABLES	x
LIST OF ABBREVIATIONS	xi
CHAPTER 1: INTRODUCTION	1
1.1 Pancreatic Cancer	1
1.2 Breast Cancer	12
1.3 Figures	20
CHAPTER 2: PANCREATIC DUCTAL ADENOCARCINOMA (PDA) MICE LACKING MUCIN 1 HAVE A PROFOUND DEFECT IN TUMOR GROWTH AND METASTASIS	35
2.1 Abstract	35
2.2 Introduction	36
2.3 Materials and Methods	38
2.4 Results	42
2.5 Discussion	50
2.6 Figures	53
CHAPTER 3: VESICULAR STOMATITIS VIRUS AS AN ONCOLYTIC AGENT AGAINST PANCREATIC DUCTAL ADENOCARCINOMA	59
3.1 Abstract	59
3.2 Introduction	60
3.3 Materials and Methods	63
3.4 Results	71
3.5 Discussion	81

	vi
3.6 Figures	88
CHAPTER 4: ONCOLYTIC VESICULAR STOMATITIS VIRUS IN AN IMMUNOCOMPETENT MODEL OF PANCREATIC DUCTAL ADENOCARCINOMA	102
4.1 Abstract	102
4.2 Introduction	104
4.3 Materials and Methods	107
4.4 Results	117
4.5 Discussion	126
4.6 Figures	131
CHAPTER 5: ENHANCING THE EFFICACY OF A MUC1 TARGETED BREAST CANCER VACCINE	138
5.1 Abstract	138
5.2 Introduction	140
5.3 Materials and Methods	145
5.4 Results	152
5.5 Discussion	158
5.6 Figures	162
CHAPTER 6: CONCLUSIONS AND FUTURE DIRECTIONS	172
REFERENCES	178

LIST OF FIGURES

FIGURE 1: Pancreatic Structure.	20
FIGURE 2: The incidence of pancreatic cancer is rapidly increasing and it is projected to become the 2 nd leading cause of cancer related deaths by 2015	21
FIGURE 3: Pancreatic cancer progression model.	22
FIGURE 4: Hematoxylin and eosin staining of PanIN lesions in human specimens.	23
FIGURE 5: Detection of MUC1 using a specific MUC1 CT antibody.	24
FIGURE 6: MUC1 cytoplasmic tail interactions.	25
FIGURE 7: Detection of MUC1 using MUC1 specific TAB004 antibody.	26
FIGURE 8: In a cancer setting there is a loss of polarity.	27
FIGURE 9: Hypothetical binding sites for cell signaling molecules on the MUC1 cytoplasmic tail.	28
FIGURE 10: Metastasis of cancer cells.	29
FIGURE 11: Mouse models utilized in pancreatic cancer experiments.	30
FIGURE 12: Oncolytic virotherapy is a cancer therapy that uses viruses to specifically infect cancer cells.	31
FIGURE 13: Model of breast carcinogenesis.	32
FIGURE 14: Mechanism of action for cyclooxygenase and indoleamine-2,3 dioxygenase pathways.	33
FIGURE 15: Signaling pathways activated by the EP receptors for PGE ₂ .	34
FIGURE 16: KCKO mice have lower tumor burden, metastasis and levels Of VEGF and PGE ₂ with higher survival compared to KC and KCM mice.	53
FIGURE 17: Significantly decreased tumor burden and increased survival in syngeneic C57/BL6 mice challenged with KCKO versus KCM cells.	54

	viii
FIGURE 18: Significantly altered rate of cell division and progression through the cell cycle in KCKO versus KCM cells.	55
FIGURE 19: Significantly lower proliferation and invasion index in KCKO versus KCM cells.	56
FIGURE 20: Differential protein expression profile in MUC1-expressing vs. Muc1-null cells.	57
FIGURE 21: Treatment with MEK1/2 inhibitor, U0126, abrogates proliferation of KCM but not KCKO cells.	58
FIGURE 22: Viruses used in this study.	88
FIGURE 23: PDA cell viability following infection with viruses.	89
FIGURE 24: Kinetics of cytopathogenicity of VSV- Δ M51-GFP in PDA cells.	90
FIGURE 25: Permissiveness of PDA cell lines to different viruses.	91
FIGURE 26: Permissiveness of selected PDA cell lines to virus infection.	92
FIGURE 27: Surface expression of CAR.	93
FIGURE 28: Analysis of viral protein accumulation in cells at 16 h p.i.	94
FIGURE 29: One-step growth kinetics of VSVs in PDA cell lines.	95
FIGURE 30: Early viral RNA levels in infected cells.	96
FIGURE 31: Type I interferon sensitivities of PDA cell lines.	97
FIGURE 32: Type I interferon production by PDA cell lines.	98
FIGURE 33: Efficacy of VSV- Δ M51-GFP and CRAAd-dl1520 in nude mice bearing human PDA tumors.	99
FIGURE 34: Generation of KCM and KCKO cell lines.	131
FIGURE 35: Characterization of human MUC1 expression of KCM and KCKO.	132
FIGURE 36: KCM and KCKO viability following infection with viruses.	133

FIGURE 37: Cells were infected with VSV- Δ M51-GFP at cell line specific .001 or 5 MOIs.	134
FIGURE 38: Panc02.MUC1 and Panc02.Neo expression of human MUC1.	135
FIGURE 39: Efficiency of VSV- Δ M51-GFP in human MUC1 transgenic immunocompetent mice bearing KCM tumors.	136
FIGURE 40: Treatment Schedule for human MUC1 transgenic immunocompetent mice bearing KCM or KCKO tumors.	137
FIGURE 41: Characterization of the MTAG.MUC1 cell line.	162
FIGURE 42: Indomethacin treatment with vaccination is the only combination that reduces tumor burden.	163
FIGURE 43: Indomethacin treatment with vaccination is the only combinations that has a trend indicating reduced tumor burden.	164
FIGURE 44: Celecoxib and Indomethacin both reduce PGE2 metabolite levels in combination with vaccination.	165
FIGURE 45: Immune analysis (MDSCs and Tregs) of combinational MUC1 vaccine therapy.	166
FIGURE 46: Immune analysis (T cells) of combinational MUC1 vaccine Therapy.	167
FIGURE 47: Combinational treatment of Vaccine + Indomethacin significantly reduces tumor burden.	168
FIGURE 48: Combinational treatment of Vaccine + Indomethacin significantly reduces tumor wet weight.	169
FIGURE 49: Indomethacin reduces PGE2 metabolite levels alone and in combination with vaccination.	170
FIGURE 50: Potential pathways involved in the enhanced efficacy of Vaccine + Indomethacin.	171

LIST OF TABLES

TABLE 1: Early viral RNA synthesis in cells infected with VSV- Δ M51-GFP.	100
TABLE 2: Correlation between IFN sensitivity, production, and resistance of PDA cells to VSV.	101

LIST OF ABBREVIATIONS

Δ M51	deletion of methionine at position 51
1-MT	1-methyl tryptophan
³ H	tritium
aa	amino acid
ANOVA	analysis of variance
APC	antigen presenting cell
BSA	bovine serum albumin
CAR	coxsackievirus and adenovirus receptor
CDK5	cyclin-dependent kinase 5
CFSE	carboxyfluorescein succinimidyl ester
CIU	cell infectious units
COX	cyclooxygenase
COX-1	cyclooxygenase-1
COX-2	cyclooxygenase-2
CpG ODN	CpG oligodeoxynucleotides
CRAds	conditionally replicative adenoviruses
CT	cytoplasmic tail
CT2	antibody directed against the cytoplasmic tail of muc1
CTL	cytotoxic T lymphocyte
d	days
DAB	3,3'-diaminobenzidine tetrahydrochloride hydrate
DMEM	dulbecco's modified eagles medium

DMSO	dimethyl sulfoxide
DNA	deoxyribonucleic acid
ECL	enhanced chemiluminescence
EGF	epidermal growth factor
ELISA	Enzyme-linked immunosorbent assay
ELISPOT	Enzyme-linked immunosorbent spot
EMT	epithelial to mesenchymal transition
ER	estrogen receptor
F	fusion
FBS	fetal bovine serum
FITC	fluorescein isothiocyanate
GFP	green fluorescent protein
GM-CSF	granulocyte macrophage colony stimulating factor
h	hours
HER2	human epidermal growth factor receptor 2
H&E	hematoxylin and eosin
h.p.i.	hours post infection
HBS	HEPES buffered saline
HMFG2	anti-milk fat globule 2 monoclonal antibody
HPDE	human pancreatic duct epithelial cell line
HRP	horse radish peroxidase
HSV-1	herpes simplex virus type 1
hTERT	human telomerase reverse transcriptase

IACUC	institutional animal care and use committee
ICC	immunocytochemistry
IDO	indoleamine 2,3 dioxygenase
IFN	interferon
Ig	immunoglobulin
IHC	immunohistochemistry
Indo	indomethacin
IP	intraperitoneal
IPMN	intraductal papillary mucinous neoplasms
IT	intratumoral
KC	Cre-LSL-KRAS ^{G12D} mouse model of PDA
KCKO	PDA mice lacking MUC1/Muc1
KCM	PDA mice expressing MUC1
M	matrix protein
MAPK	mitogen activated protein kinase
MCN	mucinous cystic neoplasms
MDSCs	myeloid derived suppressor cells
MEM	modified eagle's medium
MFI	mean fluorescence intensity
mg	milligrams
MHC	major histocompatibility complex
min	minutes
MMP-9	matrix metalloproteinase

MMTV	mouse mammary tumor virus
MOI	multiplicity of infection
mRNA	messenger RNA
MTAG	middle T antigen
MTT	3-(4,5-dimethyl-2-thiazolyl)-2,5-diphenyl-2H-tetrazolium bromide
MUC1	human mucin-1
Muc1	mouse mucin-1
MUC1.Tg	human MUC1 transgenic
NEO	transfected with neomycin empty vector
NIH	national institute of health
NNS	nonsegmented negative-strand RNA
OD	optical density
ONYX-15	CRAAd-dl1520
OPD	o-Phenylenediamine
ORF	open reading frame
OV	oncolytic virus
p.i.	post infection
p.t.i.	post tumor injection
PanIN	pancreatic intraepithelial neoplasia
PBS	phosphate buffered saline
PCNA	proliferating cellular nuclear antigen
PCR	polymerase chain reaction
PDA	pancreatic ductal adenocarcinoma

PDGF	platelet derived growth factor
PE	phycoerythrin
PFA	paraformaldehyde
PGE ₂	prostaglandin E ₂
PGEM	prostaglandin E ₂ metabolite
PI	propidium iodide
PR	progesterone receptor
PVDF	polyvinylidene difluoride
PyVMT	polyoma virus middle T antigen
rm-	recombinant mouse
RNA	ribonucleic acid
RNase	ribonuclease
RSV	respiratory syncytial virus
RT	room temperature
SDS-PAGE	sodium dodecyl sulfate polyacrylamide gel electrophoresis
SEM	standard error of the mean
SeV	Sendai virus
SFM	serum free medium
TGF β	transforming growth factor- β
TM	transmembrane
TR	tandem repeat
Tregs	T regulatory cells
U	units

Vacc	vaccine
VEGF	vascular endothelial growth factor
VNTR	variable number of tandem repeats
VSV	vesicular stomatitis virus
VVT7	vaccinia virus containing T7 RNA polymerase gene
wk	week
wt	wild-type

CHAPTER 1: INTRODUCTION

1.1 Pancreatic Cancer

Pancreatic Structure and Function

The pancreas is a glandular organ which has dual functions. It is located deep within the abdomen, behind the stomach. It is composed of a head, uncinata process, neck, body and tail. It has both endocrine functions as well as exocrine functions. The endocrine, or hormone producing, portion of the pancreas consists of cell clusters called the islet of Langerhans, which is made up of four main types of cells, α cells, β cells, delta cells, or PP cells (gamma cells). Each of these cell types performs a distinct function. The α cells are known to secrete glucagon, the β cells secrete insulin, whereas the delta cells are known to secrete somatostatin and the PP cells secrete pancreatic polypeptide, all of which are important in glucose metabolism as well as regulating blood glucose concentration. The exocrine portion of the pancreas, consisting of ductal and acinar cells, is responsible for the secretion of digestive juices. Pancreatic ductal cells line the ducts of the pancreas, which open into sac-like-structures called acinar cells (Figure 1). The acinar cells produce the digestive enzymes, which are then transported via the ducts of the pancreas to the stomach or duodenum. The digestive enzymes that are produced then assist in the breakdown of carbohydrates, proteins, and lipids.

Pancreatic Cancer

Pancreatic cancer is estimated to be the 4th leading cause of cancer related death in the United States. The incidence of pancreatic cancer is rapidly increasing and it is projected to become the 2nd leading cause of cancer related deaths by 2015 (published by the Pancreatic Cancer Action Network; Figure 2). Pancreatic cancers can arise from the exocrine and endocrine parts of the pancreas. Cancer of the exocrine portion (the portion responsible for secretion of digestive enzymes) accounts for >95% of pancreatic cancers. This includes cancer of the ductal epithelium, acinar cells, the connective tissue, and lymphatic tissue. Tumors may also develop in the endocrine portion (or the hormone producing portion), and are thus referred to as pancreatic neuroendocrine tumors; however this type of pancreatic cancer is rare. Cystic neoplasms also occur, but account for less than 1% of pancreatic cancers. Roughly 75% of all pancreatic cancers arise in the head or neck of the pancreas, 15-20% in the body of the pancreas, and 5-10% in the tail.

Pancreatic Ductal Adenocarcinoma

In 2010 alone, there were an estimate 43,140 new cases and 36,800 deaths attributed to pancreatic cancer in the US [1]. Pancreatic Ductal Adenocarcinoma (PDA) is the most common type of pancreatic cancer, accounting for >90% of pancreatic cancers. It is the most lethal type of digestive cancer, with a 5 year survival rate of only 3-5% [2-5]. PDA ranks the 10th most commonly diagnosed cancer, and the 4th among cancer-related deaths [1].

Risk Factors

Several environmental risk factors and genetic conditions for the development of pancreatic cancer have been identified. Age is a primary risk factor, given that pancreatic

cancer is rarely diagnosed before the age of 40, with a median age of diagnosis at 73 years old (<http://seer.cancer.gov/>). Males are more susceptible than females (12.8 vs. 10 cases per 100,000 individuals). Race is also a risk factor, with more African Americans diagnosed than Caucasians (14.9 vs. 11.1 per 100,000 cases) (<http://seer.cancer.gov/>). Cigarette smoking is the leading preventable cause of pancreatic cancer [6-8] Moreover, conditions such as diabetes, obesity, genetic predisposition, and chronic pancreatitis have been linked to increased susceptibility to pancreatic cancer [9-12]. These causes of organ dysfunction have been known to result in the production of reactive oxygen species, and result in chronic inflammation, which has been correlated with transformation of the ductal cells of the pancreas. Moreover, several mutations in tumor suppressor genes are known to be linked to the development of pancreatic cancer, including: *BRCA1*, *BRCA2*, *INK4A*, *MLH1*, *PRSS1*, and *STK11/LKB1* [13-15]. Activating mutations in the *K-RAS* oncogene are thought to represent an initiating event in the development of PDA. Mutations in the 12th codon of the *K-RAS* gene (from G to D) are detected in 30% of early neoplasms and 100% of PDA [16-18].

Diagnosis and Treatment Options for PDA

Early stage diagnosis is very rare for pancreatic cancer, as patients are generally asymptomatic until advanced disease is present. The symptoms patients may present with include fever, nausea, lower back pain, lack of appetite and the resulting weight loss. However, these symptoms are very common to a wide-array of diseases. Moreover, there are no specific markers for pancreatic cancer, although *CA-19-9*, a sialylated mucin glycoprotein present on Lewis^a blood group antigen and *CA-242*, another mucin glycoprotein [19] have been utilized as non-invasive diagnostic markers for monitoring

disease progression. These are not used for screening due to false positive rates associated with these markers. Over 75% of pancreatic cancer patients present with locally unresectable tumors. These patients have a median survival rate of 3-6 months [20-23]. Only 5 –25% of pancreatic cancer cases are eligible for surgery. Post-operative patients have a two-year survival rate of 20% – 40% with surgery, however, recurrence or metastasis occurs in more than 50% of the patients. Adjuvant therapy including radiation and chemotherapy remain largely ineffective as the tumors tend to develop resistance. Several of these therapies also produce undesirable side effects. Gemcitabine, with or without erlotinib, has been the standard chemotherapeutic adjuvant therapy, however, only modest benefits have been identified. The combination of gemcitabine with erlotinib is the only combination that has demonstrated a significant increase in survival of patients. However, a number of drug combinations have been tested to no avail, including gemcitabine in combination with platinum based agents such as topoisomerase inhibitors, taxanes, bevacizumab and cetuximab, or gemcitabine in combination with vaccine therapy [24-28].

Pancreatic Ductal Adenocarcinoma Progression

Precursor lesions are detectable prior to progression of an invasive PDA. There are three main types of precursor lesions that have been identified thus far. These include pancreatic intraepithelial neoplasias (PanIN), mucinous cystic neoplasms (MCN) and intraductal papillary mucinous neoplasms (IPMN) [29]. MCN precursor lesions as of yet, have not been very well characterized, however, it is known that MCN precursors are more likely to occur in women, and MCN precursors present with a distinct ovarian type stroma [30]. IPMN lesions and PanIN lesions are much more difficult to differentiate.

IPMN generally arise in the main pancreatic duct, and present with a papillary structure [31]. PanIN lesions are the most frequently occurring and thus, most extensively studied lesion. PanIN lesions are subclassified into three categories depending on the degree of dysplasia and atypia, PanIN-1, PanIN2, and PanIN3, respectively [31, 32].

Molecular abnormalities are present at different stages of progression. For instance, genomic alterations can be detected in K-ras and telomere length, as early as PanIN-1, whereas alterations in p16/CDKN2A are detectable at the PanIN-2 stage, and SMAD-4 and BRCA-2 alterations are first detected in the PanIN-3 stage [33-35]. The most notable of these genetic alterations is the K-ras mutation, known to be an activating and initiating event in pancreatic cancer [29]. These genomic alterations are also accompanied by phenotypic changes. Normal cells present with a cuboidal phenotype and uniform round nuclei; however as they progress to PanIN-1 stage, the cells present with a more columnar phenotype, yet the polarity is still maintained with basally located nuclei. Once the cells are categorized as PanIN-2, they present with moderate nuclear atypia, and a loss of polarity is observed. PanIN-3 lesions are characterized by severe nuclear atypia, clusters of cells budding off, and a total loss of polarity (Figure 3, Figure 4). This eventually progresses to invasive adenocarcinoma.

Mucins in Pancreatic Cancer: Highlight on MUC1

As can be seen in Figure 3, MUC1 expression is altered as early as PanIN-1A lesions. Using an antibody against the cytoplasmic tail of MUC1 (CT-2), we have shown that MUC1 expression can be detected in early stages of PDA and low grade PanIN lesions (Figure 5). Most pancreatic cancers are known to express a variety of mucins, including MUC1, MUC3, MUC4, and MUC5AC [36]. To date, 11 members of the

Mucin family have been identified. These include the membrane tethered mucins: MUC1, MUC3, MUC4, MUC11, MUC12, and MUC13, as well as the secreted mucins MUC2, MUC5AC, MUC5B, MUC6, and MUC7 [37]. MUC1 expression during pancreatic cancer progression has long been identified; however its role has yet to be fully elucidated due to a lack of appropriate mouse models. MUC1 (CD227) is a type I membrane tethered mucin glycoprotein which is normally expressed on the apical surface of glandular epithelial cells, including expression in the pancreas, breast, stomach, colon, lung, salivary glands, and to a lesser extent on immune cells. The normal function of MUC1 is to play a key role in anti-adhesion and immune protection. It has been shown to be important for hydration, lubrication, and protection.

MUC1 has a unique N-terminal extracellular domain consisting of variable number tandem repeats (VNTR) of 20 amino acids (PDTRPAPGSTAPPAHGVTSA) that are extensively modified by O-glycosylation (Figure 6). The C-terminal domain of MUC1 includes a 53 amino acid (aa) extracellular region, a transmembrane domain (TM) and a 72 aa cytoplasmic tail (CT) [38]. The TM and CT domains of MUC1 are highly conserved (88% identical), suggesting important functional roles [39]. The 72 amino acid tail contains 7 tyrosines, six of which are 100% conserved. MUC1 is encoded by a single transcript which gives rise to two separate subunits after post-translational cleavage to form a stable, non-covalently bonded heterodimer. It is generally found as a heterodimer, however, several MUC1 variants have been discovered due to differential mRNA splicing events. MUC1 has been shown to be expressed while lacking either the cytoplasmic tail or the tandem repeat portions [40-43]. Additionally, it has been shown that the extracellular portion of MUC1 can be cleaved enzymatically and secreted [44,

45]. MUC1 is known to be heavily O-glycosylated at the hydroxyl groups of the serine and threonine residues found in the extracellular domain. Depending on the extent of O-glycosylation, the molecular weight (mw) can range anywhere from 100kDa to 500kDa.

MUC1 Functions as a Biomarker and Target

MUC1 is overexpressed and aberrantly glycosylated in many human adenocarcinomas including pancreas, breast, and ovaries [46-52]. MUC1 is overexpressed in >60% of pancreatic cancers and >80% of PDA [51, 53]. MUC1 staining of human pancreatic cancer sections has been detected using MUC1 specific antibody, TAB004 (Figure 7). Tumor associated MUC1 is hypoglycosylated, and thus, the immunogenic protein core is exposed. Tumor associated MUC1 is therefore considered to be a promising target, and has recently been designated by the National Cancer Institute as the 2nd most targetable tumor antigen [54]. Moreover, a number of studies have focused on utilizing MUC1 as a biomarker for cancer detection, as the extracellular domain of MUC1 can be shed in the serum of patients. MUC1 has already been detected in patients with pancreatic cancer [55] ovarian [56], colon [57], prostate [58] and breast cancer. Moreover, in a cancer setting, there is a loss of polarity such that MUC1 is expressed around the entire surface of the cell such that it can interact with growth factor receptors, normally located on the basolateral surface (Figure 8).

Signaling of the Cytoplasmic Tail of MUC1

MUC1 interacts with a number of proteins implicated in carcinogenesis through both its tandem repeat and cytoplasmic domains. The cytoplasmic tail of MUC1 contains 7 tyrosines. Tyrosines in the MUC1 CT have been shown to be phosphorylated, for instance by members of the Src family of kinases, such as lyn [59], c-Src [60], and Lck

[61]. The phosphorylated CT of MUC1 is known to play a role in a number of signaling events. For instance, MUC1 is known to interact with β -catenin at the SAGNGGSSL sequence in the CT [62]. Recently, it has been shown that MUC1 also complexes with α -catenin [63], and with γ -catenin [64] suggesting a role of MUC1 in stabilizing and enhancing nuclear localization of catenins. GSK3 β , a serine kinase has been shown to binds directly to MUC1 and decrease the ability of β -catenin to bind *in vitro* and *in vivo* [65]. Recently, MUC1 has been shown to bind Grb2/SOS (Figure 9), which are signaling mediators of a number of receptor kinases [66]. Moreover, MUC1 is known to interact with the erbB receptors (EGFR or erbB1, erbB2, erbB3, and erbB4) [67]. Activation of these receptors results in activation of a variety of effector proteins including Grb2/SOS and the downstream activation of MAP kinases [68].

Metastasis

Pancreatic cancer is commonly diagnosed in the later stages of the disease, as early stage diagnosis remains rare due to a lack of symptoms. Pancreatic cancer can be highly invasive; once the disease becomes metastatic it is unlikely to be curable. In fact, more than 90% of cancer related deaths are as a result of metastasis [69]. Metastasis is a complicated process in which the primary tumor grows such that it is able to invade the local environment and intravasate into the vasculature. If the cells are able to survive in circulation, they can then extravasate from the vasculature and grow in secondary organ sites, known as metastases (Figure 10). There is a lot of cross-talk that occurs between the primary tumor cells and the local tumor microenvironment in order for metastatic spread to occur [70, 71]. Cancer associated fibroblasts, for instance, are well known to secrete chemokines and growth factors known to enhance proliferation and invasion of

cancer cells. Moreover, immune cells in the local tumor microenvironment have been known to suppress immune responses and enhance invasiveness [70, 71].

Epithelial to mesenchymal transition (EMT) is known to be associated with enhanced invasiveness, motility of cancer cells, and metastasis [72, 73]. During EMT, epithelial cells acquire a fibroblastic phenotype and hence become more motile. During EMT, Snail expression has been shown to cause a functional loss of E-cadherin [74-76]. Our lab recently demonstrated that MUC1 expression in PDA cells increases their invasiveness and both *in-vitro* and *in-vivo* and that this was associated with an increase in EMT [77]. Specifically, MUC1 expression was associated with a decreased expression of mesenchymal markers such as vimentin, Snail and Slug and an increased expression of epithelial markers such as E-cadherin. However, cells transfected with the MUC1 plasmid lacking the tyrosines in the cytoplasmic tail did not display epithelial and mesenchymal markers and therefore less invasive. We have also demonstrated that MUC1-induced invasion and proliferation occurs through the increased exogenous production of Platelet-Derived Growth Factor-A, one of the major drivers of tumor growth, angiogenesis, and metastasis in PDA [78]. Moreover, we have recently shown that MUC1 associates with Hif1- α , a known transcription factor controlling PDGFA transcription and facilitates Hif1- α translocation to the nucleus [78].

Pancreatic Cancer Mouse Models

Early mouse models of pancreatic cancer utilized tumor grafts in either immunodeficient or immunocompetent mice. The first transgenic mice developed utilized acinar specific promoters such as elastase, however, this resulted in neoplasia of the acinar cells, not the ductal cells [79]. In 2003, Dr. Tuveson's group described the first

mouse model of pre-invasive and invasive ductal pancreatic cancer that recapitulates the full spectrum of human PanINs. The PanINs were highly proliferative, showed indications of histological progression, and trigger signaling pathways normally inactive in normal ductal epithelium [80]. Mice developed ductal lesions very similar to all three stages of human PanINs. Tuveson's model expressed $Kras^{G12D}$ through Cre-mediated recombination driven by pancreas specific promoter Pdx1 or p48. Both of which are expressed in the progenitor cells of the pancreas. In our studies, we have backcrossed these mice onto the blk6 background, and mated them with either MUC1.Tg mice, or MUC1 null mice (Figure 11). From these mouse models cell lines were generated that are unique to our lab and are critical for the MUC1 scientific community. These models provide us with the capability to fully examine the oncogenic role of MUC1 in tumor progression.

Oncolytic Virotherapy

Several cancer therapies proven successful in other tumor types have had little effect in treating PDA. Surgical resection complemented by chemotherapy is the primary treatment option [81]. The few treatment options available for patients suffering from PDA indicate a critical need for the development of novel therapeutics. Oncolytic virotherapy is an anti-cancer approach that utilizes replication-competent viruses to target and kill tumor cells. Importantly, several tumors are known to be deficient in their intracellular defenses such as the loss of Type I IFN induction and signaling [82]. These defects can offer the tumor growth advantages; however, it also renders the cells susceptible to viral infection. The premise of oncolytic virotherapy then, is to specifically target tumor cells using replication-competent viruses (Figure 12). Virus replication

within the tumor cell can lead to releasing new infectious viral particles that then go and infect neighboring tumor cells. Thus, ultimately leading to tumor cell death [82]. Several oncolytic DNA and RNA viruses have already shown to be effective at the clinical level including adenoviruses, vaccinia virus, herpesviruses, reovirus and paramyxoviruses [83]. Moreover, vesicular stomatitis virus (VSV) has already been tested and shown promise in a number of cancers, including prostate [84-86], breast [87-90], melanoma [88, 91], colorectal [92-94], liver [95-97], glioblastoma [98-100] and other cancers [101] however its potential in pancreatic ductal adenocarcinoma (PDA) has not been studied.

VSV is the prototypic member of the nonsegmented negative strand RNA viruses [102]. VSV is known to exhibit sensitivity to early innate immune responses such as the Type I IFN response [102]. This sensitivity allows VSV to specifically replicate in tumor cells. Healthy tissues are still able to mount a successful immune response against VSV infection. In addition to the sensitivity to type I IFN, VSV has potential as a successful oncolytic therapy for a number of reasons: (i) replication occurs in the cytoplasm of host cells so there is no risk of host cell transformation, (ii) there is no cell cycle dependency for infection and cellular uptake occurs rapidly, (iii) the genome is easily manipulated with the possibility for expression of foreign genes, and (iv) VSV is not considered a human pathogen [101]. Investigating the ability of VSV to specifically target and kill PDA tumor cells, therefore, can provide an alternative strategy for the treatment of PDA.

Conclusions

Pancreatic cancer is a devastating disease with very few treatment options. Radiation therapies and chemotherapies remain largely ineffective, while incident and death rates remain high. Numerous studies have focused on MUC1 signaling in

pancreatic cancer, and therapeutically targeting MUC1. However, the precise role of MUC1 had yet to be elucidated due to a lack of appropriate model systems. Therefore, we first hypothesized that MUC1 may play an imperative role in the development and progression of the disease [36, 103, 104]. We sought to further our understanding of the oncogenic role of MUC1 in pancreatic cancer, and its potential impact on design and implementation of therapeutic strategies. In Chapter 2, we utilize newly developed mouse models and cell lines in order to examine the oncogenic role of MUC1 in pancreatic cancer. In Chapter 3, we sought to investigate the potential of VSV as a noncolytic agent against pancreatic cancer. We test a panel of human pancreatic cancer cell lines, and analyze the ability of VSV to infect and kill tumor cell lines. We also test the oncolytic ability of VSV in vivo, in an immunodeficient mouse model. In Chapter 4, we develop a system for testing the efficacy of VSV in an immunocompetent mouse model, as well as testing VSV in combination with chemotherapeutic agent, gemcitabine.

1.2 Breast Cancer

Breast Cancer: Statistics, Risk Factors, and Pathogenesis

Breast cancer is the second most common cancer in the United States and contributes to 40,000 deaths a year. It is estimated that 226,870 women will be diagnosed in 2012 alone, and that nearly 3 million women in the US have a history of invasive breast cancer. For tumors confined within the breast, surgical removal can result in a favorable outcome. However, tumors have the ability to metastasize to distant sites, such as lymph nodes, lungs, liver or brain.

A number of risk factors have been identified for breast cancer, including gender (more women affected than men), age, and familial history. Other modified risk factors

include hormonal changes, obesity (specifically in the postmenopausal range) as well as dietary factors including alcohol intake and dietary fat intake [105]. Pathogenesis of breast cancer is similar to other epithelial carcinomas (Figure 13). Specifically, there are an accumulation of cellular events that result in a dysplastic appearance. This is accompanied by a number of genotypic and phenotypic changes including uncontrolled cell proliferation, and the eventual progression to carcinoma.

As discussed previously, hormonal changes play a large role in the development and progression of breast cancer. In fact, hormonal changes play a critical role in approximately 70% of all breast cancer cases [106]. Therefore, a large number of studies focusing on chemotherapeutics have focused their attention on targeting breast cancers that are hormonally responsive [107]. Estrogen-receptor positive breast cancers are generally treated with one of two types of drugs, aromatase inhibitors or estrogen receptor modulators. Estrogen is a key hormone, in that it has been shown to promote cell division and proliferation within the breast in both normal and malignant cells. However, estrogen-receptor negative breast cancer accounts for approximately 20-30% of breast cancers [108]. Triple negative breast cancers, lacking estrogen receptor(ER), progesterone receptor (PR), as well as lacking over-expression of human epidermal growth factor receptor 2 (HER2), have the worst prognosis. Therefore, other treatment options are needed for patients, including, agents such as tyrosine kinase inhibitors (TKIs), cyclooxygenase-2 (COX-2) inhibitors, vitamin D receptor (VDR), and others.

Cancer vaccines

Complications from metastatic disease are the leading causes of cancer-related deaths. Therefore, newly developed cancer vaccines are being developed with the hope

that they can delay recurrence, prolong survival, and perhaps even be utilized as a preventative measure [109, 110]. Cancer vaccines are designed to immunize individuals to antigens present on tumors, in order to stimulate the patient's own immune system to combat the disease processes. The advantage of this approach is that it can act specifically against the tumor cell, without causing damage to normal tissues. In addition to providing active immunization, immunotherapy can also generate memory immune responses, which should assist in prevention of recurrence. Several immune-based strategies have been employed in preclinical and clinical settings already [47, 111-116].

MUC1 Expression in Cancer: Potential Vaccine Therapy

In recent years there has been great interest in cancer vaccines, which have the potential of controlling disease, prolonging time to recurrence, and ultimately even serving as a preventive measure. Novel therapies such as cancer vaccines that target tumor associated antigens (TAA) present an attractive alternative therapy with the hopes of preventing metastasis and recurrence. Importantly, MUC1 is a transmembrane mucin glycoprotein that is overexpressed in >90% of breast carcinomas [48, 50, 117-119]. As in pancreatic cancer, the extracellular domain is normally extensively *O*-glycosylated [48, 50, 117-119]. However, in a tumor setting, MUC1 hypoglycosylated and is no longer restricted to the apical surface, as polarity is lost. Moreover, tumor associated MUC1 has an aberrant glycosylation pattern [46]. Interestingly, patients with breast, pancreatic and ovarian tumors have exhibited spontaneous immune responses to MUC1. This is evidenced by the presence of antibodies and T cells specific for MUC1 [120-124]. These attributes have long made MUC1 an interesting target molecule for immunotherapeutic strategies [46, 125].

Importantly, MUC1 was designated by the National Cancer Institute as the second most targetable tumor antigen in 2009.

Treatments that work by modulating the immune response are amongst the most widely used and accepted medical treatments. Several preclinical and clinical trials using MUC1 peptide vaccines have elicited anti-MUC1 CTLs [47, 113, 115, 120, 126, 127]. The recent description of MUC1 as a target for cytotoxic T lymphocytes (CTLs) has raised interest in using this protein as a target for immunotherapy. So far, these approaches have generated only modest and infrequent clinical responses [128]. Immunotherapy as an approach to cancer has yet to live up to its expectations. However, tumors create an abnormal local microenvironment that allows them to escape immune detection and destruction. Thus, immune evasion is one major obstacle that has to be addressed prior to designing and delivering successful immunotherapy. There are opposing forces that control the immune system: immunity and tolerance. Most efforts thus far in cancer immunotherapy have focused only on enhancing immunity. These observations indicate that in most instances, tumors are still able to utilize immune evasion tactics. Thus, as tumors progress, immune evasion dominates over anti-tumor immunity.

Immune Suppression

Immunotherapy has been shown to elicit tumor-specific immune responses that infiltrate the spontaneously arising breast tumor. However, a number of studies have shown that the effector cells become non-functional within the tumor microenvironment [129, 130]. Tumor escape is one of the major obstacles that must be addressed prior to designing and delivering successful immunotherapy. Interestingly, a set of genes that marks and mediates breast cancer metastasis has been identified recently [131]. Eighteen

genes were listed as 'lung metastasis signature genes'. Amongst these were two genes, one in the COX-2/PGE₂ pathway, and one in the IDO pathway.

There are two isoforms of COX, COX-1 and COX-2, that have been identified [132]. Although they both catalyze the formation of prostaglandins from arachidonic acid, they have different biological roles. COX-1 is constitutively expressed in many tissues and is thought to be involved in maintaining cellular homeostasis [133]. COX-2 is an enzyme that is induced during carcinogenesis and inflammation, over-expressed in several human cancers, including breast cancer. COX-2 affects multiple pathways of tumorigenesis including angiogenesis, invasion and tumor-induced immune suppression. COX-2 induces its immunosuppressive effects through PGE₂, which targets both cytotoxic (CTL) and T helper lymphocyte (Th) functions [134, 135]. Inhibitors specific for COX-2 have shown significant effects in reducing the incidence and progression of tumors in animal models and in cancer patients. Cyclooxygenase inhibitors or nonsteroidal anti-inflammatory drugs (NSAIDs) are substances that block either the cyclooxygenase site of enzyme cyclooxygenase type 1 or 2 (COX 1 and COX 2, respectively), or its peroxidase site. Drugs known to inhibit enzymatic activity include ibuprofen, indomethacin (further explored in Chapter 5), rofecoxib, celecoxib, among others. Recently, we have discovered a novel mechanism by which COX-2 may regulate immunosuppression within the tumor microenvironment. Using a transgenic model of spontaneous mammary gland tumors, our lab has found that Cyclooxygenase 2 (COX2) over-expression and subsequent Prostaglandin E₂ (PGE₂) production are immunosuppressive, as they reduce T cell and dendritic cell function in patients with

breast cancer [136]. Further, COX-2 inhibition, via celecoxib administration reduced breast tumor levels of indolamine 2, 3-dioxygenase (IDO; Figure 14) [136].

IDO is an enzyme that catabolizes L-tryptophan to L-kynurenine. Its activity is increased under pathological conditions including tumor development [137, 138]. IDO was first identified in maintaining maternal tolerance towards the antigenically foreign fetus during pregnancy [139] and in suppressing T cell responses [140]. Tumor cells are known to exploit this mechanism to prevent rejection by tumor-specific T cells [139, 141]. IDO is overexpressed in many types of tumors as well as on antigen presenting cells including a subset of specialized DCs, known as plasmacytoid dendritic cells [137, 142-144]. These dendritic cells induce suppressor T cells leading to immune tolerance. IDO is emerging as a key player in suppressing T cell function and in the induction of immune tolerance to tumors [137, 144-147]. It has been shown to suppress T-cell responses through depleting the local tryptophan levels [148, 149]. Tryptophan is an essential amino acid required for T cell survival and proliferation. The effects of tryptophan depletion are mediated in part via a stress-activated kinase, GCN2 [150]. Transfection of tumor cells with IDO renders tumor cell lines immunosuppressive *in vitro* [151] and treatment with a competitive inhibitor, 1-methyl-dl-tryptophan (1MT) significantly delayed tumor outgrowth in a model of lung carcinoma.

COX-2 is known to be responsible for the high production of prostaglandins [152]. PGE₂, one of the major prostaglandins produced in the COX-2 pathway. PGE₂ exerts its effects via binding to G protein-coupled E prostanoid (EP) receptor. There are four EP receptors, each coupled to distinct G proteins. The four EP receptors that have been identified, named EP1, EP2, EP3, and EP4 respectively [153]. Activation of EPs leads to alterations in intracellular calcium and cAMP concentrations.

Specifically, EP1 is coupled to the G_q protein and signals through phospholipase C (PLC) and intracellular Ca^{2+} and activation of PKC. EP2 and EP4 are coupled to the G_s protein, signaling through elevation of cAMP level and activation of PKA. Importantly, there are specific EP antagonists that can be utilized in studying the effects of PGE_2 . Specifically, there exists a known EP1, EP2, EP3, and DP antagonist, AH6809 as well as an EP4 antagonist AH23848 which have displayed inhibitory effects on PGE_2 . This provides us with new opportunity to develop novel immunotherapeutic combinations for the treatment of metastatic breast and pancreas cancer (Figure 15).

Conclusions

Breast cancer is the 2nd most common cancer and affects 40,000 individuals annually. With the advent of breast cancer vaccines, there is promise for better patient outcome, however challenges still exist. First and foremost, tumors have the ability to undergo immune evasion tactics. These include expression of immunosuppressive enzymes. We hypothesize that inhibiting immune suppression and activating anti-tumor immunity combined will exert maximal anti-tumor effect in the treatment of breast cancer. Therefore, in Chapter 5, we evaluate the efficacy of our MUC1 vaccine that consists of two MHC class I-restricted MUC1 peptides, one MHC class II helper peptide mouse, CpG ODN, and GM-CSF in the context of combating immune suppression. We test the vaccine in combination with COX inhibitors, celecoxib and indomethacin. Moreover, we test the vaccine in combination with an EP 1-3 receptor antagonist, AH6809, or an IDO inhibitor, 1-MT (1-Methyl Tryptophan). In these studies, we use MUC1.Tg mice that are on a C57bl6 background. These mice express human MUC1 under its own promoter and therefore express human MUC1 in a tissue specific manner. These mice exhibit T and B cell tolerance

when immunized with human MUC1 antigen which makes it a relevant model to study MUC1-based vaccines [154]. Of key importance is that the tumors arise in immune competent mice and undergo immune evasion tactics similar to humans. It is therefore, a particularly challenging and relevant situation in which to study a combinatorial MUC1 based vaccines.

1.3 Figures

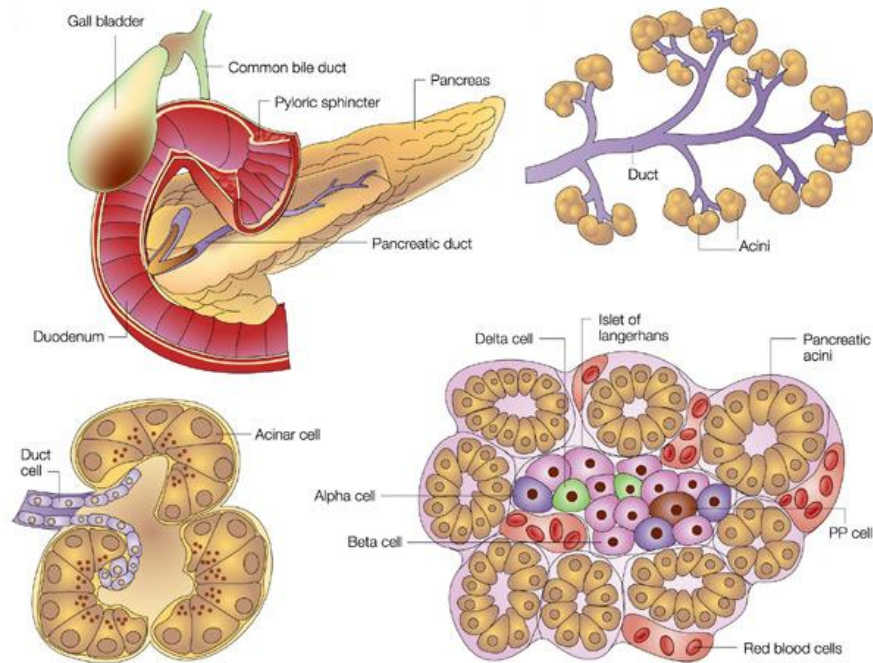


Figure 1. Pancreatic Structure. Adapted from Bardeesy et al., “Pancreatic cancer biology and genetics” *Nature Reviews Cancer* 2002. Figure displays the pancreas, and the cell types of the pancreas.

1.3 Figures continued

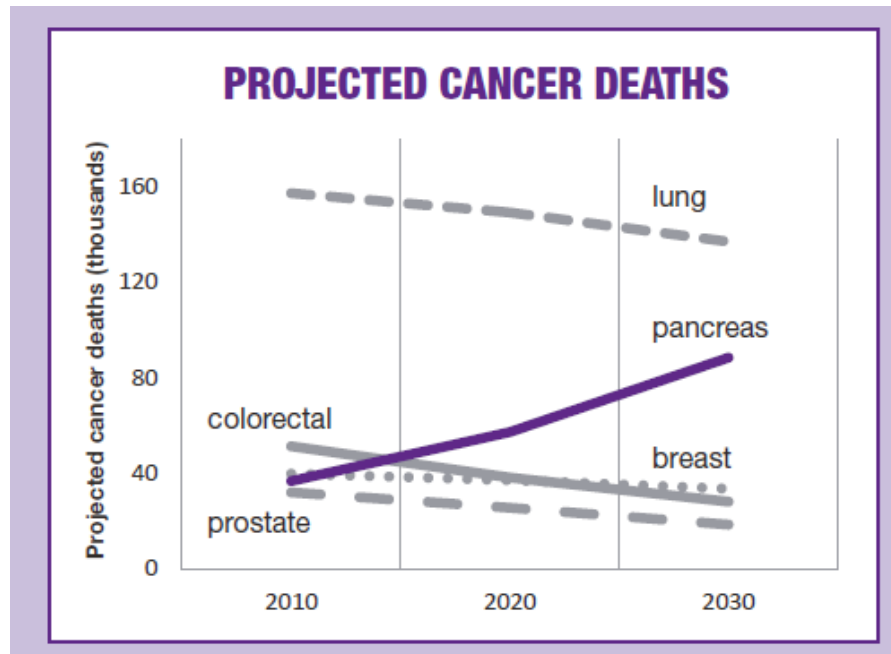


Figure 2: The incidence of pancreatic cancer is rapidly increasing and it is projected to become the 2nd leading cause of cancer related deaths by 2015. Published by the Pancreatic Cancer Action Network

1.3 Figures continued

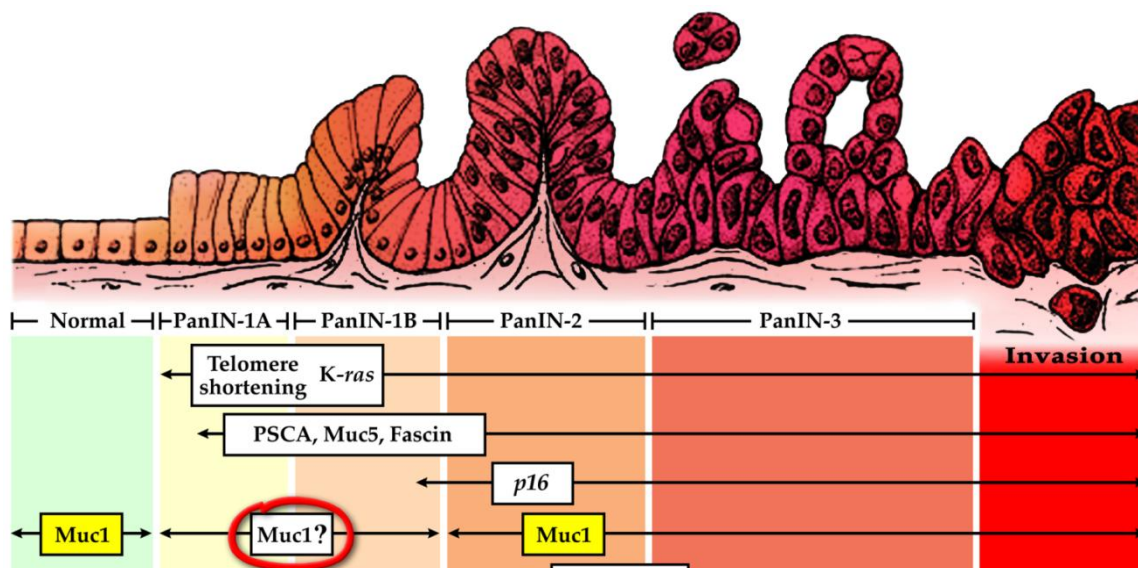


Figure 3. Pancreatic cancer progression model. PanIN lesions are subclassified into three categories depending on the degree of dysplasia and atypia, PanIN-1, PanIN2, and PanIN3, respectively. Adapted from Maitra et al. "Pancreatic Cancer" Annual Review Pathology 2008

1.3 Figures continued

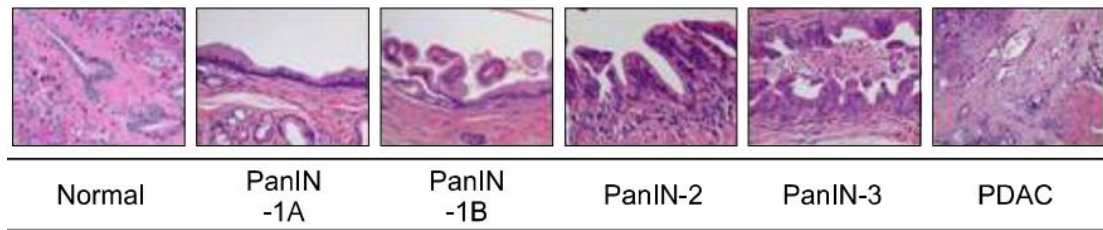


Figure 4: Hematoxylin and eosin staining of PanIN lesions in human specimens. Note the degree of atypia as PanIN lesions are scored higher. Adapted from Yonezawa et al. "Precursor lesions of pancreatic cancer" *Gut and Liver*. 2008.

1.3 Figures continued

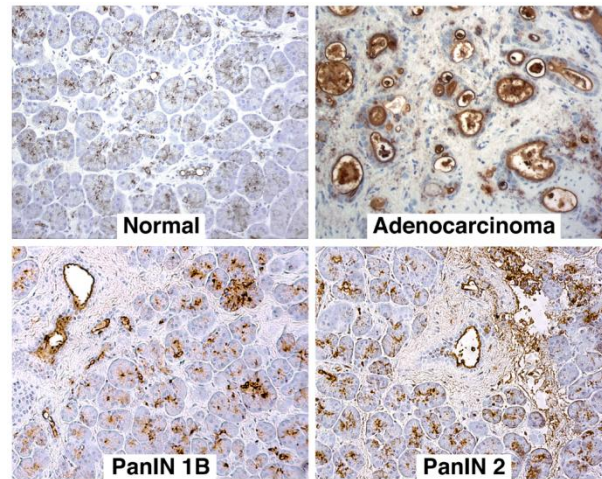


Figure 5: Detection of MUC1 using a specific MUC1 CT antibody. Our lab has demonstrated that over expression of MUC1 is detected in early and late stage human pancreatic cancer specimens.

1.3 Figures continued

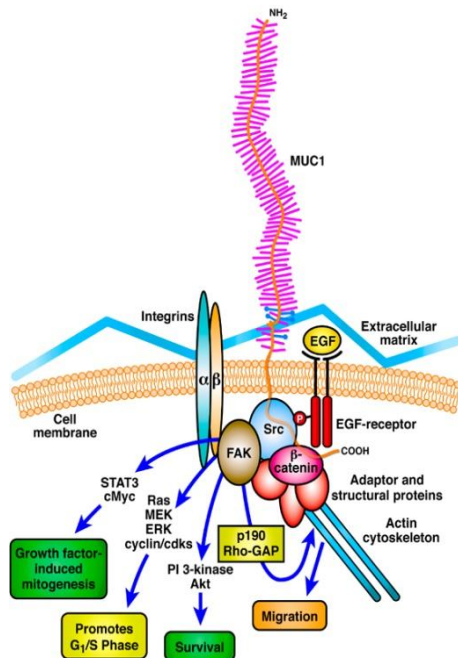


Figure 6: MUC1 cytoplasmic tail interactions. The cytoplasmic tail is involved in a variety of functions including mitogenesis, survival, and migration. Adapted from [www.functional glycomics.org](http://www.functionalglycomics.org)

1.3 Figures continued

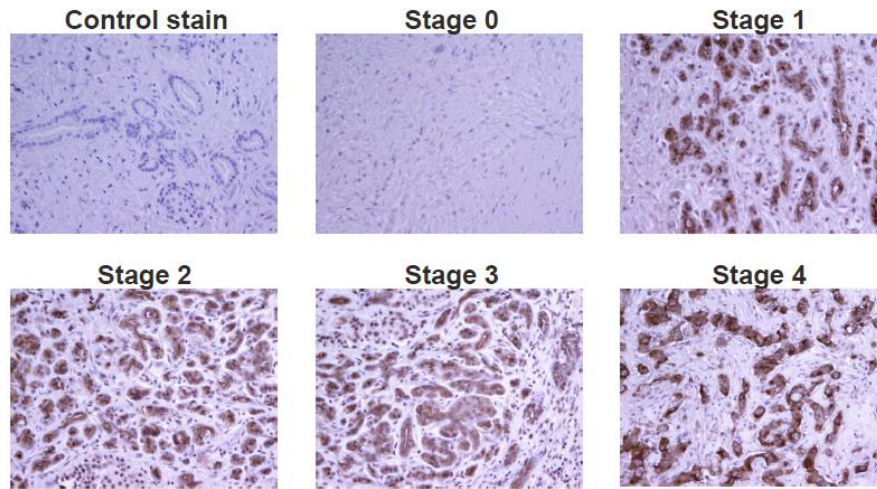


Figure 7: Detection of MUC1 using MUC1 specific TAB004 antibody. Our lab has detected MUC1 overexpression in early and late stage human pancreatic cancer specimens.

1.3 Figures continued

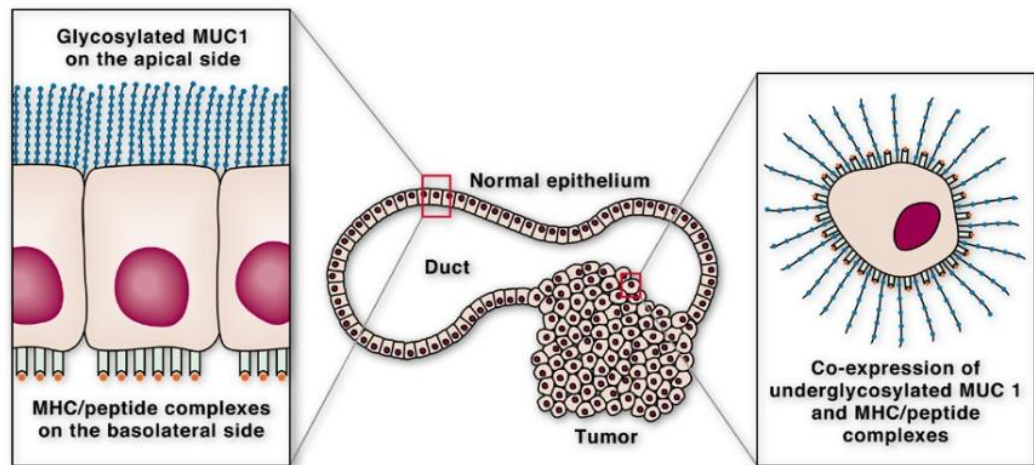


Figure 8: In a cancer setting there is a loss of polarity. MUC1 is no longer restricted to the apical surface, and has an aberrant glycosylation pattern. Adapted from www.genusoncology.com

1.3 Figures continued

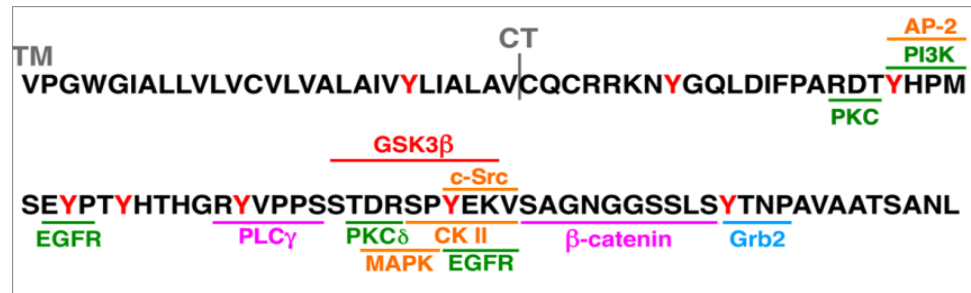


Figure 9: Hypothetical binding sites for cell signaling molecules on the MUC1 cytoplasmic tail. The MUC1 CT has a number of putative binding sites for a number of cell signaling molecules including c-Src, β -catenin, Grb2, EGFR and many others. Figure utilized with the permission of Dr. Pinku Mukherjee.

1.3 Figures continued

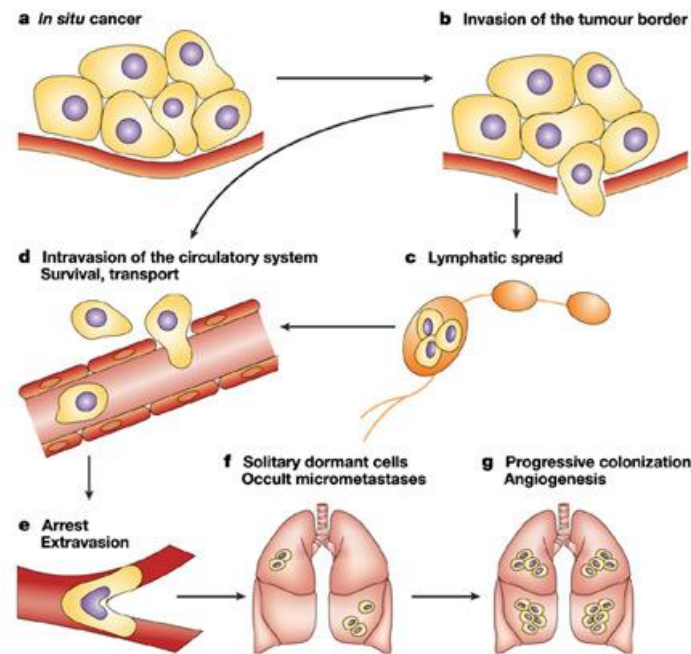


Figure 10. Metastasis of cancer cells. The primary tumor grows such that it is able to invade the local environment and intravasate into the vasculature. If the cells are able to survive in circulation, they can then extravasate from the vasculature and grow in secondary organ sites. Adapted from Steeg et al., “Metastasis is a complex, multistep process”, *Nature Reviews Cancer*, 2003.

1.3 Figures continued

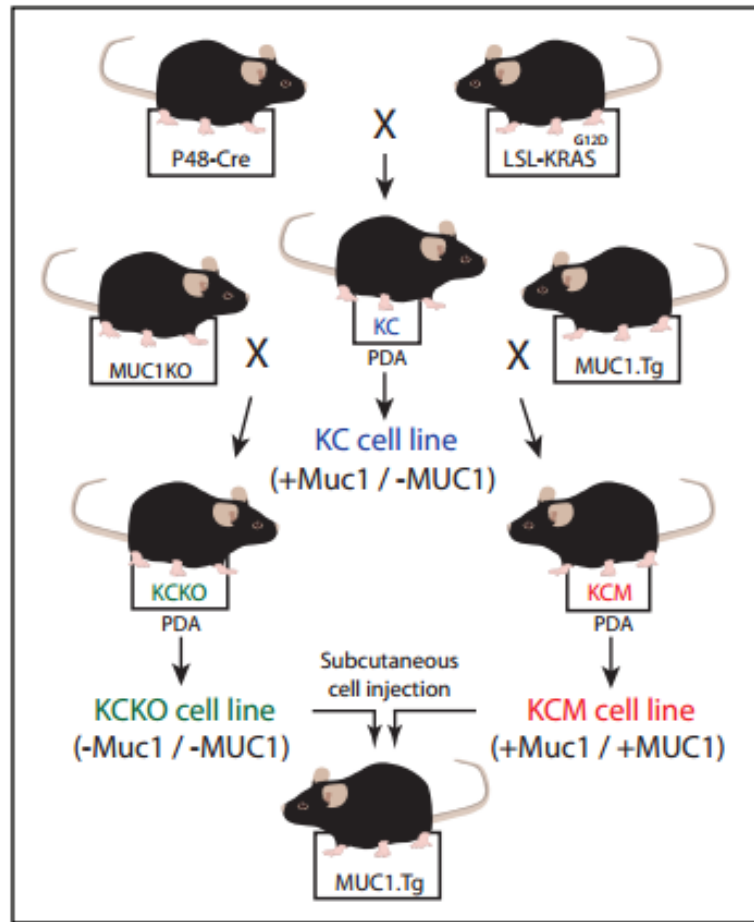


Figure 11: Mouse models utilized in pancreatic cancer experiments. C57BL/6 mice with KRAS^{G12D}-driven spontaneous PDAs were crossed with mice expressing human MUC1 (MUC1.Tg) or null (MUC1 KO) were used to generate the MUC1 positive KCM or MUC1 null KCKO cell lines, respectively.

1.3 Figures continued

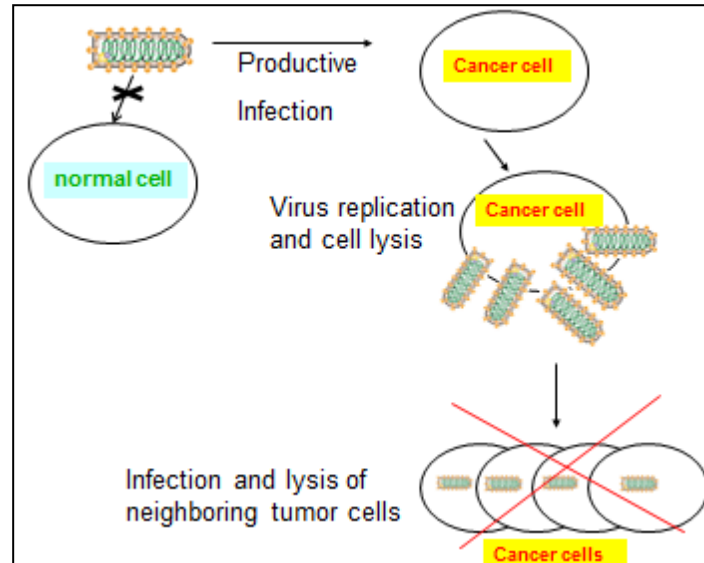


Figure 12: Oncolytic virotherapy is a cancer therapy that uses viruses to specifically infect cancer cells. It cause cell lysis and then newly released infectious virus particles can go onto infect neighboring tumor cells and this cycle of infection ultimately leading to tumor regression. Picture utilized with the permission of Dr. Andrea Murphy.

1.3 Figures continued

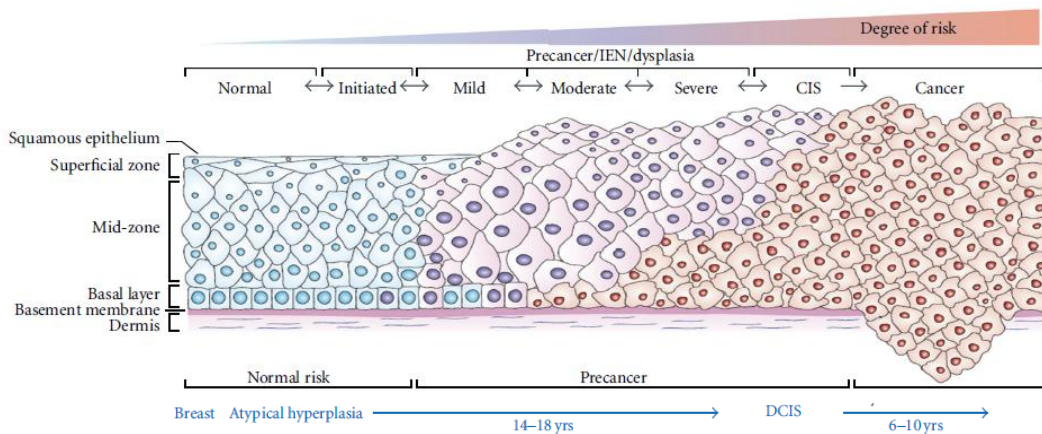


Figure 13: Model of Breast carcinogenesis. Specifically, there are an accumulation of cellular events that result in a dysplastic appearance. Adapted from Cazzaniga et al. "Breast Cancer Chemoprevention: Old and New approaches" Journal of Biomedicine and Biotechnology 2012.

1.3 Figures continued

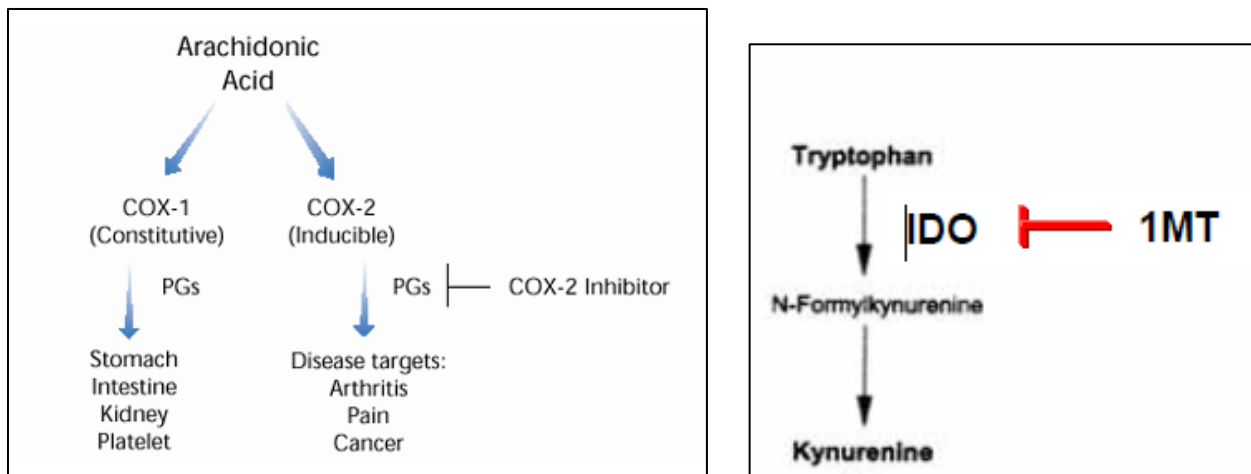


Figure 14: Mechanism of action for cyclooxygenase and indoleamine-2,3 dioxygenase pathways. Cyclooxygenase converts arachidonic acid to prostaglandins. IDO is the enzyme responsible for converting Tryptophan to Kynurenine. Figure on the left, adapted from Seibert et al “COX-2 Inhibitors-Is there a cause for concern?” *Nature Medicine* 1999. Figure on the right, adapted from Mellor et al. “IDO expression: tolerance and tryptophan catabolism” *Nature Reviews* 2004.

1.3 Figured continued

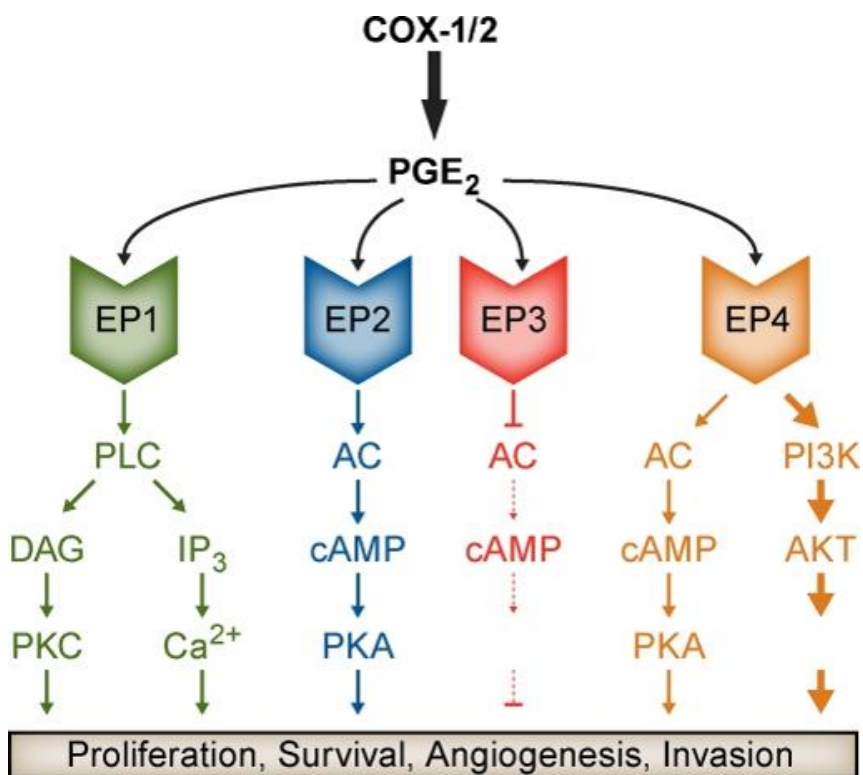


Figure 15: Signaling pathways activated by the EP receptors for PGE₂. Induction of COX-2 and its product, PGE₂ results in tumor promotion, specifically affecting proliferation, survival, angiogenesis, and invasion. PGE₂ binds to and activates for G-protein coupled E receptors. Adapted from Rundhaug et al. "The role of the EP receptors for prostaglandin E2 in skin and skin cancer" *Cancer Metastasis Review* 2011.

CHAPTER 2: PANCREATIC DUCTAL ADENOCARCINOMA (PDA) MICE LACKING MUCIN 1 HAVE A PROFOUND DEFECT IN TUMOR GROWTH AND METASTASIS

2.1 Abstract

MUC1 is over expressed and aberrantly glycosylated in >60% of pancreatic ductal adenocarcinomas. The functional role of MUC1 in pancreatic cancer has yet to be fully elucidated due to a dearth of appropriate models. In the present study, we have generated mouse models that spontaneously develop pancreatic ductal adenocarcinoma (KC), which are either Muc1-null (KCKO) or express human MUC1 (KCM). We show that KCKO mice have significantly slower tumor progression and rates of secondary metastasis, compared to both KC and KCM. Cell lines derived from KCKO tumors have significantly lower tumorigenic capacity compared to cells from KCM tumors. Therefore, mice with KCKO tumors had a significant survival benefit compared to mice with KCM tumors. KCKO cells have reduced proliferation and invasion and failed to respond to epidermal growth factor (EGF), platelet-derived growth factor (PDGF), or matrix metalloproteinase-9 (MMP9). Further, significantly fewer KCKO cells entered the G₂M phase of the cell cycle compared to the KCM cells. Proteomics and western blotting analysis revealed a complete loss of cdc-25c expression, phosphorylation of MAPK, as well as a significant decrease in Nestin and Tubulin α -2 chain expression in KCKO cells. Treatment with a MEK1/2 inhibitor, U0126, abrogated the enhanced proliferation of the KCM cells but had minimal effect on KCKO cells, suggesting that MUC1 is necessary

for MAPK activity and oncogenic signaling. This is the first study to utilize a Muc1-null PDA mouse in order to fully elucidate the oncogenic role of MUC1.

2.2 Introduction

Pancreatic ductal adenocarcinoma (PDA) is the fourth leading cause of cancer-related deaths in the United States [155]. It is one of the most deadly cancers due to its aggressive nature and relatively few treatment options. With a 5-year survival rate of only 5%, it has the poorest prognosis among all cancers. To date, the only potential curative is surgical resection, of which only 20% of patients are eligible. Alternative therapies, such as radiotherapy and chemotherapy remain largely ineffective. The development and evaluation of novel targeted therapeutic agents for improving the outcome of patients are of paramount importance.

Importantly, MUC1 is a membrane-tethered mucin glycoprotein expressed on the apical surfaces of normal glandular epithelia but is over expressed and aberrantly glycosylated in >60% of human PDA and in 100% of metastatic lesions [156, 157]. In human cancers, MUC1 is commonly detected in high grade but not in low-grade pancreatic intraepithelial neoplasia (PanIN) [51, 53]. Recently, the contribution of MUC1 on invasive and metastatic properties of pancreatic cancer cell line has been shown [158]. Thus MUC1 may play an important role in the development and progression of PDA [36, 103, 104]. Over expression of MUC1 in pancreatic cancer has been known for quite some time; however its function has not been clearly elucidated mainly due to the lack of an appropriate pancreatic cancer model.

Activating mutations in the KRAS proto-oncogene are found in over 90% of invasive pancreatic ductal adenocarcinoma and are thought to represent an initiating

event. Recently a transgenic mouse model has been created that expresses physiological levels of oncogenic KRAS with a glycine to aspartate substitution at codon 12, in the progenitor cells of mouse pancreas [159]. These mice, designated as KC or Cre-LSL-KRAS^{G12D}, develop the full spectrum of pancreatic ductal adenocarcinoma. We have further crossed the KC mice to the human MUC1 transgenic (MUC1.Tg) mice which express MUC1 in a pattern and level consistent with that in humans (designated KCM) [157]. KC mice were also crossed with the Muc1KO mice (designated KCKO), creating a Muc1-null PDA model. These mouse models provide us with a unique opportunity to fully evaluate the role of MUC1 in pancreatic cancer development.

This study is the first to utilize a model of pancreatic cancer that is Muc1-null in order to fully elucidate the oncogenic role of MUC1. In this study, we show that lack of Muc1 significantly decreased proliferation, invasion, and mitotic rates both and . Importantly, treatment with MEK1/2 inhibitor, U0126, completely abrogated the enhanced proliferation of the KCM cells. These data, therefore, may have implications in the future design of MUC1-targeted therapies for pancreatic cancer.

2.3 Materials and Methods

Spontaneous Mouse Models and Tissue Culture.

KC mice were generated in our laboratory on the C57BL/6 background by mating the P48-Cre with the LSL-KRAS^{G12D} mice [80, 160]. They were further mated to the MUC1.Tg mice to generate KCM mice [157, 161] or to the Muc1KO mice [162] to generate KCKO mice. Tumors were excised at predetermined time points and weighed. Gross metastasis was evaluated in the lung, liver and peritoneum. Tumors were dissociated using collagenase IV (Worthington Biochemical) and cell lines generated in our laboratory. Cell lines are designated KCKO for those cells lacking Muc1 and KCM for those cells expressing MUC1. Since we have been unable to generate the KC cell lines, we have compared KCM with KCKO. The cells were maintained in complete DMEM (Invitrogen) supplemented with 10% FBS (HyClone), 1% glutamax (Invitrogen), and 1% penicillin/streptomycin.

ELISA.

PGE₂ levels in the tumor lysate were determined using a specific ELISA kit for PGE₂ metabolite (PGE-M) (Cayman Pharmaceuticals). VEGF levels were also determined by specific ELISA (RayBiotech).

³H-Thymidine Incorporation.

KCM and KCKO cells were serum-starved for 24hrs and treated for 30 mins with rm-PDGF-CC (Peprotech), rm-EGF (Peprotech), and rm-MMP9 (R&D systems) at a concentration of 50ng/mL, or MEK1/2 inhibitor at 10μM concentration. Cell proliferation was determined by using ³H -thymidine incorporation, in which 1μCi of ³H-thymidine was added per well for 24hrs prior to harvesting. Incorporated thymidine was

evaluated using the Topcount micro-scintillation counter. All determinations were performed in triplicate.

CFSE Dilution Assay.

Cells were stained using the CellTrace CFSE Kit (Molecular Probes). CFSE was added to the cells at a final concentration of $2\mu\text{M}$, incubated for 15min at 37°C , and 0.5×10^6 removed for initial positive staining. The remaining cells were plated in triplicate. Cells were harvested at predetermined time-points and CFSE dilution was determined by flow cytometry (Beckman Coulter). Analysis was conducted using FlowJo (Treestar, Ashland, OR).

Cell Cycle Analysis.

Cells were harvested, fixed by resuspending in 10ml of 70% ethanol for 30min, and washed in ice-cold PBS. The pellets were resuspended in 0.5ml PBS, and 1mL of DNA extraction buffer was added. Cells were incubated, washed and resuspended in DNA staining solution containing $20\mu\text{g/ml}$ propidium iodide (Sigma-Aldrich) and $100\mu\text{g/ml}$ RNase (Invitrogen). DNA content was determined by flow cytometry and analyzed using FlowJo.

Invasion Assays.

Cells (serum starved for 24hrs) were treated with rm-PDGF, rm-EGF, or rm-MMP-9 for 30min, trypsinized, washed, and resuspended in SFM. Cells were plated over transwell inserts (BD Biosciences) pre-coated with growth-factor reduced Matrigel™ (BD Biosciences), and permitted to invade towards serum contained in the bottom chamber for 48hrs. Percent invasion was determined as described in [163].

Western Blots and Proteomics.

Tumor lysates were run on SDS-PAGE gels and western blotting carried out as previously published [163]. MUC1 CT antibody CT2, was made in Mayo Clinic Immunology Core [163]. MUC1 TR antibody was provided by Dr. Joyce Taylor-Papadimitriou. ERK1/2 antibodies: phospho-p44/42 and p44/42 were purchased from Cell Signaling Technologies. All other antibodies (p53, CDKN1A, c-myc, TGF β -R1, MEK1, Cyclin B1, Wee 1, Cdc2-p34, Cdc-25c, and β -actin) were purchased from Santa Cruz Biotechnologies and used according to manufacturer's recommendations. Proteomics analysis was determined as previously described [163].

Tumor Growth.

Ten week and nine month old mice were injected with 1×10^6 KCM or KCKO cells (in 50 μ l of PBS combined with 50 μ L of growth factor-reduced MatrigelTM) into the flank of the mice (n=8). Mice were palpated starting at 6 days post tumor injection. Tumor weight was calculated according to the formula: grams=(length in centimeters x (width)²)/2 [163]. Upon sacrifice, the tumors were weighed, prepared for lysates, and fixed for immunohistochemistry. In accordance with IACUC, for survival studies, tumors were allowed to grow until reaching 10% of the body weight.

Hematoxylin/Eosin (H&E) Staining.

Tissues were fixed in 10% neutral-buffered formalin. Paraffin-embedded blocks were prepared by the Histology Core at The Mayo Clinic and 4-micron thick sections were cut for staining. Slides were H&E stained, and examined under light microscopy. Images were taken at 100X and 200X-magnification.

Statistical Analysis.

Data were analyzed using GraphPad software. Results are expressed as mean \pm SEM and are representative of greater than or equal to three separate experiments. Comparison of groups was performed using one-way or two-way ANOVA followed by the post-test for multiple comparisons (* p <0.05, ** p <0.01, *** p <0.001). Survival was assessed using a Kaplan Meier estimator.

2.4 Results

In the Absence of Muc1, Pancreatic Tumor Burden and Secondary Metastasis are Decreased.

Mice were sacrificed at 6, 16, 26, and 40 weeks of age. The pancreas weight was used as the indicator of tumor weight. At 6wks of age, there was no statistical difference between KCKO and either KC or KCM. However, by 16wks of age and thereafter, KC and KCM mice had significantly higher tumor burden than KCKO mice (Figure 16A). It must be noted that the KCM mice had significantly higher tumor burden than KC mice confirming our previous results that over expression of MUC1 augments pancreatic tumor progression [157]. Most importantly, pancreas weight did not increase from 6 to 40wks of age in mice lacking Muc1 suggestive of a stable disease (Figure 16A).

At 36-40wks of age, mice were euthanized and lungs, liver and peritoneum were evaluated for macroscopic gross lesions. Interestingly, 61% of KCM mice developed lung metastasis, 33% developed liver metastasis and 23% developed peritoneal metastasis (n=13). This is in stark contrast to the KCKO mice which had 10% of mice develop metastasis in any of the three organs (n=10). Thirty percent of the KC mice (n=13) had developed lung metastasis, 20% had developed liver metastasis, and 10% had developed peritoneal metastasis. As an example, a representative H&E image of a lung showing clear metastatic lesion is provided in Figure 16B.

We have previously shown that MUC1-expressing PDA have higher levels of VEGF and PGE-M [157], leading to higher angiogenesis and metastasis [164]. Therefore, we evaluated the circulating levels by specific ELISA. Both VEGF and PGE-M levels were significantly lower in the KCKO mice compared to KC and KCM mice and most notably the levels did not increase with age in the KCKO mice as noted in KC

and KCM mice (Figure 16C). PGE₂ is an end-product of the cyclooxygenase-2 (COX-2) pathway and is known to induce tumor cell proliferation and increase motility [165, 166].

H&E stained pancreas sections were examined from 6, 24, and 40-week old KC, KCM and KCKO mice. Clearly, abnormal duct with low grade PanIN lesions were visualized in the KCM pancreas as early as 6-weeks of age (Figure 16D). At this time-point, the pancreas from KC and KCKO mice looked relatively normal. By 24 and 40-weeks of age, both KC and KCM pancreas showed PanIN lesions of varying grades with KCM pancreas showing signs of higher grade PanIN lesions and adenocarcinoma (Figure 16D). This data confirms our previously published analysis of the PanIN lesions in KC and KCM pancreas as a function of age [157]. Most notably, pancreas from KCKO mice did not show high-grade PanIN lesions even at 24 and 40-weeks of age (Figure 16D). The data from these spontaneous models clearly point toward the critical role of MUC1 in the progression of pancreatic cancer. Further, pancreas from KCM and KC mice were highly proliferative compared to KCKO pancreas by Proliferating Cell Nuclear Antigen (PCNA) staining (data not shown).

Muc1-null Tumor Cells Have Significantly Lower Tumorigenic Capacity Compared to Their MUC1-expressing Counterpart.

To further decipher the underlying mechanism of enhanced proliferation and progression in MUC1-expressing tumors, we generated several cell lines from the KCM and KCKO tumors and first studied their tumor forming ability in both young and old mice. In the 8-10 week old mice (n = 4), both cell lines formed palpable tumors by 6d post-injection. By 12d post tumor challenge, KCM tumors grew faster (p<0.001), and continued the same trend until sacrifice at 21d post injection (Figure 17A). By 21d, the

tumor burden in mice injected with KCM (n=5), as determined by caliper measurement had grown to an average of 1017mg whereas; those mice injected with KCKO had a tumor burden of 461mg (n=6). During necropsy, tumors were excised and weighed. KCM tumors weighed on an average of 700mg whereas KCKO remained at 500mg (Figure 17A).

Because the median age of pancreatic cancer patients is >65 years of age, we assessed whether this observation would hold true in aged mice. In nine month old mice (Figure 17B, n=5 mice per group), tumor burden was again significantly higher with KCM versus KCKO cells starting at 12d post-injection ($p<0.05$) and continued until 21d reaching a tumor weight of 1300mg for KCM versus 300mg for KCKO (Figure 17B). It must be noted that in the aged mice, the KCM cells grew more aggressively than in the younger mice and reached a much higher tumor burden at 21d (compare Figure 17A and B), but that KCKO growth remained consistent.

Survival is Significantly Higher in Mice Injected with Pancreatic Cancer Cells Lacking MUC1.

In order to assess survival, mice were injected with KCM and KCKO cells and tumors were allowed to grow until reaching 10% of the body weight or until ulcerations developed, whichever came first (Figure 17C). Survival was significantly increased in mice injected with KCKO compared to KCM cells ($p<0.001$). By 25d post tumor challenge, none of the mice injected with KCM cells survived (n=7), while 100% of mice injected with KCKO cells (n=6) survived at that age (Figure 17C). Mice injected with KCKO survived until ~40d post tumor injection. Tumor weight, derived from caliper measurements, shows a steady growth rate of tumors injected with KCM, while the

KCKO tumor growth remains stunted and does not exceed ~500mgs (Figure 17D). These data recapitulate the data from the spontaneous model of PDA in Figure 16.

Cell Division and Cell Cycle Progression is Significantly Altered in Pancreatic Cancer Cells Lacking Muc1/MUC1.

To further analyze the effects of MUC1 on the kinetics of cellular division, KCKO and KCM were subjected to the CFSE dye dilution assay, which fluorescently labels cells and is depleted as they divide. Initial staining of KCM cells with CFSE resulted in a MFI of 2499. By the end of 48hrs, CFSE had already been diluted to a MFI of 96. Initial staining of KCKO cells resulted in a MFI of 1500. At the end of 48hrs, CFSE had been diluted to a MFI of 73 (Figure 18A). Although the KCM cells initially stained with greater intensity than did the KCKO cells, the CFSE was diluted much faster as can be seen by the slope of the line displaying MFI dilution over time (Figure 18B).

Since we observed that MUC1 affects cell division, we next investigated how the cell cycle was affected by MUC1 expression. Cells were stained with Propidium iodide (PI) and the DNA content was determined by flow cytometry. KCM cells progress through the cell cycle at a steady rate. At 12hrs post plating, 26.9% of KCM cells were in the G0/G1, 34.3% in S, and 32.5% in G2/M phase of the cell cycle (Figure 18C). In contrast, KCKO cells that lack Muc1 had a significantly different distribution at both 12hr and 24hr time points ($p < 0.001$, Figure 18B bottom panel). At 12hrs post plating, KCKO cells had 31.1% of cells in G0/G1, 52.9% in S, and 13.3% of cells in G2/M phase. This distribution remained relatively similar, in both cell types by 24hrs post plating (Figure 18C). KCKO cells clearly enter and accumulate in the S-phase where the DNA

doubling occurs more rapidly than KCM cells but thereafter, KCKO cells do not progress to the G2 and mitotic phase as efficiently as KCM cells.

KCKO cells fail to proliferate or invade in response to EGF, PDGF, and MMP9.

To assess if KCKO cells would respond to growth factors known to induce cell division, proliferation and invasion of cancer cells, KCKO and KCM cells were subjected to a proliferation assay, as determined by ³H-thymidine uptake. First, KCM cells displayed a significantly higher rate of proliferation compared to KCKO cells.

Stimulation with EGF, PDGF, or MMP9, did not induce proliferation in KCKO cells (Figure 19 A-C). With regards to invasion, the basal level invasion index of the KCKO cells was found to be significantly lower than KCM cells (Figure 19D, $p < 0.001$). More importantly, KCKO cells did not respond to any of the exogenous factors to increase its invasion index (Figure 19D). It should be noted that neither did the KCM cells, however that may be because of the high basal invasion index. Taken together the data suggests a failure of the KCKO cells to respond to exogenous EGF, PDGF or metalloproteinase.

Complete loss of cdc-25c expression and decreased phosphorylation of MAPK in KCKO cells may account for lower mitosis, proliferation, and invasion.

Once it was confirmed that cell cycle progression and proliferation was altered in cells lacking MUC1, we began to investigate what specific proteins and markers were altered to cause such drastic differences. KCKO and KCM cells were subjected to both western blot analysis and proteomics. We probed for those proteins typically involved in cell cycle regulation pathways. Most notable was the complete loss of the tumor suppressor proteins, p53 and downstream p21, in the KCM cells but not in the KCKO cells. Associated with this was the complete loss of the M phase inducer phosphatase,

cdc-25c, in the KCKO cells (Figure 20A). Furthermore, there was a significant down-regulation of levels of phosphorylated MAPK p44/42 in the KCKO cells compared the KCM cells (Figure 20A). Cdc-25c is a tyrosine phosphatase that directs dephosphorylation of cyclin B-bound CDC2 and triggers entry into mitosis. Thus, it becomes plausible to speculate that KCKO cells do not enter the mitotic phase efficiently because of the absence of Cdc-25c expression. Cdc-25c is also known to suppress p53-induced growth arrest which possibly explains why cells lacking Cdc25-c and lacking Muc1 do not lose p53 and p21 expression, do not phosphorylate MAPK and therefore do not divide, proliferate and invade effectively.

MUC1 Increases Expression of Tubulin α -2 Chain and Nestin Proteins.

These alterations in cell cycle regulation were coupled with differential transcription of genes associated with proliferation and metastasis. Proteomics analyses of a total of 2874 cancer progression-associated proteins showed down regulation of 757 proteins in KCKO versus KCM cells. Genes with a two-fold decrease and below were considered to be significant and are shown in Figure 20B and C. It is extremely relevant that the most pronounced down regulation was seen in Tubulin α -2 chain and Nestin in KCKO cells, and therefore these proteins were highly up regulated in KCM cells (Figure 20B). Tubulin α -2 is a major constituent of microtubules and is required for mitotic spindle organization, mitosis, growth and cell migration. Similarly, Nestin is a marker of proliferating and migrating cells and highly expressed in mitotically active cells.

Treatment with MEK1/2 Inhibitor, U0126, Completely Abrogates the Enhanced Proliferation in KCM cells.

Since MEK1 phosphorylation is a critical signaling event for proliferation of KCM cells, we treated KCKO and KCM cells with U0126. As a positive control, cells were treated with 20% FBS. As was expected, the basal level of activated MEK1 was higher in KCM cells than in KCKO cells (Figure 21A). Similar to the cell lines, lysates from primary tumors of 26wk old KCKO mice showed reduced phosphorylation of MAPK versus tumors from the KCM mice (Figure 21A). This confirmed that activated MEK is a function of MUC1 expression and is critical in the progression of pancreatic cancer. When cell lines were treated with U0126, activation of MEK1/2 was completely abolished (Figure 21A). To assess if MEK1/2 is responsible for MUC1-enhanced cellular division and proliferation, KCM and KCKO cells treated with U0126 were subjected to CFSE dilution and ³H-Thymidine uptake assays. CFSE dilution assay results are displayed as change in mean fluorescence intensity (MFI) at 6, 12, and 24hrs (Figure 21B). Within 6hrs, KCM cells have already undergone rapid cell division as compared to KCKO cells (Figure 21B, $p < 0.001$) and treatment with the inhibitor did not significantly reduce cell division in either cell lines. However, at 12hrs and 24hrs post treatment, cell division was significantly lower in KCM cells with treatment ($p < 0.001$ as compared to basal cell division) but there was no significant change in the KCKO cells with U0126 treatment (Figure 21B). Both sets of cells supplemented with 20% FBS have significantly increased cell division albeit KCM always showed significantly rapid cell division compared to KCKO cells ($p < 0.001$, Figure 21B). It is noteworthy that addition of the MEK1/2 inhibitor reduced cell division of the KCM cells to the level of KCKO cells at all time points.

Similar results were obtained using the ^3H -Thymidine uptake assay. At 6 and 12hrs post treatment with U0126, proliferation of KCM cells was significantly decreased from its basal level proliferation (Figure 21C, $p < 0.001$) and reached the level of KCKO cells. At 24hrs after treatment, there was no statistical significance between KCKO treated with U0126 and KCM treated with U0126. KCKO on the other hand did not respond to the inhibitor such that the basal proliferation and inhibitor treated proliferation remained similar suggesting that these cells do not require MEK1 activation. As expected, KCM cells were significantly more proliferative than KCKO cells ($p < 0.001$) at all time points.

2.5 Discussion

MUC1 is aberrantly over expressed in pancreatic cancer [104]. Over expression of MUC1 is detectable during the early stages of pancreatic cancer development and is further increased in invasive carcinoma in humans and mice [51, 157]. However, it is not known if pancreatic cancer cells are dependent on MUC1 for their growth and survival. Using appropriate mouse models, we show unequivocally for the first time that pancreatic cancer cells depend on MUC1 to grow and survive, by directly suppressing p53 and its major transcriptional target p21Cip (Figure 20) while activating MAPK, cdc-25-c, tubulin- α -2, and Nestin (Figure 20). This in turn stimulates proliferation and mitosis (Figure 18 and 19). Further, for survival, MUC1 expression causes the up-regulation of several multidrug resistance proteins and pro-survival factors that protect them from undergoing apoptosis (Figure 20). This is in stark contrast to what occurs in Muc1-null cells, in which the oncogenic signaling is shut down even though the KRas oncogene remains active. Muc1 deficiency leads to the failure to form tumors (Figure 17) and decreased proliferation and invasion (Figures 16-19).

The first evidence that MUC1 is required for pancreatic tumor growth came from the observation that the pancreas tumor weight remained unchanged between 6 and 40wks of age in Muc1-null mice, whereas, the tumor weight increased significantly in wild type mice (Figure 16A). This lack of tumor growth in the Muc1-null mice was further substantiated when cell lines generated from tumors in these mice resulted in stable disease when injected (Figure 17A-D) and had low proliferative index even when supplemented with exogenous growth factors known to enhance tumor cell proliferation (Figure 18 A-C). Further, MUC1 was shown to regulate cell cycle, as Muc1 deficiency lead to fewer cells entering the (G₂M) phase of the cell cycle (Figure 19B). In addition,

MUC1 drove Cdc-25c expression, a tyrosine phosphatase that triggers entry into mitosis. Since activated ERK1/2 is known to interact with Cdc-25c during interphase and phosphorylate Cdc-25c during mitosis [167], increased levels of ERK activation may be partially responsible for the up-regulation of cdc-25c and thereby enhanced mitosis and entry into the G₂M phase of the cell cycle. To that effect, treatment with U0126, reduced proliferation of MUC1-expression cells to that of Muc1-null cells (Figure 21A-B).

MUC1 regulation of cell cycle checkpoints, proliferation, and invasion could also be attributed to strikingly higher levels of Tubulin α -2 chain and Nestin proteins (Figure 20B-C). Nestin, a marker for proliferating and invading cells, is differentially expressed during the cell cycle and promotes cell proliferation [168, 169]. Nestin is also known to interact with Cyclin-dependent kinase 5 (CDK5), a kinase which phosphorylates MEK1. Thus, we hypothesize that MUC1 regulation of Nestin may activate CDK5 and thereby enhance phosphorylation of MEK1. Interestingly, inhibition of the ERK pathway has been shown to suppress the expression of nestin [168], once again, making the MAPK/ERK pathway an especially attractive target. Tubulin α -2 is a major constituent of microtubules and is required for mitotic spindle organization, mitosis, growth, and cell migration, thus emphasizing another important role of MUC1 in cell division. Currently, small molecule inhibitors of tubulin are clinically used as anti-mitotic drugs [170]. Importantly, these anti-mitotic drugs have shown efficacy against multidrug-resistant tumors.

We postulate that the strong oncogenic signaling motifs reside in the cytoplasmic tail of MUC1 (MUC1 CT). MUC1 CT is a trans-membrane receptor that is known to function as an oncoprotein [46, 171, 172]. The tyrosines in MUC1 CT are essential for

the oncogenic signal to occur in pancreatic cancer cells [163] and contains a YTNP site that, when phosphorylated, interacts with the proteins of the MAPK pathway. Our data and the above findings enable us to postulate that MUC1 contributes to pancreatic cancer cell growth and survival by promoting activation of the MAPK pathway, as pharmaceutically inhibiting this pathway inhibited proliferation in MUC1-expressing cells.

Finally, we have previously shown that treatment with a MUC1-based vaccine in combination with celecoxib was extremely effective in halting tumor progression in the KCM mice [161]. Further, we have recently shown that the tyrosines in MUC1 CT was essential for epithelial to mesenchymal transition and invasion [173]. Thus, targeting MUC1 CT may be an attractive approach, especially since the activation of MAPK pathway in pancreatic cancer cells may occur in part via MUC1 CT phosphorylation and interaction with β -catenin [173].

2.6 Figures

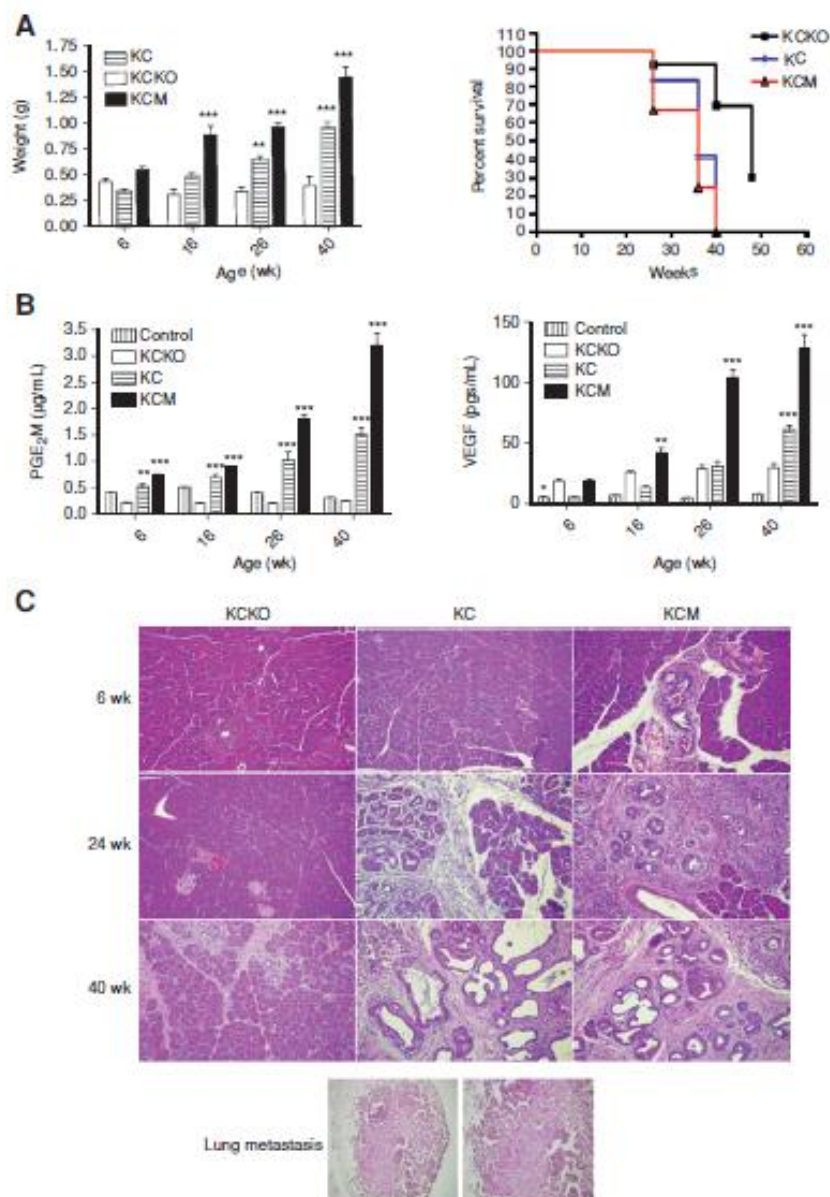


Figure 16: KCKO mice have lower tumor burden, metastasis, and levels of VEGF and PGE₂ with higher survival compared to KC and KCM mice. A. Pancreas weight and survival of KCKO, KC, and KCM mice. (pancreas weight: ** $p < 0.01$; *** $p < 0.001$ compared to KCKO; survival: * $p < 0.01$ compared to KCM and KC). B. Circulating levels of PGE₂M and VEGF in C57Bl/6, KCKO, KC, and KCM mice (** $p < 0.01$; *** $p < 0.001$ compared to KCKO). C. Representative IHC images of pancreas from KCKO, KC, and KCM mice as a function of age (200X). Representative H&E of lung metastasis (100 and 200X)

2.6 Figures continued

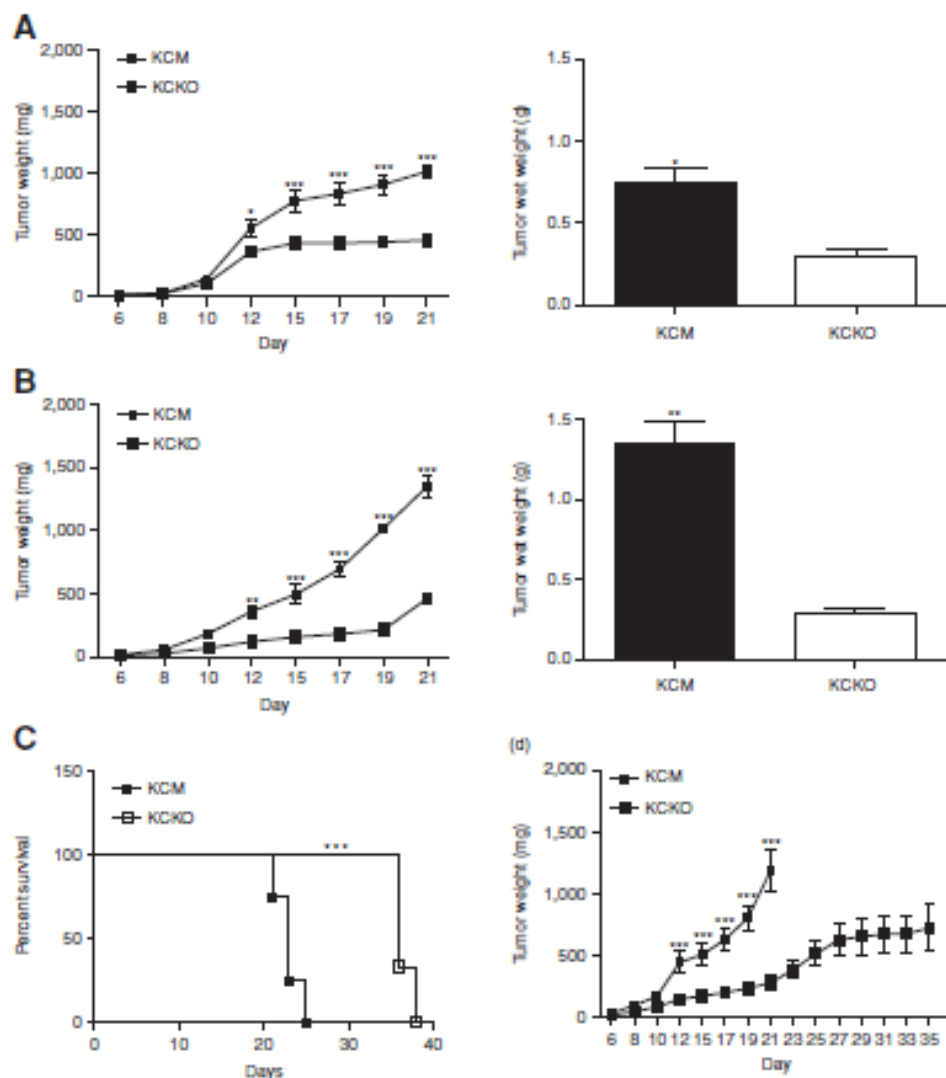


Figure 17: Significantly decreased tumor burden and increased survival in syngeneic C57/BL6 mice challenged with KCKO versus KCM cells. A. Tumor growth curve and tumor wet weight in 8–10wk and nine month old mice. Significantly higher tumor weight in mice injected with KCM versus KCKO cells (* $p < 0.05$, *** $p < 0.001$). B. Tumor growth curve and tumor wet weight in 9-month old mice. Significantly higher tumor weight in mice injected with KCM versus KCKO cells (** $p < 0.01$, *** $p < 0.001$). C. Survival curve of 8–10wk old mice challenged with KCKO and KCM cells ($n = 7$). Significantly higher survival in mice injected with KCKO versus KCM tumors (*** $p < 0.001$). D. Tumor growth curve of KCM versus KCKO cells of mice in the survival study (*** $p < 0.001$).

2.6 Figures continued

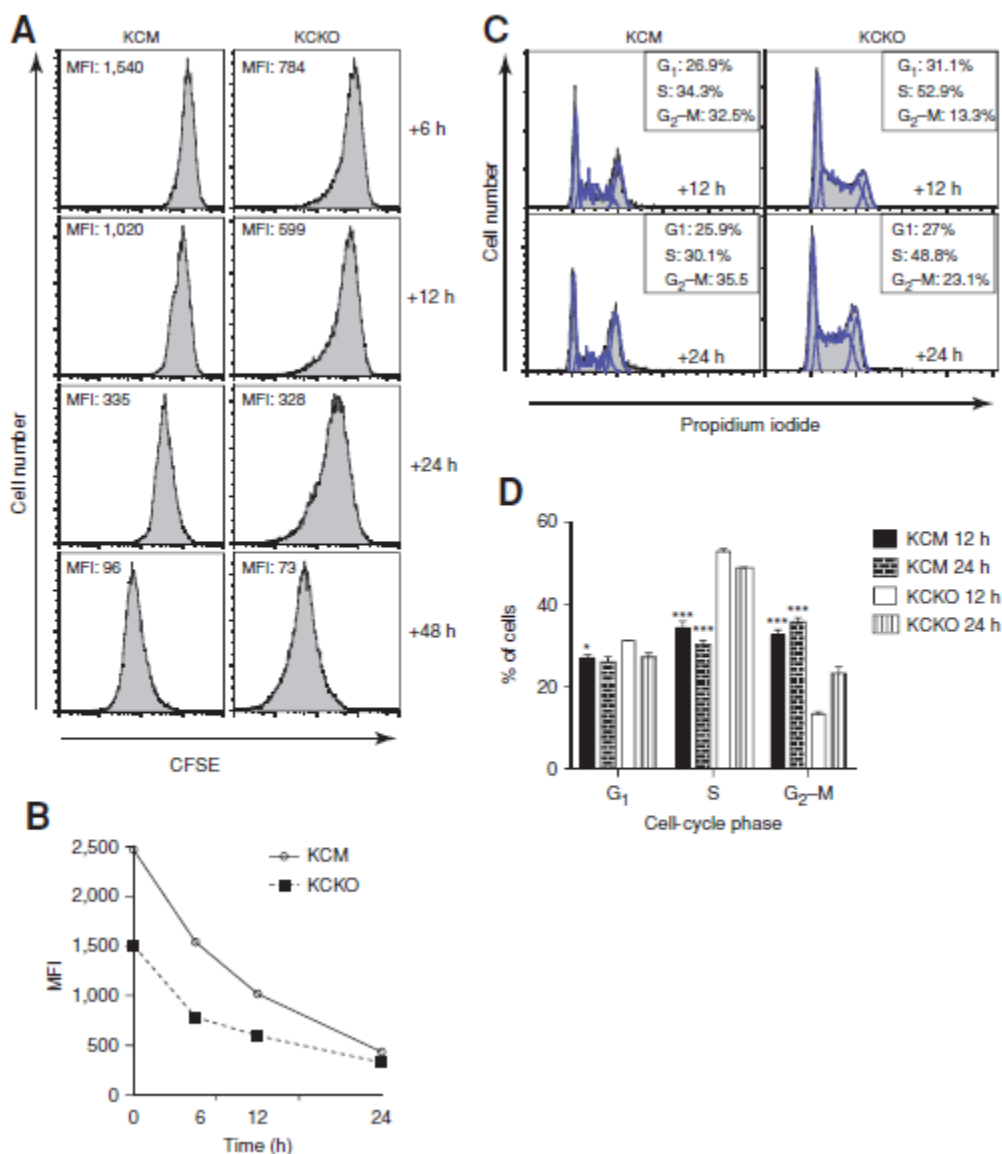


Figure 18: Significantly altered rate of cell division and progression through the cell cycle in KCKO versus KCM cells. A. Histogram representing CFSE staining in KCM and KCKO cells by flow cytometry. At time zero, KCM cells had MFI of 2499, by 48hrs, CFSE had been diluted to an MFI of 96. Whereas, in KCKO cells, the initial MFI was 1500, and by 48hrs, CFSE had been diluted to MFI of 73. B. Graph representing average MFI of CFSE staining in KCM and KCKO cells as a function of time in 3 experiments. C. Representative histograms of cell cycle analysis of KCM and KCKO cells by flow cytometry at 12 and 24hrs. D. Percentage of KCM and KCKO cells in the G₀/G₁, S, and G₂M phase of the cell cycle. Average of 3 experiments is shown

2.6 Figures continued

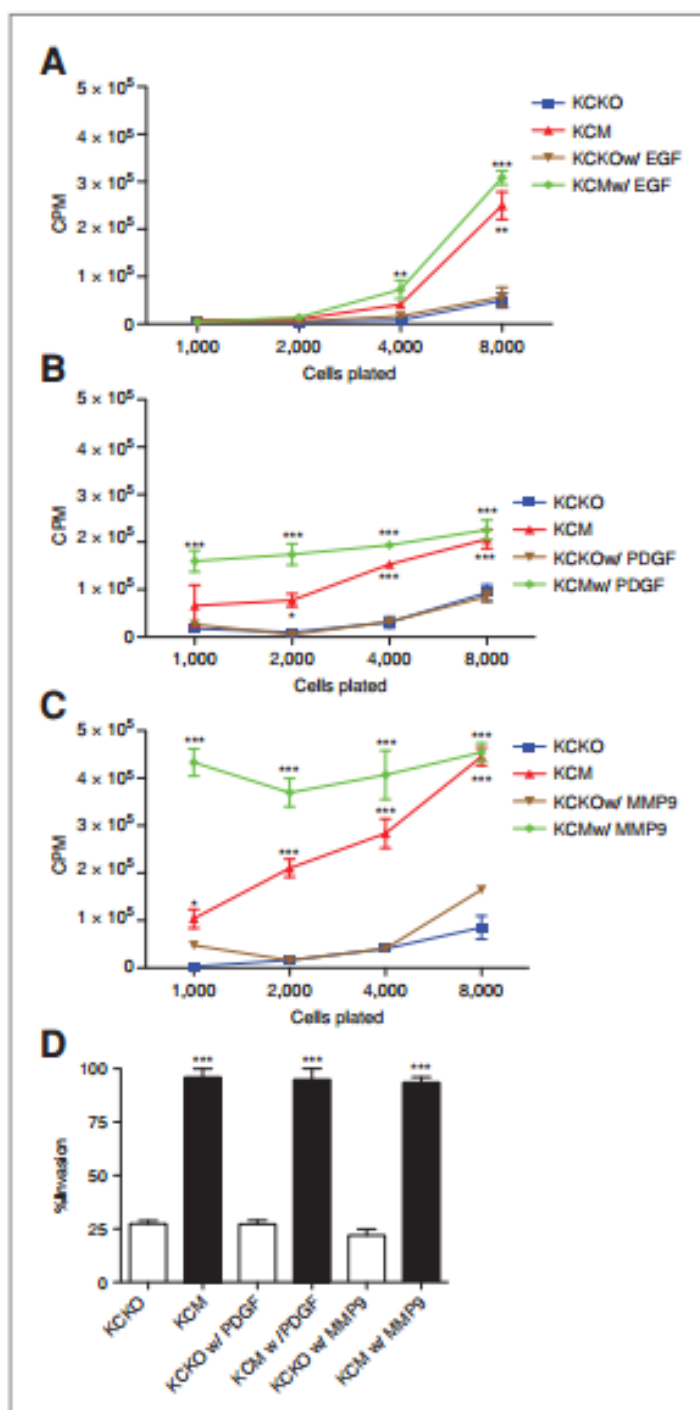


Figure 19: Significantly lower proliferation and invasion index in KCKO versus KCM cells. A – C. Proliferation as measured by ^3H -thymidine uptake in response to A. EGF, B. PDGF, and C. MMP9. Significantly higher proliferation was observed in KCM versus KCKO cells (* $p < 0.05$, *** $p < 0.001$). D. Percentage of KCM and KCKO cells that invaded in response to PDGF and MMP9 (*** $p < 0.001$).

2.6 Figures continued

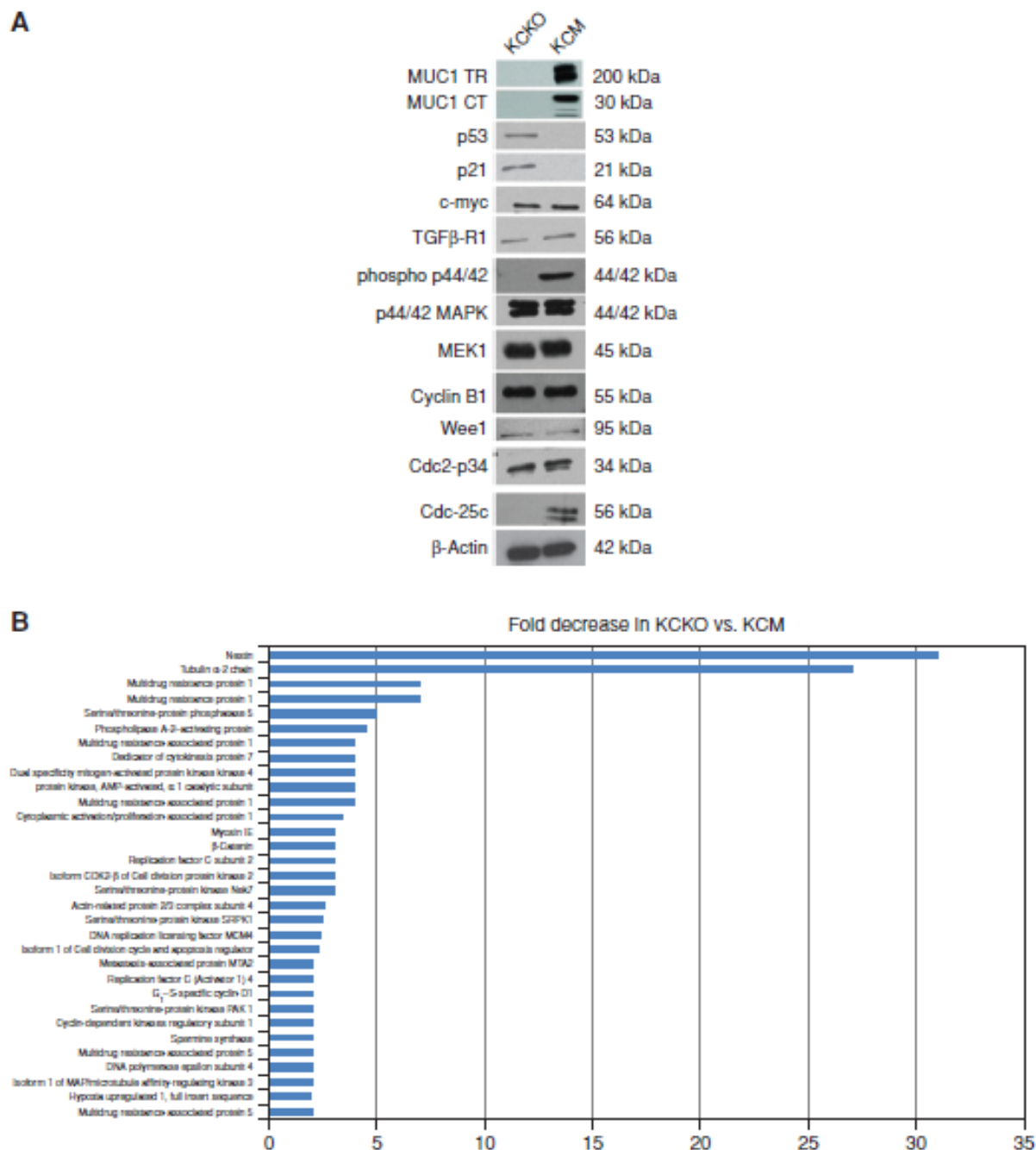


Figure 20: Differential protein expression profile in MUC1-expressing vs. Muc1-null cells. A. Western blotting analysis of KCM and KCKO cell lysates probed various proteins. B. Proteomics data from KCKO and KCM cell lysates (average of n=2 with each experiment conducted in triplicate). Data displayed as fold increase in KCM compared to KCKO cells. Only proteins that were changed >2-fold are shown.

2.6 Figures continued

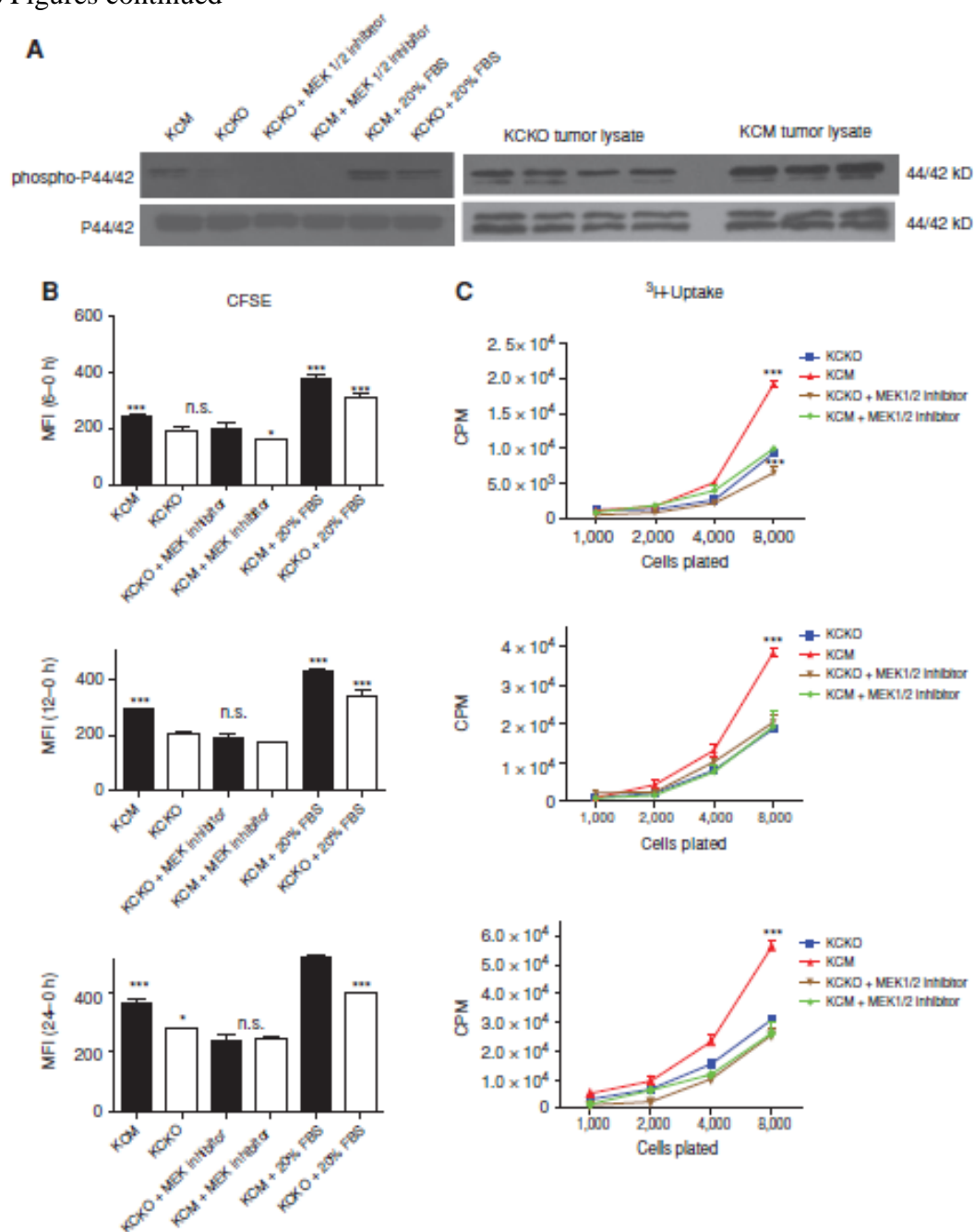


Figure 21: Treatment with MEK1/2 inhibitor, U0126, abrogates proliferation of KCM but not KCKO cells. A. Western blotting analysis showing phosphorylation of MAPK was completely abrogated with the addition of U0126, the MEK 1/2 inhibitor B and C. Proliferation of KCM and KCKO cells 6, 12, and 24hrs post treatment with U0126 using the B. CFSE dilution assay and C. ^3H -thymidine uptake assay. Experiments were repeated three times in triplicate.

CHAPTER 3: VESICULAR STOMATITIS VIRUS AS AN ONCOLYTIC AGENT AGAINST PANCREATIC DUCTAL ADENOCARCINOMA

3.1 Abstract

Vesicular stomatitis virus (VSV) is a promising oncolytic agent against a variety of cancers. However, it has never been tested in any pancreatic cancer model. Pancreatic ductal adenocarcinoma (PDA) is the most common and aggressive form of pancreatic cancer. In this study, the oncolytic potential of several VSV variants was analyzed in a panel of 13 clinically relevant human PDA cell lines and compared to conditionally replicative adenoviruses (CRAds), Sendai virus and respiratory syncytial virus. VSV variants showed superior oncolytic abilities compared to other viruses, and some cell lines that exhibited resistance to other viruses were successfully killed by VSV. However, PDA cells were highly heterogeneous in their susceptibility to virus-induced oncolysis and several cell lines were resistant to all tested viruses. Resistant cells showed low levels of very early VSV RNA synthesis, indicating possible defects at initial stages of infection. Unlike permissive PDA cell lines, most of the resistant cell lines were able to both produce and respond to interferon, suggesting that intact Type I interferon responses contributed to their resistance phenotype. Four cell lines that varied in their permissiveness to VSV- Δ M51 and CRAd dl1520 were tested in mice, and in vivo results closely mimicked those in vitro. While our results demonstrate VSV is a promising oncolytic agent against PDA, further studies are needed to better understand the molecular mechanisms of resistance of some PDAs to oncolytic virotherapy.

3.2 Introduction

Oncolytic virus (OV) therapy is an anticancer approach that utilizes replication-competent viruses to specifically kill tumor cells [82, 174, 175]. Such selectivity is possible because many tumors are characterized by defective innate immune responses or tumor-related abnormalities in regulation of mRNA translation or certain cellular signaling pathways, facilitating selective replication of viruses in cancer cells. For example, many cancer cells have defective Type I interferon (IFN) responses, which provides growth advantages to tumor cells; however, it also makes them more susceptible to viral infections [176, 177]. As a result, OV can infect, replicate within and kill tumor cells. Successful virus replication in cancer cells leads to the release of newly formed infectious virus particles that go on to infect neighboring tumor cells.

Vesicular stomatitis virus (VSV) is a promising OV and has demonstrated preclinical success against a variety of malignancies, including prostate [84-86], breast [87-90], melanoma [88, 91], colorectal [92-94], liver [95-97], glioblastoma [98-100] and other cancers [101]. As a result, at least two VSV OV have been considered for clinical trials by the NIH Recombinant-DNA Advisory Committee [99]. However, VSV oncolytic potential has never been studied in any pancreatic cancer models. About 95% of pancreatic cancers are pancreatic ductal adenocarcinomas (PDA) which are highly invasive with aggressive local growth and rapid metastases to surrounding tissues [178]. PDA is considered one of the most lethal abdominal malignancies with annual deaths closely matching the annual incidence of the disease [179, 180], resulting in a 5-year survival rate of 8-20%. Several cancer therapies proven successful in other tumor types have shown little efficacy in treating PDA. Chemotherapy is the primary treatment available; however, patients exhibit little improvement or develop chemoresistance [178].

Therefore, development of new treatment strategies for patients suffering from PDA is of utmost importance.

OV therapy with several viruses, including adenoviruses [181-183], herpesviruses [184-188] and reoviruses [189-191], has recently shown promise in several PDA tumor models. However, there are several advantages of using VSV as an anticancer therapy. VSV is the prototypic nonsegmented negative-strand RNA (NNS) virus (order *Mononegavirales*, family *Rhabdoviridae*), and its basic biology and interactions with host immune responses have been extensively studied [102]. This knowledge has led to the development of rationally designed VSV vectors for use in vaccines, gene therapy and OV therapy [101, 192]. While VSV is very sensitive to IFN-mediated antiviral responses (and therefore unable to productively infect healthy cells), it can specifically infect and kill tumor cells, majority of which are believed to be defective in Type I IFN production and responses [101, 193]. Also, the mechanisms of VSV-mediated killing by apoptosis have been established [194]. In addition to tumor specificity, VSV has several important advantages as an OV: (i) replication occurs in the cytoplasm of host cells with no risk of host cell transformation, (ii) cellular uptake in many mammalian cell types occurs rapidly and there is no cell cycle dependency, (iii) the genome is easily manipulated with the possibility for strong and adjustable levels of foreign gene expression to enhance oncolysis and specificity, and (iv) there is no preexisting immunity against VSV in humans [101]. While VSV is not considered a significant human pathogen, it can cause neurotoxicity in mice, nonhuman primates and even humans [195]. However, several VSV mutants have been generated which are not neurotropic but retain their oncolytic

activity [98, 196, 197]. In this study, we focused on two such VSV mutants, VSV- Δ M51-GFP and VSV-p1-GFP [98].

In our study, the oncolytic potential of VSV variants was analyzed in a panel of 13 clinically relevant human PDA cell lines and compared to conditionally replicative adenoviruses (CRAds), Sendai virus (SeV) and respiratory syncytial virus (RSV). VSV showed superior oncolytic abilities compared to all other viruses tested, and was effective in killing the majority of tested PDA cell lines. However, we identified some PDA cell lines that showed general resistance to oncolysis by all tested viruses. These results were confirmed for several PDA cell lines in vivo in nude mice. We also conducted initial analysis of PDA resistance to virus-induced cell death. Our in vitro and in vivo results demonstrate that VSV has good potential as an OV against PDA, while further studies are needed to better understand the molecular mechanisms of resistance of some PDA cell lines to virotherapy.

3.3 Materials and Methods

Cell lines.

Human PDA cell lines used in this study: CFPAC-1 (ATCC CRL-1918), Hs766T (ATCC HTB-134), Capan-2 (ATCC HTB-80), T3M4 [198], AsPC-1 (ATCC CRL-1682), HPAF-II (ATCC CRL-1997), Suit2 [199], HPAC (ATCC CRL-2119), BxPC-3 (ATCC CRL-1687), MIA PaCa2 (ATCC CRL-1420), SU.86.86 (ATCC CRL-1837), Capan-1 (ATCC HTB-79), and Panc-1 (ATCC CRL-1469). In addition, the immortal human pancreatic duct epithelial cell line (HPDE) [200] was used in this study and maintained in Keratinocyte-SFM (Gibco). This cell line, which was generated by introduction of the E6 and E7 genes of human papillomavirus 16 into normal adult pancreas epithelia, retains a genotype similar to pancreatic duct epithelia and is non-tumorigenic in nude mice [200]. The mouse breast cancer cell line 4T1 (ATCC CRL-2539), the baby hamster kidney fibroblasts BHK-21 (ATCC CCL-10), the human cervix adenocarcinoma cell line HeLa (ATCC CCL-2), the African green monkey kidney cells Vero (ATCC CCL-81) and the human epidermoid cancer cells Hep-2 (ATCC CCL-23) were used to grow viruses and/or as controls for viral replication. CFPAC-1, Suit2, HPAC, MIA PaCa2, Capan-1, Panc-1, 4T1, and Vero cells were all maintained in Dulbecco's modified Eagle's medium (DMEM, Cellgro). Capan-2, T3M4, AsPC-1, BxPC-3 and SU.86.86 cells were maintained in Roswell Park Institute medium-1640 (RPMI, Hyclone). HPAF-II, Hs766T, BHK-21, A549 and HeLa cells were maintained in modified Eagle's medium (MEM, Cellgro). All cell lines were supplemented with 9% fetal bovine serum (Gibco). For all experiments, PDA cell lines were passaged no more than 10 times.

Viruses.

The following viruses were used in this study: recombinant wild-type (wt) VSV (Indiana serotype) [201]; VSV-p1-GFP; VSV- Δ M51-GFP (p5); CRAd-dl1520 (“ONYX-015”); CRAd-hTERT (Adv-TERT_p-E1A); SeV-GFP; and RSV-GFP. VSV-p1-GFP has the green fluorescent protein (GFP) open reading frame (ORF) inserted at position one of the viral genome [98]. VSV- Δ M51-GFP has a deletion at amino acid position 51 of the matrix (M) protein, as well as the GFP ORF inserted in position 5 of the viral genome [98]. Both attenuated VSV recombinants have been shown to retain their oncolytic activity while lacking neurotoxicity in vivo [98, 197]. CRAd-dl1520 is attenuated by deletion of a large part of the coding sequence for the E1b55k viral gene product and selectively replicates in and kills cancer cells [202, 203]. CRAd-hTERT is a human telomerase reverse transcriptase (hTERT)-promoter-dependent CRAd, which selectively replicates in and kill cells with active hTERT (85–90% of tumor cells) [204]. SeV-GFP (SeV-GFP-F_{mut}) has the GFP ORF at position one of the viral genome and a mutation in the cleavage site of the fusion (F) protein allowing for F activation and production of infectious virus particles in cells without acetylated trypsin in the medium through a ubiquitous furin-like protease [205]. RSV-GFP has the GFP ORF at position one of the viral genome [206]. All VSV variants were grown in BHK-21 cells, SeV-GFP was grown in Vero, CRAbs were grown in HeLa, and RSV-GFP was grown in Hep-2 cells. For animal experiments, VSV- Δ M51-GFP was dialyzed (Slide-A-Lyzer, Pierce) in 2 L chilled dialysis buffer [25 mM Tris pH 7.4, 140 mM NaCl, 5 mM KCl, 0.6 mM Na₂HPO₄, 0.5 mM MgCl₂, 0.9 mM CaCl₂, and 5% (w/v) sucrose] for 2 hour (h) at 4°C and then 4 h at 4°C in fresh dialysis buffer. CRAd-dl1520 was dialyzed in 10 mM Tris

pH 8, 135 mM NaCl, 1 mM MgCl₂ and 50% (v/v) glycerol three times for 1 h each at 4°C. Dialyzed viruses were tested for infectivity on A549 cells.

Cell Viability Assay.

Cells were seeded in 96-well plates so that they reached 80% confluency at 24 h, and then virus-infected at a multiplicity of infection (MOI) of 1 or 0.01 CIU (cell infectious units) per cell (based on VSV titration on 4T1 cells) or mock infected in MegaVir HyQSFM4 serum-free media (SFM, Hyclone). One h post infection (p.i.) virus was aspirated and cells were incubated in growth media containing 5% FBS. Cell viability was analyzed at 5 days (d) p.i. by an MTT cell viability assay (Biotium). To determine the kinetics of virus-associated cytopathogenicity, cells were seeded in 96-well plates so that they reached 50% confluency at 24 h. Cells were then mock infected or infected with VSV-ΔM51-GFP at low (0.001 CIU/cell), intermediate (0.1 CIU/cell), or high MOI (1 CIU/cell). At 1 h p.i., virus was aspirated and cells were overlaid with growth media containing 5% FBS. An MTT cell viability assay was performed at 1, 16, 24, 48, and 72 h p.i.

Permissiveness of Cells to Virus Infection.

Cells were incubated with serial dilutions of VSV-wt, VSV-GFP(p1), VSV-ΔM51-GFP, SeV-GFP, CRAd-dl1520, or CRAd-hTERT in SFM for 1 h. At 1 h p.i., virus was aspirated and growth media containing 5% FBS was added to each well. The infectious foci of VSV-ΔM51-GFP, VSV-GFP(p1) and SeV-GFP were analyzed by fluorescent microscopy at 24 and 48 h p.i. respectively. The infectious foci of CRAd-dl1520 and CRAd-hTERT were analyzed by immunocytochemistry (ICC) at 5 d p.i. Briefly, cells were washed with phosphate buffered saline (PBS) and fixed in 3%

paraformaldehyde (PFA, Sigma) for 10 min followed by permeabilization for 2 min on ice with a solution containing 20 mM HEPES (pH 7.5), 300 mM sucrose, 50 mM NaCl, 3 mM MgCl₂, and 0.5% Triton X-100. Cells were then blocked with 5% bovine serum albumin (BSA, Sigma) in PBS for 20 min and incubated with anti-adenovirus hexon primary antibodies (1:600, US Biologicals, Cat # A0880-14) for 1.5 h. Cells were washed, incubated with peroxidase conjugated goat anti-mouse IgG antibodies (1:300, Jackson ImmunoResearch) for 1.5 h, and detected by addition of the peroxidase substrate 3,3'-diaminobenzidine tetrahydrochloride hydrate (DAB, Amresco). The infectious foci of VSV-wt were also analyzed by ICC as described above but using 1:100 rabbit polyclonal anti-VSV antibodies (raised against VSV virions) and anti-rabbit secondary antibodies. Cells were infected with serial dilutions of VSV-wt in triplicate and infectious foci were analyzed by ICC at 48 h p.i.

One-step Virus Growth Kinetics.

Selected PDA cells were seeded in 96-well plates to reach confluency at 24 h. They were infected in duplicate with VSV-wt, VSV- Δ M51-GFP, or VSV-p1-GFP at MOI 10 CIU/cell based on the reference cell line 4T1. At 1 h p.i. virus was aspirated, cells were washed twice with PBS (to prevent carryover of virions) and overlaid with growth media containing 5% FBS. At 1, 24, 50 and 72 h p.i. supernatant was collected from wells and flash frozen at -80°C. Virus titers were later determined by plaque assay analysis. Briefly, BHK-21 cells were incubated with serial dilutions of the samples for 1 h. Virus was aspirated and cells were overlaid with a SFM / 2% BactoAgar mixture to limit virus spread. Infectious foci were counted by light and fluorescence microscopy at 16 h p.i.

Type I Interferon Sensitivity and Production.

Cells were seeded in 96-well plates so that they reached 80% confluency at 24 h. For Type I interferon sensitivity, cells were either treated with 5000 U/ml interferon alpha (IFN- α , Calbiochem, Cat # 407294) in SFM or with SFM only. Twenty-four h post treatment, cells were infected with serial dilutions of VSV- Δ M51-GFP, and infectious foci were analyzed 16 h p.i. by fluorescent microscopy. Treatments and infections were performed in duplicate. For Type I interferon production, cells were infected with VSV- Δ M51-GFP at MOI 10 CIU/cell or mock-treated with SFM only. One h p.i. virus was aspirated and cells were incubated in SFM. Eighteen h p.i. supernatant was harvested and analyzed by ELISA for production of human IFN- β (PBL, Cat # 41410-1) or human IFN- α (multi-subtype, PBL, Cat # 41105-1) per manufacturer's instructions (PBL InterferonSource). Infections were performed in triplicate.

Western Blot.

Cellular lysates were prepared by mock infecting cells or infecting them with VSV- Δ M51-GFP at MOI 1 or 10 CIU/cell. One h p.i. virus was aspirated, cells were extensively washed and incubated in growth media containing 5% FBS. Cells were harvested at 16 h p.i. and lysed in lysis buffer containing 1% Triton-X-100, 20mM Hepes, 0.15 M NaCl, 2 mM EDTA and supplemented with c-inhibitor (2X, Roche). Total protein concentration was determined by Bradford assay. Three μ g (for VSV detection) or 30 μ g (for GFP detection) of total protein was separated by electrophoresis on 10% or 12% SDS-PAGE gels respectively, and electroblotted to polyvinylidene difluoride (PVDF) membranes. Membranes were blocked using 5% non-fat powdered

milk in TBS-T [0.5 M NaCl, 20 mM Tris (pH 7.5), 0.1% Tween20], which was also used for antibody dilutions. Membranes were incubated with 1:10000 rabbit polyclonal anti-VSV antibodies (raised against VSV virions) or 1:3000 mouse anti-GFP clone 9F9.F9 (Rockland). Detection was with 1:5000 goat anti-rabbit or 1:5000 goat anti-mouse horseradish peroxidase-conjugated secondary antibodies (Jackson ImmunoResearch) using the Enhanced Chemiluminescence Plus (ECL+) protein detection system (GE Healthcare). Membranes were reprobbed with mouse anti-actin clone C4 [207] to verify sample loading. Image capture and densitometry analysis were performed using VisionWorksLS v6.8 software (UVP).

Northern Blot.

The pVSVFL(+).g.1 plasmid, which encodes a complete cDNA copy of the VSV (Indiana strain) antigenome [201], was used as a template for addition of a SP6-promotor to the 3' end of a 279 bp fragment of N by PCR using the following primers: 5'-ATCCAGTGGAATACCCGGCAGATT-3' and 5'-ATTAGGTGACACTATAGAAGTGCTCGTCAGATTCAAGCTCAGGCTG-3'. A probe for detection of N mRNA and VSV anti-genomic RNA was synthesized from the PCR product by in vitro transcription in the presence of ³²P-UTP using the MAXIscript T7 kit (Ambion). Cells were mock treated or treated with 100 µg/ml cycloheximide for 30 min prior to mock infection or infection with VSV-ΔM51-GFP at MOI 10 and continuing treatment with cycloheximide. At 4 h p.i. cells were collected and total RNA extracted using the Quick-RNA MiniPrep kit (Zymo Research). For each sample, 1 µg of RNA was separated on a 1.2% agarose-formaldehyde gel containing ethidium bromide for confirmation of RNA loading by visualization of rRNA. The RNA was transferred to

a nylon membrane and incubated with probe overnight at 58°C. Bands were detected using a phosphoimager and quantitated using Image Quant 5.2 (Molecular Dynamics).

Animal Experiments.

Mice were handled and maintained under veterinary supervision in accordance with institutional guidelines and under a University of North Carolina at Charlotte Animal Care and Use Committee (IACUC) approved protocol. 6-8 week old, male, athymic nude mice (Hsd:Athymic Nude-Foxn1^{nu}, Harlan Laboratories, Inc., Frederick MD) were subcutaneously injected with one of 4 human PDA cell lines. All cell lines used in animal experiments were tested negative for an extended panel of pathogens (MIA PaCa2, SU.86.86, and Panc-1 were tested by Charles River Laboratories and HPAF-II was tested by Bioreliance). Based on preceding titration experiments (data not shown), mice were injected with: 5×10^6 Mia PaCa2, 5×10^6 Panc-1, 3×10^6 HPAF-II, and 3×10^6 SU.86.86 cells (in 100 μ l of PBS) into the right flank (n=18 per group). Two additional untreated age-matched mice were used in this experiment to compare body weights with the treated experimental mice. Mice were palpated starting at 9 d post tumor injection. Tumors were established by day 13 and mice were randomly divided into 3 groups (n=6 per group). One group served as a control and received one intratumoral (IT) administration of 50 μ l PBS only. The other two groups were administered once with VSV- Δ M51-GFP or CRAd-dl1520 IT with a dose of 5×10^7 CIU in 50 μ l PBS. Dose was determined based on CIU established on A549 cells for both viruses. Tumor size was monitored by caliper measurements every other day, and body weight was measured once weekly. Tumor weight was calculated according to the formula: grams = [(length in cm) x (width in cm)²]/2. Upon sacrifice, tumor and brain tissue were harvested and tested for

the presence of VSV- Δ M51-GFP. Data were analyzed using GraphPad software and are expressed as mean \pm standard deviation.

3.4 Results

Susceptibility of PDA Cell Lines to Viral Oncolysis.

The susceptibility of human PDA cells to virus-mediated oncolysis was tested in a panel of 13 clinically relevant PDA cell lines derived from primary PDA tumors or PDA metastases to the liver and lymph nodes. In addition to PDA cell line, the immortal human pancreatic duct epithelial cell line (HPDE), which retains a genotype similar to pancreatic duct epithelia and is non-tumorigenic in nude mice [200], was employed as a “benign” control cell line to determine virus specificity towards PDA cells. In addition to VSV-wt, we tested two additional VSV variants: VSV- Δ M51-GFP and VSV-p1-GFP (Figure 22), with a particular focus was on VSV- Δ M51-GFP [98]. Several previous studies showed that VSV mutants with the deletion of methionine at position 51 (Δ M51) of the matrix (M) protein exhibited good oncolytic potential but lack undesirable neurotoxicity [95, 98, 197, 208-210]. A similar phenotype was recently demonstrated for VSV-p1-GFP [98]. To evaluate the relative efficacy of VSV as an OV, we compared VSV variants to four other viruses: SeV-GFP, RSV-GFP, CRAd-dl1520, and CRAd-hTERT (Figure 22). SeV-GFP and RSV-GFP are also NNS RNA viruses shown to have oncolytic potential [211-216], while CRAds have shown some success in several PDA cell lines in vitro and in vivo [181-183], although they have not been tested in most of the PDA cell lines used in this study. The inclusion of additional viruses would also help to discriminate between a virus-specific and general resistance phenotype if any PDA cell lines were identified as non-permissive to VSV.

To analyze the ability of viruses to kill cancer cells, PDA cell lines were infected at either a low MOI (0.01 CIU/cell) or a higher MOI (1.0 CIU/cell) and at 5 d p.i. an

MTT cell viability assay was performed. The MOI values for each virus/cell line combination are relative and calculated based on titration of all VSV variants and SeV on 4T1 cells, and RSV and CRAds on HeLa cells. These two reference cell lines (4T1 and HeLa) were selected based on their abilities to support robust replication of viruses used in this study. Therefore, for each MOI, the same amount of virus stock was added to each cell line. VSV-wt, VSV- Δ M51-GFP, and VSV-p1-GFP all caused significant death in the majority of cell lines at both high (Figure 23A) and low (Figure 23B) MOI compared to mock infected cells. In general, at the higher MOI, VSVs and CRAds caused more significant cell death than to SeV-GFP and RSV-GFP (Figure 23A). At the lower MOI VSVs caused more significant cell death compared to all other viruses including CRAds (Figure 23B).

Several PDA cell lines showed various degrees of resistance to oncolysis by VSVs, with HPAF-II, Hs766T, and BxPC-3 displaying the strongest resistance. Interestingly, we observed a substantial difference in the susceptibilities of HPAF-II, Hs766T, and benign HPDE cells to oncolysis with different VSV variants. These cell lines were effectively killed by VSV-wt (both MOIs) and VSVp1-GFP (HPAF-II at the high MOI only) at 5 days p.i. but were resistant to VSV- Δ M51-GFP, even at an MOI of 1. Importantly, all three PDA cell lines were also among the most resistant to other tested viruses, suggesting that general antiviral mechanisms may contribute to their phenotype (see below).

To analyze the kinetics of PDA cell death following VSV- Δ M51-GFP (Figure 24) or VSV-wt (data not shown) infection, cells were infected at MOI 0.001, 0.1 or 1 CIU/cell (Figure 24) and cell viability was analyzed at different time points. The majority

of cell lines had significantly decreased viability after infection with VSV- Δ M51-GFP at any tested MOI. Consistent with the data presented in Figure 23, HPAF-II, Hs766T, and BxPC-3 cells were most resistant to VSV-mediated cell death in the presence of any amount of VSV- Δ M51-GFP. CFPAC-1, HPAC, and benign HPDE cells were resistant to VSV- Δ M51-GFP only when infected at the lowest MOI (0.001)

Permissiveness of PDA Cell Lines to Viral Infection

The failure of OVVs to kill cancer cells can be explained by their inability to infect and/or replicate in these cells, although cellular defects in apoptosis may also be responsible for the defect in virus-mediated oncolysis. To determine whether variations in viral oncolysis observed between different PDA cell lines were due to different levels of permissiveness of these cell lines to virus infection, monolayer cultures of PDA cells were infected with serial virus dilutions. To test whether the differences between cell line levels of permissiveness to virus infection were specific for VSVs or general (e.g., if they have intact antiviral responses), we examined all viruses (Figure 22) except RSV. The infectious foci of VSV- Δ M51-GFP, VSV-p1- GFP, and SeV-GFP were analyzed by fluorescence microscopy at 24 (VSV) or 48 (SeV) h p.i. The number and size of viral plaques produced by VSV-wt, CRAd-dl1520, and CRAd-hTERT were analyzed by ICC as described in Materials and Methods. The virus permissiveness shown in Figure 25 is expressed as the ratio of the virus titer on the pancreatic cell line under study to the titer on a reference cell line (4T1 or HeLa), and higher numbers indicate greater permissiveness.

The degree of curvature in Figure 25 indicates that that the adenoviruses have less variability among PDA cells than VSV and SeV. Interestingly, while BxPC-3 and

Hs766T were resistant to all tested viruses, HPAF-II showed an intermediate permissiveness to infection by both adenoviruses (Figure 25; Figure 26 for CRAd-dl1520), although this PDA cell line was resistant to virus-mediated oncolysis by either CRAd (Figure 23). As shown in Figure 25, the majority of cell lines were highly permissive to VSV- Δ M51-GFP infection, with a relative ratio greater than or close to 1 ($\log_{10}=0$) (AsPC-1, SU.86.86, Capan-1, Panc-1, MIA PaCa2, Suit2, and Capan-2). In these cell lines, we observed rapid spread of VSV- Δ M51-GFP forming large infectious foci (filled circles in Figure 25; large GFP foci in Figure 26). Cell lines that were less permissive to VSV- Δ M51-GFP infection include benign HPDE cells (6.6 times less, with very small foci), as well as T3M4 (2.2 times less than 4T1), CFPAC-1 (3.8 times less), and HPAC (10 times less), all of which also formed smaller infectious foci at 16 h p.i. BxPC-3, HPAF-II, and Hs766T cells appeared highly resistant to VSV- Δ M51-GFP infection, with relative susceptibilities much less than that of 4T1 (62, 971, and 25,385 times less, respectively), and infectious foci were much smaller than those of all the other cell lines tested (Figure 26). VSV- Δ M51-GFP was also analyzed at 5 days p.i., when the majority of cell lines highly permissive to VSV- Δ M51-GFP infection was no longer viable and had detached from the culture plastic. However, HPAF-II, BxPC-3, and Hs766T cells remained attached to the plastic with decreased GFP intensity, again indicating that VSV- Δ M51-GFP infection is restricted in these cell lines (data not shown).

SU.86.86 showed a very intriguing phenotype by being highly permissive to VSVs and SeV, but resistant to both CRAd-dl1520 and CRAd-hTERT. To test whether this cell line may lack Coxsackievirus and adenovirus receptor (CAR) required for

adenovirus attachment (which would explain this phenotype) [181-183], we analyzed all PDA cell lines for CAR expression by flow cytometry and found that SU86.86 was the only cell line completely lacking CAR (Figure 27), while all other cell lines (including HPAF-II, Hs766T and BXPC-3 displaying general resistance phenotype) had varying but detectable levels of CAR (data not shown) which is in agreement with our data (Figure 25 and 26), indicating that these cell lines (unlike SU86.86) have reasonably good susceptibility to both adenoviruses and also suggesting that they are not defective in CAR expression. Although other factors may also contribute to the resistance of SU86.86 to CRAds, the lack of CAR expression alone might be sufficient to cause the phenotype.

To examine if reduced permissiveness to VSV- Δ M51-GFP also resulted in a decrease in new viral protein synthesis, lysates were prepared from uninfected cells and from cells infected with VSV- Δ M51-GFP at MOIs of 1 and 10 CIU/cell and harvested at 16 h p.i. Equal amounts of total protein were then examined by Western blotting for both VSV proteins and GFP expression. The expression levels of viral proteins within the different cell lines were in agreement with GFP expression (Figure 28). Protein expression (GFP level measurements are shown in Figure 28) was also generally consistent with cell line permissiveness and oncolysis, especially when protein accumulation levels were compared after lower-MOI infection. Viral protein expression was strongly reduced in BxPC-3, HPAF-II, Hs766T, and benign HPDE cells, which are the most “nonpermissive,” and all demonstrated small focus sizes when infected with VSV- Δ M51-GFP (Figure 25). Viral protein expression was also reduced in CFPAC-1 and HPAC cells, which had reduced permissiveness and medium focus sizes.

To directly examine the growth potential of VSVs in resistant cell lines, we tested all 3 VSVs in the majority of PDA cell lines (and in benign HPDE cells) using a standard one-step growth kinetics assay (Figure 29). In general, our data show that, while all tested cell lines were able to support productive replication of VSVs, the lowest production was observed in benign HPDE cells and in most PDA cell lines displaying a resistant phenotype. Also, most cells showed very similar growth kinetics for all 3 viruses, while HPAF-II supported a significantly lower level of VSV-M51-GFP production than other VSVs. This result may explain, at least partially, why HPAF-II cells were particularly resistant to VSV- Δ M51-GFP (Figure 23A). BxPC-3 cells showed a surprisingly high level of new particle production when infected at an MOI of 10. However, it is important to note that an MOI of 10, used for one-step growth kinetics, is never attainable during oncolytic treatment. The experiments on virus-mediated cell death shown in Figure 23 and 24 were conducted at more realistic MOIs of 0.001 to 1 (maximum).

Timing and Cellular Factors of Resistance of PDA Cell Lines to VSV- Δ M51-GFP

To analyze why PDA cells differ in their permissiveness to VSV- Δ M51-GFP, we looked at the early stages of virus replication and at cellular characteristics that could explain the observed differences.

Antigenome and VSV N mRNA synthesis was determined by northern blot of total RNA isolated at 4 h p.i. from cells untreated or treated with cycloheximide and infected with VSV- Δ M51-GFP at MOI 10 (Figure 28B and Table 1). Cycloheximide blocks new protein synthesis and thereby viral genome synthesis and secondary transcription. Expression of both VSV N mRNA and anti-genomic RNA were strongly reduced in BxPC-3, HPAC, HPAF-II, Hs766T and somewhat reduced in CFPAC-1 cells,

consistent with the reduced viral protein synthesis and permissiveness to VSV- Δ M51-GFP infection seen in these cells lines. Interestingly, RNA synthesis in “benign” HPDE cells was quite robust despite low protein synthesis 16 h p.i. (Figure 28A) and reduced permissiveness in this cell line, suggesting a block at a later stage of viral replication. In all cases where secondary transcription was reduced, primary transcription was reduced proportionately (Table 1). This suggests that in cell lines with lower mRNA synthesis, viral genome release into the cytoplasm was inhibited, and that for genomes that were released, early replication proceeded normally.

VSV is sensitive to Type I IFN responses. However, many different tumor types are known to lack these responses, allowing VSV to productively infect cancer cells while sparing healthy cells [193, 217]. Here, we wanted to test the hypothesis that the resistance of some PDA cell lines to VSV (and other viruses) was a result of their intact IFN responses. To determine if PDA cell lines were sensitive to Type I IFN, all cells were mock treated or treated with 5000 U/ml IFN- α for 24 h prior to infection with serial dilutions of VSV- Δ M51-GFP. A titer ratio for mock treated to IFN- α treated cells was determined for each PDA cell line (Figure 29). We observed that certain cell lines did not significantly suppress VSV- Δ M51-GFP replication in response to IFN- α . VSV- Δ M51-GFP titers were no more than 26-fold reduced following IFN treatment in Panc-1, SU.86.86, MIA PaCa2, and HPAC cells, while Capan-2, Hs766T, T3M4 and benign HPDE cells showed an intermediate sensitivity to IFN- α (Figure 31). HPAC displayed an interesting phenotype with comparable titers with or without IFN treatment; however, IFN treated HPAC cells required an additional day for visible foci to appear. Surprisingly, several PDA cancer cell lines were highly responsive to IFN- α (Capan-1,

AsPC-1, HPAF-II, BxPC-3, Suit2 and CFPAC-1). Among these IFN-sensitive cells are AsPC-1, Capan-1 and Suit2, which support robust replication of VSV- Δ M51-GFP in the absence of IFN- α pre-treatment.

To further study the role of IFN in the resistance of PDA cells to VSV, we examined the abilities of PDA cell lines to produce IFN alpha and/or beta in response to VSV- Δ M51-GFP infection (MOI of 10 CIU per cell) at 18 h p. i. As expected, significant amounts of IFN-beta were produced by benign HPDE cells, which are expected to retain normal antiviral responses (Figure 30). Importantly, all three cell lines (HPAF-II, HPAC and Hs766T) producing significant amount of IFN-beta at 18 h p.i. were among the most resistant cell lines (Figure 30). As illustrated in Table 2, except for BxPC-3, all PDA cell lines highly resistant to VSV show an HPDE-like phenotype characterized by both the production of IFN-beta and sensitivity to IFN treatment. In addition, our data experimentally explain the phenotypes AsPC-1, Suit2, and Capan-1 which are sensitive to IFN but support robust virus replication without added IFN, as they all are defective in IFN production. Interestingly, we were unable to detect any significant production of IFN-alpha in response to virus infection by any tested cell line at 18 h p.i. (data not shown), however it is produced later than IFN-beta. Future experiments will analyze PDA cells for production of various IFNs at different time points after infection.

Together, our data show surprising diversity among PDA cells in regards to their ability to produce and respond to Type I IFN. Moreover, we demonstrate that a combination of IFN sensitivity and IFN-beta production may be used to predict responsiveness of most PDA cells to oncolytic treatment.

Efficacy of VSV- Δ M51-GFP and CRAd-dl1520 in Nude Mice Bearing Human PDA Tumors.

To test the efficacy of VSV- Δ M51-GFP *in vivo* and to determine the relevance of our *in vitro* results to an *in vivo* situation, we chose four cell lines for *in vivo* testing based on our *in vitro* virus permissiveness and oncolysis experiments. MIA PaCa2 and Panc-1 are highly permissive to both VSV- Δ M51-GFP and CRAd-dl1520, SU.86.86 is highly permissive to VSV- Δ M51-GFP but not CRAd-dl1520, and HPAF-II has limited permissiveness to both VSV- Δ M51-GFP and CRAd-dl1520 (Figure 23-26). These human pancreatic cancer cell lines were injected subcutaneously into the right flank of male nude mice (n=18 per cell line). Once the mice developed palpable tumors (5-7 mm) they were divided equally into three groups (n=6). A control group received an IT injection of PBS, one group received an IT injection of 5×10^7 CIU VSV- Δ M51-GFP, and one group received an IT injection of 5×10^7 CIU CRAd-dl1520. The mice were monitored daily for signs of distress and tumor size was measured every other day for 14 days. VSV- Δ M51-GFP and CRAd-dl1520 had the greatest therapeutic effect in mice bearing Panc-1 and MIA PaCa2 tumors (Figure 33). VSV- Δ M51-GFP seemed to stabilize SU.86.86 tumor growth compared to treatment of SU.86.86 tumors with CRAd-dl1520 and PBS, which had no effect on tumor growth (Figure 33). SU.86.86 grew more rapidly than all other cell lines *in vivo* and several tumors became ulcerated over the course of the experiment (Figure 33). While mice bearing SU.86.86 tumors showed no signs of distress at any point during the experiment, several were euthanized at an earlier time point due to large tumor size (day 21 instead of day 25). Tumor growth continued in the presence or absence of VSV- Δ M51-GFP and CRAd-dl1520 for mice bearing HPAF-II tumors (Figure

33). In general, our in vivo experiments closely mimicked our in vitro results. Fourteen days post injection with VSV- Δ M51-GFP, CRAd-dl1520 or PBS, all mice were euthanized and tumors were harvested and wet weight and presence of virus was determined.

It has been demonstrated that VSV-wt can cause encephalitis in mice; however, VSV- Δ M51-GFP is a non-neurotropic OV [98]. In agreement with this, animals infected with VSV- Δ M51-GFP showed no signs of encephalitis or distress over the course of the experiment. Nevertheless, brain tissues of VSV- Δ M51-GFP-infected animals were analyzed for the presence of virus by standard plaque assay on BHK-21 cells with no VSV- Δ M51-GFP being detected. Interestingly, despite the robust oncolytic effect achieved for animals bearing Panc-1 and MIA PaCa2 following IT infection with VSV- Δ M51-GFP, when a similar analysis was conducted on tumor samples, only two samples (one SU.86.86 and one MIA PaCa2 sample) had detectable VSV- Δ M51-GFP present at 14 d p.i. (data not shown).

3.5 Discussion

In this study, we have evaluated for the first time VSV as an OV against pancreatic cancer cells. VSV variants showed superior oncolytic abilities compared to other viruses and were effective against the majority of the 13 tested human PDA cell lines. We also identified several cell lines highly resistant to oncolytic virotherapy by VSV and/or other tested viruses.

Among VSV variants, we focused primarily on VSV- Δ M51-GFP because several previous studies showed that VSV variants with Δ M51 mutation were effective OVs with no neurotoxicity in animals [95, 98, 197, 208-210]. To evaluate the relative efficacy of VSV as an OV, we initially compared VSV variants to four other viruses. We chose CRAd-dl1520 (also known as “ONYX-15”) as a relevant control for further in vitro and in vivo experiments, as this DNA virus is unrelated to VSV, has been tested in several clinical trials, and has shown some success in previous PDA studies [203, 218].

Our in vitro experiments indicated a great variability in permissiveness of PDA cell lines to all viruses. Overall, VSV variants were the most effective, but even for VSVs, some cell lines, including HPAF-II, Hs766T and CFPAC-1, were less effectively killed by VSV- Δ M51-GFP than by VSV-wt and VSV-p1-GFP. There are two major hypotheses explaining varying susceptibility of PDA cell lines to oncolysis by a particular virus in vitro. First, PDA cells may differ in their susceptibility to virus infection and their ability to support virus replication. This may happen because PDA cells may lack key cellular factors (e.g., receptors) required for successful virus infection and replication or because resistant cells have intact antiviral responses preventing successful virus replication. Alternatively, some PDA cells may have defective apoptotic

pathways, so that even if a virus can successfully infect and replicate in these cells, they are not efficiently killed by apoptosis.

The oncolytic potential of viruses is generally contingent on their ability to infect and replicate in these cells. In our study, PDA cell permissiveness to all viruses closely mirrored our cell death analysis, with several cell lines (HPAF-II, Hs766T and BxPC-3) showing varying degrees of resistance to all tested viruses. The six least permissive cell lines were all defective in cell killing for at least some of the MOIs tested. Five of these cell lines, BxPC-3, HPAF-II, HPAC, Hs766T and CFPAC showed low levels of early (4 h p.i.) viral RNA synthesis (including primary transcription of viral genome) when infected with VSV- Δ M51-GFP compared to the more permissive cell lines, indicating a possible defect at very early stage in replication, such as attachment, entry or endosomal escape. Experiments are underway in these PDA cell lines to further define the affected steps in viral replication and the responsible cellular mechanisms. In contrast to VSV-resistant PDA cell lines, in “benign” HPDE cells (also resistant to VSV), early viral mRNA and genome synthesis equaled that found in many permissive cell lines, but viral protein synthesis at 16 h p.i and virion production were sharply reduced, suggesting a defect at later stages of viral replication. This phenotype is expected for “benign” cells with intact innate antiviral responses.

To address differences in permissiveness to VSV in PDA cell lines, we also looked at their abilities to produce and respond to Type I IFN. . In general, many tumor cells are defective in producing Type I IFNs but may remain sensitive to Type I IFN, which could be produced by infected benign cells that surround the tumor. Still other tumor cells may retain the ability to produce their own IFN [176, 177]. Responsiveness of

cancer cells to IFN could be an important factor in predicting their behavior in vivo, where VSV infection would induce IFN production in surrounding healthy tissues, thus limiting oncolytic potential towards cancer cells sensitive to IFN. Our data showed surprising diversity among PDA cells in regard to their ability to produce and respond to Type I IFN (Table 2). With the exception of BxPC-3, all other VSV-resistant PDA cell lines were characterized by both the production of IFN-beta and sensitivity to IFN treatment. The same phenotype was shown by “benign” HPDE cells, which are expected to retain normal antiviral responses. The VSV-resistant phenotype of BxPC-3 in vitro (sensitive to IFN but does not produce IFN-beta) could be due to an IFN-independent block of virus replication. Interestingly, we identified some PDA cell lines (AsPC-1, Suit2, and Capan-1) that are responsive to IFN, but highly susceptible to infection in vitro (without added IFN) as they all are defective in IFN production. High heterogeneity in response to type I IFN has been reported in several other cancer types, including mesothelioma [219], melanomas [220, 221], lymphomas [222], bladder cancers [223], renal cancers [224], and likely in other types [209]. Our data suggest that a combination of IFN sensitivity and IFN-beta production may be used to predict responsiveness of most PDA cells to oncolytic treatment.

Together, our data suggest that VSV-resistant cell lines have more than one “defect” responsible for their virus-resistant phenotype. If their resistance was solely dependent on their intact IFN pathways, we would expect them to have a phenotype similar to that of benign HPDE cells. HPDE cells do not have any defects in early steps of VSV infection (demonstrated by “normal” RNA synthesis, including primary transcription of the viral genome at 4 h p.i.), but robust type I IFN responses inhibit

subsequent virus replication, resulting in very low protein accumulation at 16 h p.i. However, unlike HPDE cells, all PDA cell lines highly resistant to VSV also showed defective early viral RNA synthesis, suggesting that they have some defects inhibiting early steps of VSV infection (e.g., attachment or entry).

Most of our data show a correlation between the permissibility of PDA cells to VSV infection and its oncolytic potential. However, if cells are successfully infected at a high MOI (one-step infection), they are able to successfully produce new viral particles. BxPC-3 cells showed surprisingly high production of new particles when infected at an MOI of 10. Interestingly, it is also the only one of the most resistant cell lines that did not produce significant amounts of IFN- β (Figure 32 and Table 2). At the same time, BxPC-3 cells were characterized by deficient RNA synthesis at 4 h p.i., suggesting that BxPC-3 cells have some defects in virus attachment/ internalization or another early step in VSV infection. It also showed a low level of viral (and GFP) protein synthesis when BxPC-3 cells were infected at a lower MOI of 1 (Figure 28; compare AsPC1 and BxPC-3 at MOIs of 1 and 10). It is important to note that infection at an MOI of 10, used in Figure 29 for one-step growth kinetics, is never attainable during oncolytic treatment . The experiments on virus-mediated cell death shown in Figure 23 and 24 were conducted at more realistic MOIs between 0.001 and 1.

Previous studies have shown that many cancer cells are able to inhibit apoptosis to allow for prolonged proliferation [225]. As VSV has been shown to cause cell death by apoptosis via either the intrinsic or extrinsic pathway or both [99, 194, 226, 227], cell lines with decreased expression or activation of certain apoptotic proteins have the potential of limiting/delaying cell death following VSV infection. Furthermore,

differences in permissiveness to the VSV variants could be due to differences in their mechanisms of cell death induction. It has been demonstrated that VSV-wt induces apoptosis via the mitochondrial pathway due to wt M protein inhibiting gene expression, while VSV- Δ M51-GFP, with a mutant M protein, induces apoptosis primarily via the death receptor pathway [226]. While we cannot fully address these possibilities at this point, our preliminary experiments show significant increases in caspase-3 cleavage following VSV- Δ M51-GFP infection in all cell lines except Hs766T and HPAC at 17 h p.i. (data not shown). More studies are needed to determine whether reduced level of apoptotic response or the delayed induction of apoptosis in some of these cell lines plays a role in restricting VSV oncolysis. These defects could also (in addition to intact IFN pathways) explain why cell lines resistant to VSV are also resistant to other, unrelated, viruses.

Based on our in vitro studies we chose 4 cell lines with varying permissiveness to VSV- Δ M51-GFP and CRAd-dl1520 to determine if our in vitro studies are relevant in vivo. We observed in vitro that MIA PaCa2 and Panc-1 are highly permissive to both VSV- Δ M51-GFP and CRAd-dl1520, SU.86.86 is highly permissive to VSV- Δ M51-GFP but not CRAd-dl1520, and HPAF-II has limited permissiveness to both. The induced tumors in nude mice showed the same permissiveness pattern as observed in vitro indicating in vitro testing can be used to identify cancers resistant to a particular virus. It is important to emphasize that the ability of a virus to kill cancer cells in vitro or even in vivo (in nude mice) would not guarantee its efficacy in cancer patients due to complex tumor microenvironments and compromised immune responses [175]. However, our data clearly show that if cells are resistant to viral oncolysis in vitro, it is highly unlikely that

they could be effectively eliminated *in vivo*, suggesting the importance of *in vitro* pretesting (when possible) in identifying virus-resistant cancers.

There are several important characteristics of VSV that in combination make it a more attractive candidate for PDA treatment than other tested viruses: (i) there are few, if any, restrictions to VSV attachment and entry, as it is believed not to be dependent on any host receptor in target cells; (ii) there is no preexisting immunity against VSV in humans; (iii) VSV is not considered a significant human pathogen, and several VSV mutants, including VSV- Δ M51-GFP and VSV-p1-GFP, are not neurotropic but retain their oncolytic activity; (iv) cellular uptake in many mammalian cell types occurs very rapidly, and there is no cell cycle dependency; (v) our comparative analysis here demonstrated that VSV variants showed oncolytic abilities superior to those of other viruses, and some cell lines that exhibited resistance to other viruses were successfully killed by VSV.

There are several potential options for virus-resistant cancer cells. Prescreening cells against an array of different OVs could identify the best option for treating a particular tumor. For example, VSV- Δ M51-GFP is more suitable than CRAds for treating PDAs similar to SU.86.86 cells which showed a complete lack of CAR expression required for adenovirus attachment (data not shown). In the cases where cells are less permissive to VSV- Δ M51-GFP than VSV-wt or VSV-p1-GFP (HPAF-II and Hs766T), the use of VSV-p1-GFP might be a better option, especially because this virus is also non-neurotoxic *in vivo*. Combination therapies have also demonstrated some success. Virotherapy in combination with chemotherapy can enhance the oncolytic effect compared to either treatment alone [228]. Treating tumors with more than one OV

(combined virotherapy) could also potentially lead to enhanced oncolysis [229].

Importantly, understanding the mechanisms and identifying potential biomarkers of resistance is critical for the development of prescreening approaches and individualized oncolytic virotherapy against PDA.

3.6 Figures

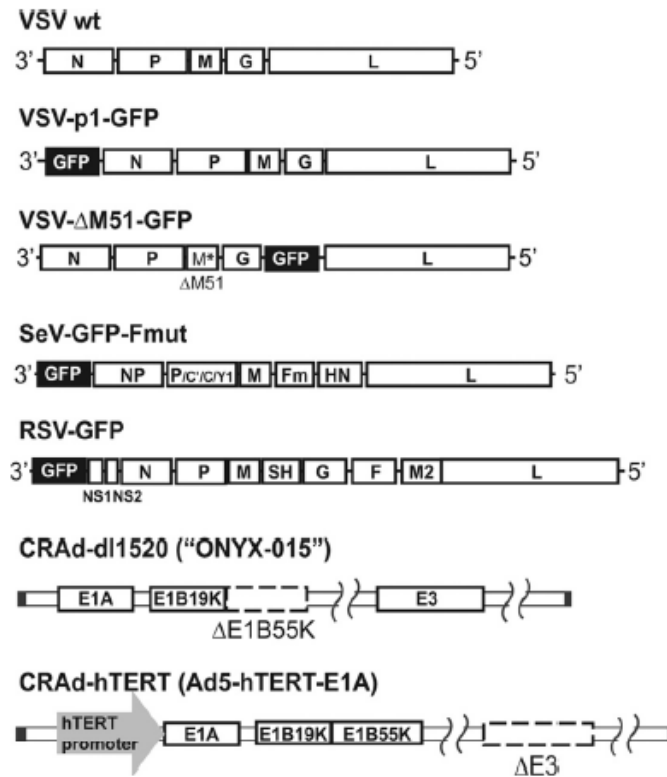


Figure 22: Viruses used in this study. VSV-p1-GFP has the GFP ORF inserted in position one of the viral genome resulting in attenuation of the virus. VSV- Δ M51-GFP has a deletion at amino acid position 51 of the matrix (M) protein reducing its ability to suppress host immunity. In addition, VSV- Δ M51-GFP has the GFP ORF inserted in position 5 of the viral genome. SeV-GFP has the GFP ORF inserted at position one of the viral genome and a mutation in the cleavage site of the fusion (F) protein allowing for F activation and production of infectious virus particles in cell without trypsin addition. RSV-GFP has GFP ORF inserted at position one of the viral genome. CRAd-dl1520 is attenuated by deletion of a large part of the coding sequence for the E1b55k viral gene product. CRAd-hTERT is a human telomerase reverse transcriptase (hTERT)-dependent CRAd.

3.6 Figures continued

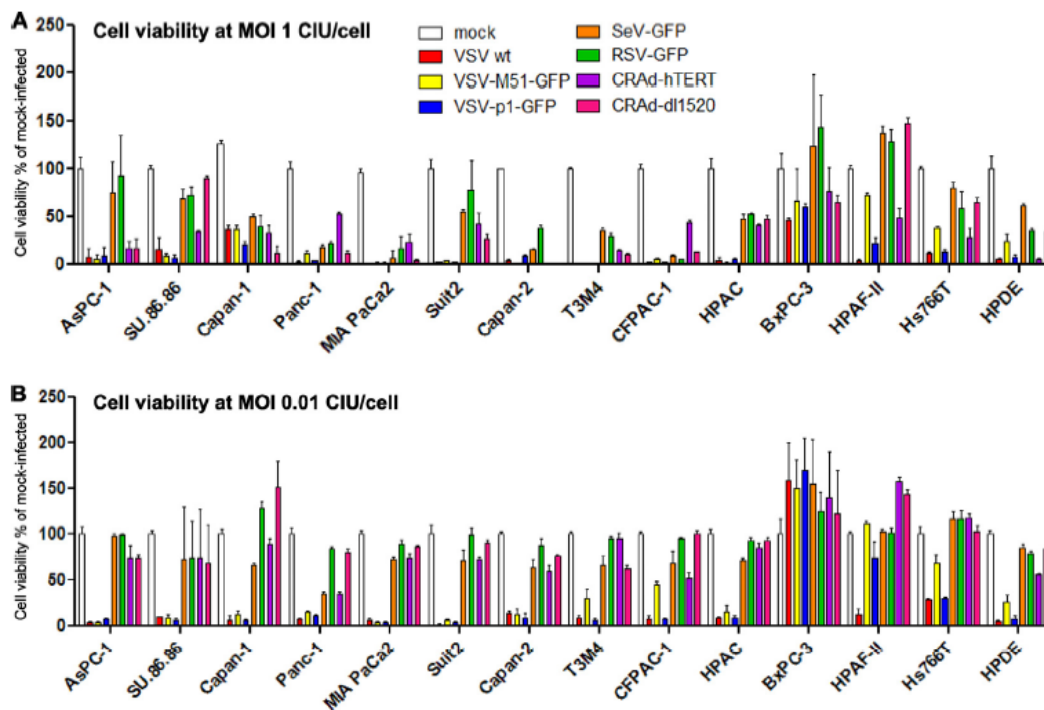


Figure 23: PDA cell viability following infection with viruses. PDA cell lines and HPDE were seeded in 96-well plates so that they reached 80% confluency at 24 h. The cells were infected with the indicated viruses at MOI of 1 (A) or 0.01 (B) CIU/cell or mock infected. Cell viability was analyzed at 5 d p.i. by an MTT cell viability assay and expressed as a ratio of virus-treated to mock-treated cells for each time point. All MTT assays were done in triplicate and the data represent the mean \pm standard deviation. Cell lines are grouped arbitrarily based on their susceptibility to virus-induced oncolysis.

3.6 Figures continued

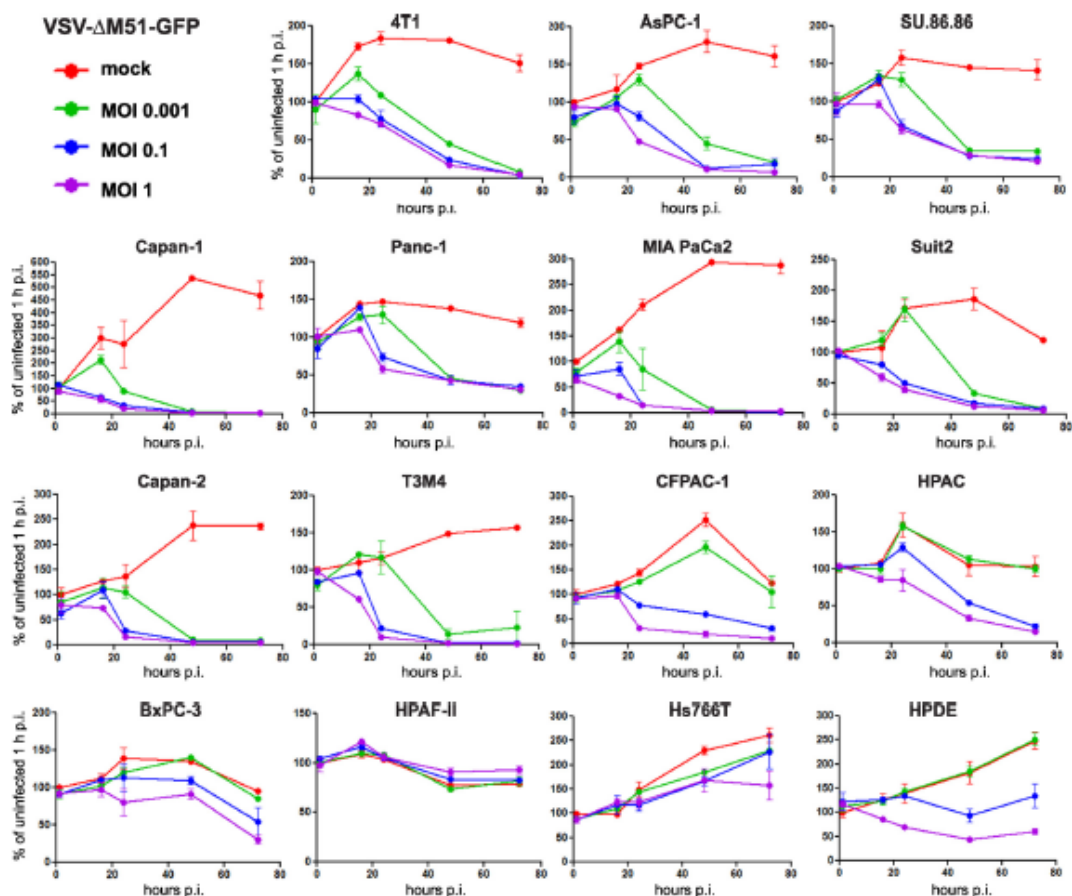


Figure 24: Kinetics of cytopathogenicity of VSV- Δ M51-GFP in PDA cells. Cells were seeded in 96-well plates so that they reached 50% confluence at 24 h. The cells were then mock infected or virus infected at low (0.001 CIU/cell), intermediate (0.1 CIU/cell), or high (1 CIU/cell) MOI. MTT cell viability assays were performed at 1, 16, 24, 48, and 72 h p.i. Cell viability is expressed as the percentage of mock-infected cells at 1 h p.i. All MTT assays were done in triplicate, and the data represent means and standard deviations.

3.6 Figures continued

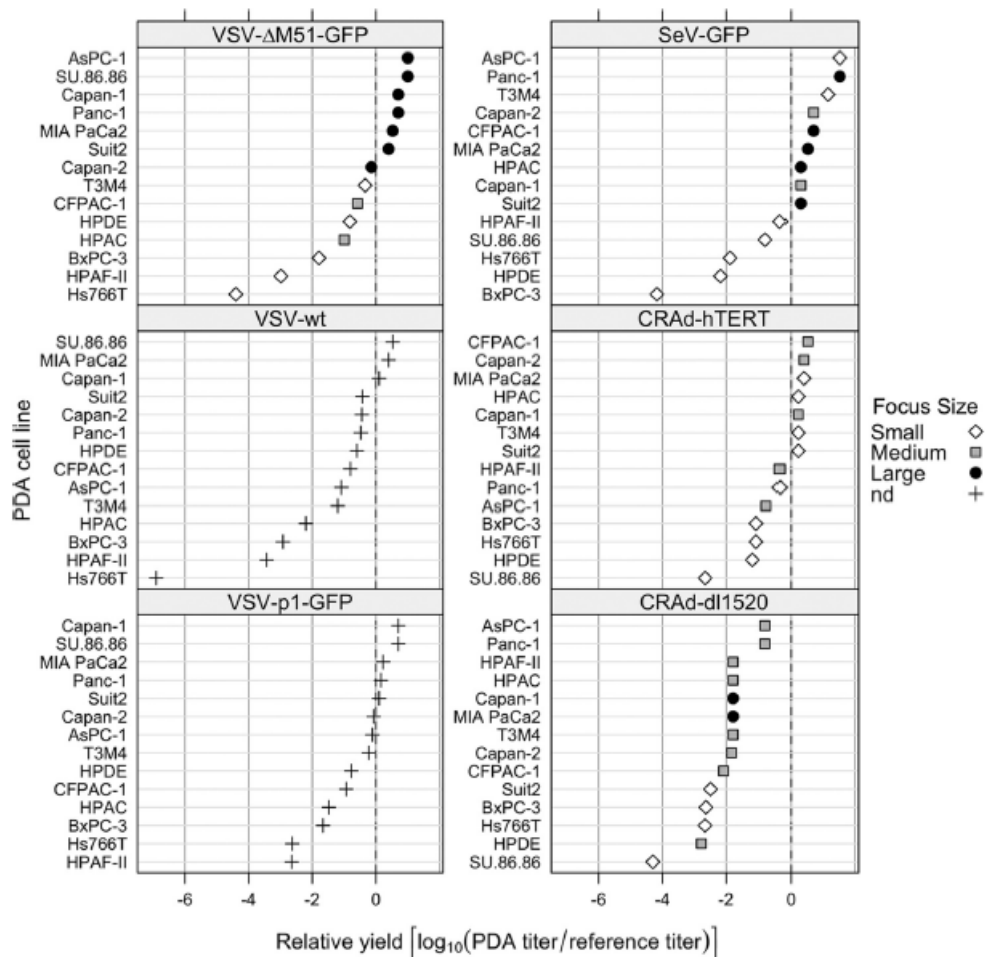


Figure 25: Permissiveness of PDA cell lines to different viruses. PDA cell lines and HPDE cells were incubated with serial dilutions of viruses. The infectious foci of VSV- Δ M51-GFP, VSV-p1-GFP (24 h p.i.), and SeV-GFP (48 h p.i.) were analyzed by fluorescence microscopy. The infectious foci of VSV-wt, CRAd-dl1520, and CRAd-hTERT were analyzed by ICC as described in Materials and Methods. Virus permissiveness (relative yield) is expressed as the \log_{10} of the ratio of the virus titer on the pancreatic cell line under study to the titer on a reference cell line (4T1 for VSV and SeV; HeLa for CRADs). The following titers were observed on reference cell lines: VSV-wt, 1.6×10^9 CIU/ml on 4T1; VSV- Δ M51-GFP, 3.3×10^8 CIU/ml on 4T1; VSV-p1-GFP, 3×10^7 CIU/ml on 4T1; SeV-GFP, 1.5×10^7 CIU/ml on 4T1; CRAd-hTERT, 1.5×10^7 CIU/ml on HeLa; and CRAd-dl1520, 4×10^8 CIU/ml on HeLa. A relative yield of 0 indicates that the PDA cell line and a reference cell line are equally permissive to the virus, while higher numbers indicate greater permissiveness for the PDA cell line. The area of infectious foci was analyzed using Image J software (NIH): small, area of <10 (surface area units); medium, area of 10 to 30; large, area of >30; nd, not done.

3.6 Figures continued

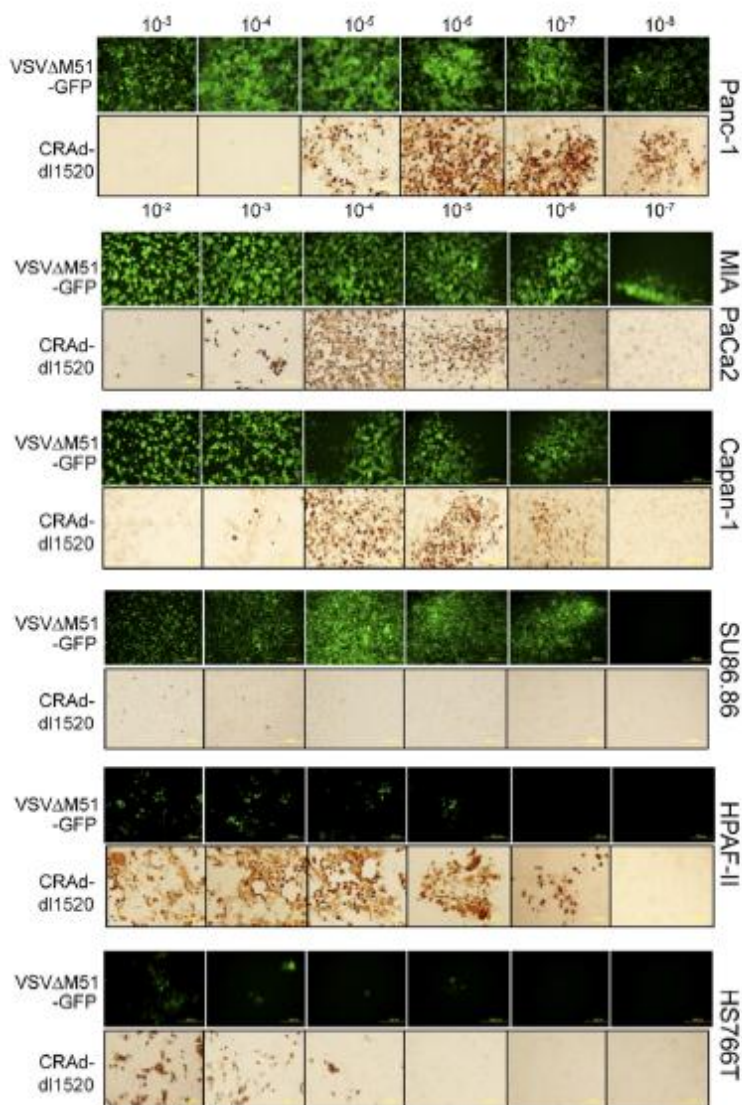


Figure 26: Permissiveness of selected PDA cell lines to virus infection. Representative PDA cell lines (not all shown) were incubated with serial dilutions of VSV-ΔM51-GFP and CRAd-dl1520. The infectious foci of VSV-ΔM51-GFP were analyzed by fluorescent microscopy at 24 h p.i. The infectious foci of CRAd-dl1520 were analyzed by ICC at 5 d p.i as described in Materials and Methods.

3.6 Figures continued

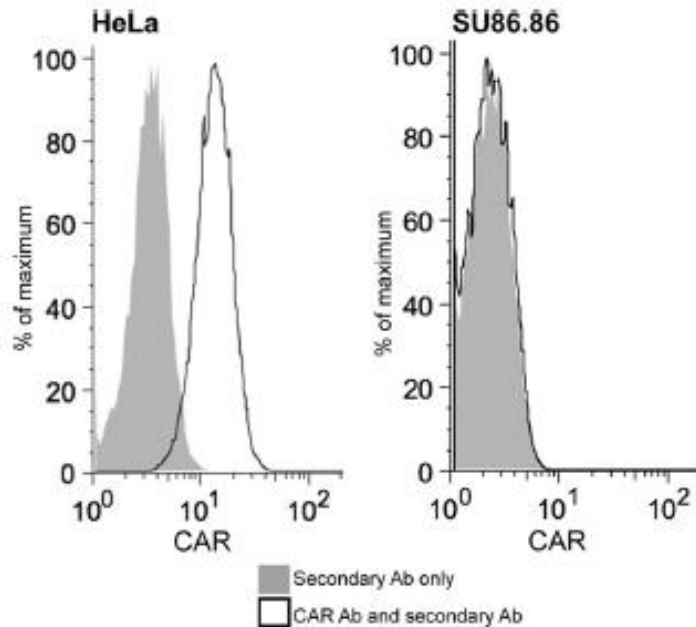


Figure 27: Surface expression of CAR. Single-cell suspensions of HeLa (positive control) or SU.86.86 (obtained without trypsin) cells were analyzed for adenovirus CAR using anti-CAR antibody and secondary IgG-FITC antibody (solid lines) or secondary IgG-FITC antibody only (gray areas). Expression of CAR was determined by flow cytometry (Beckman Coulter) and analyzed using FlowJo (Treestar, Ashland, OR) as described in Materials and Methods.

3.6 Figures continued

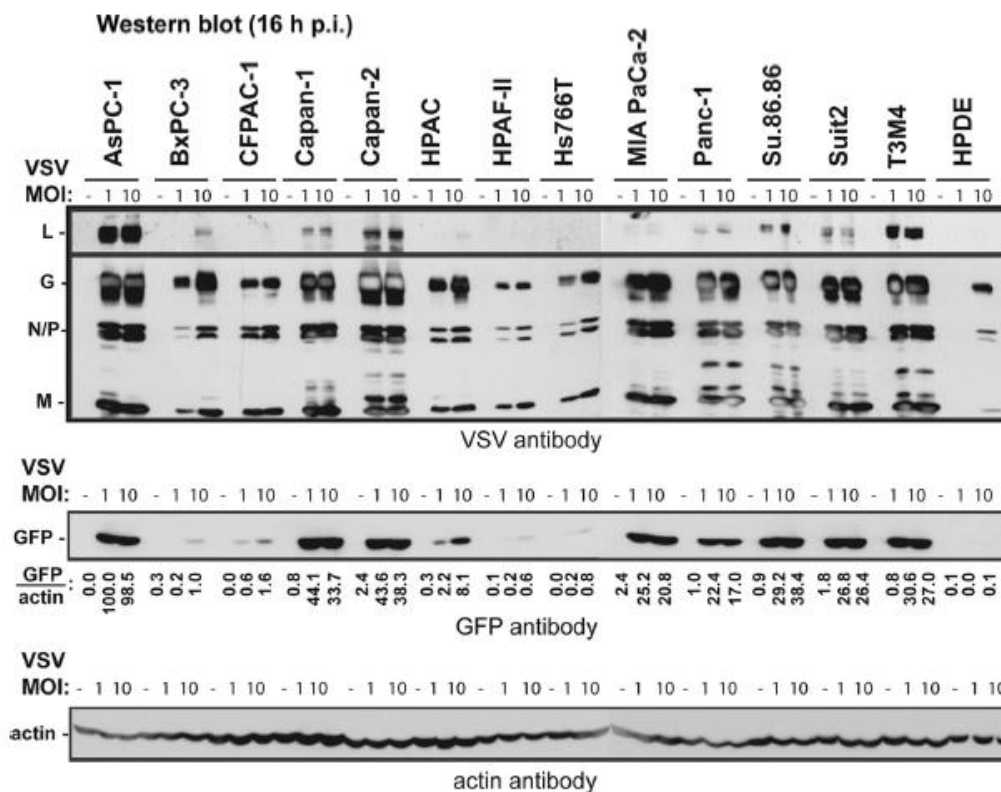


Figure 28: Analysis of viral protein accumulation in cells at 16 h p.i. Cells were mock infected or infected with VSV-M51-GFP at an MOI of 1 or 10 CIU/cell. The cells were harvested at 16 h p.i., and the cell lysates were analyzed by Western blotting for VSV proteins, GFP, or actin.

3.6 Figures continued

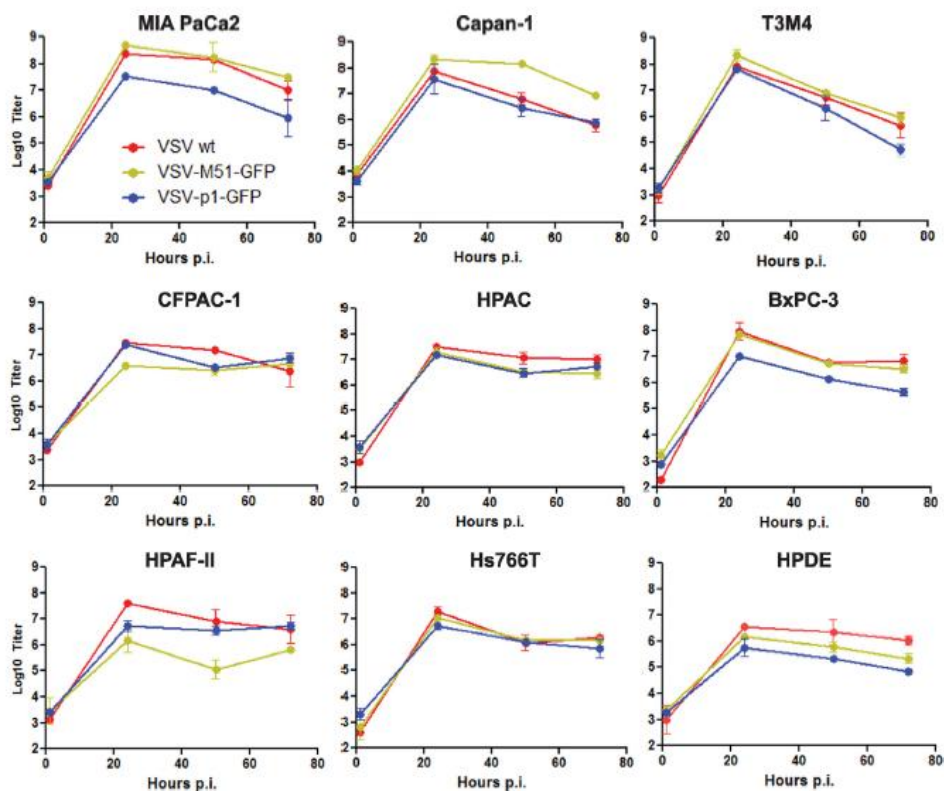


Figure 29: One-step growth kinetics of VSVs in PDA cell lines. PDA cells were infected with VSV-wt, VSV-_M51-GFP, or VSV-p1-GFP at an MOI of 10 CIU/cell, which was calculated based on the reference cell line 4T1. At 1 h p.i., the virus was aspirated and the cells were washed and overlaid with 5% growth medium. At 1, 24, 50, and 72 h p.i., the supernatant was collected, and virus titers were determined by plaque assay on BHK-21 cells. All infections were done in duplicate, and the data represent means \pm standard deviations.

3.6 Figures continued

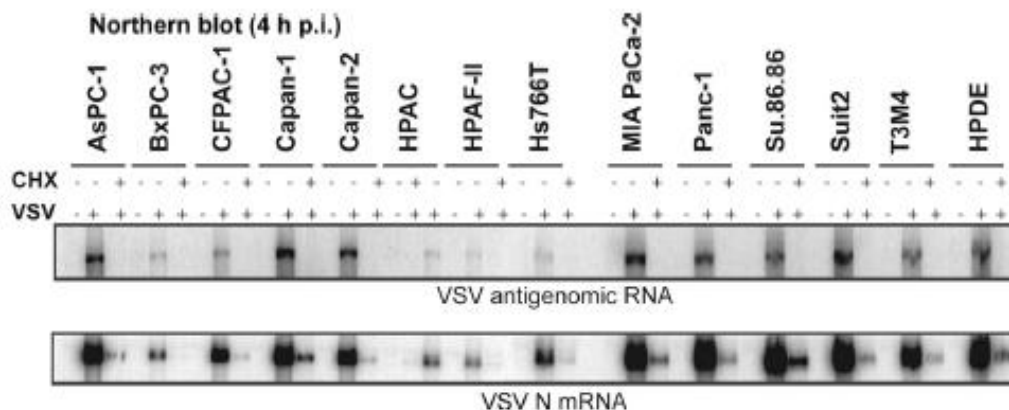


Figure 30: Early viral RNA levels in infected cells. Cells were mock treated or treated with 100 $\mu\text{g/ml}$ cycloheximide (CHX) for 30 min prior to mock infection or infection with VSV- $\Delta\text{M51-GFP}$ at an MOI of 10, and treatment was continued with CHX. At 4 h p.i., cells were collected, and total RNA was extracted and analyzed by Northern blotting for VSV antigenome RNA (top) or N mRNA (bottom).

3.6 Figures continued

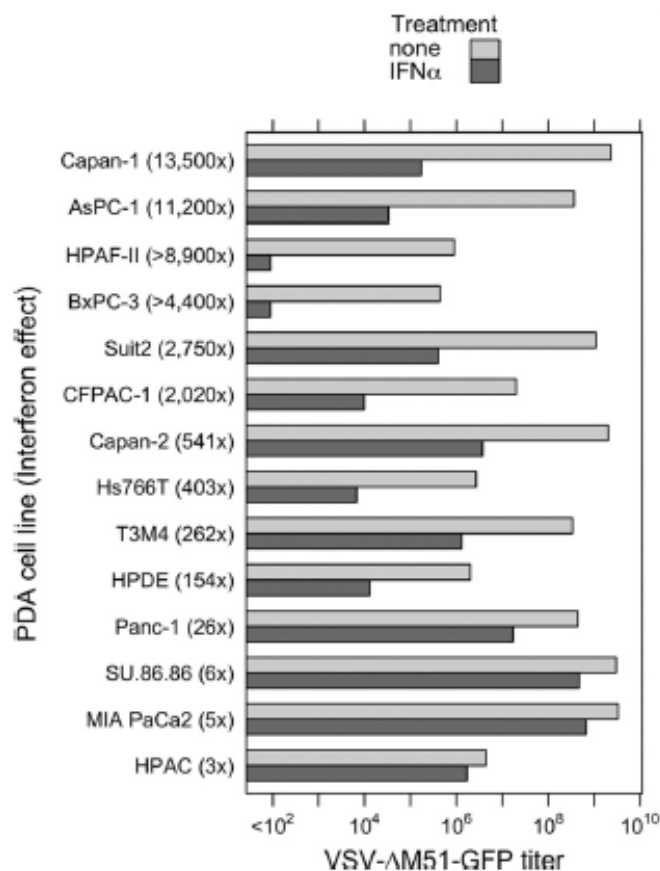


Figure 31: Type I interferon sensitivities of PDA cell lines. PDA cell lines and HPDE cells were either treated with 5,000 U/ml IFN- α in SFM or mock treated with SFM only. Twenty-four hours posttreatment, the cells were infected with serial dilutions of VSV- Δ M51-GFP, and infectious foci were analyzed 16 h p.i. by fluorescence microscopy to calculate the virus titer under these conditions. Treatments and infections were performed in duplicate, and average values are shown. For HPAC cells pretreated with IFN- α , virus-driven GFP signal was delayed by 24 h p.i.

3.6 Figures continued

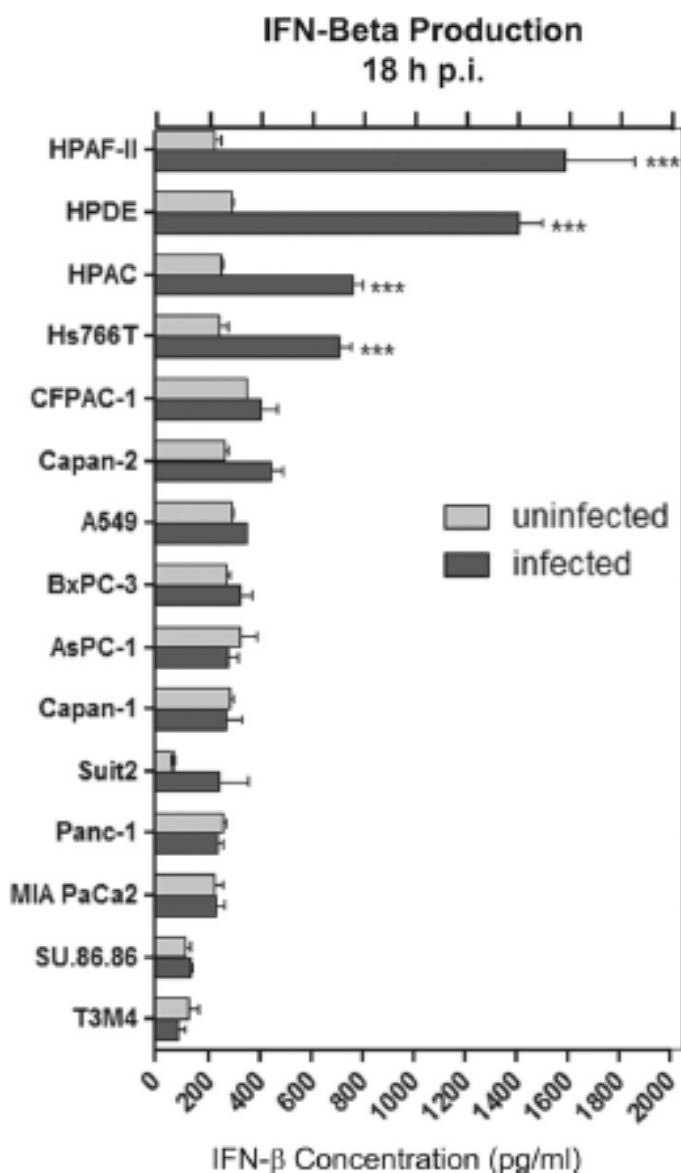


Figure 32: Type I interferon production by PDA cell lines. Cells were infected with VSV- Δ M51-GFP at an MOI of 10 CIU/cell or mock treated with SFM only. One hour p.i., the virus was aspirated and the supernatant was harvested and analyzed by ELISA for production of human IFN- β . Infections were performed in triplicate, and the data represent the means and standard deviations. Comparison of groups was done by using 2-way analysis of variance (ANOVA), followed by posttest for multiple comparisons (***, $P < 0.001$).

3.6 Figures continued

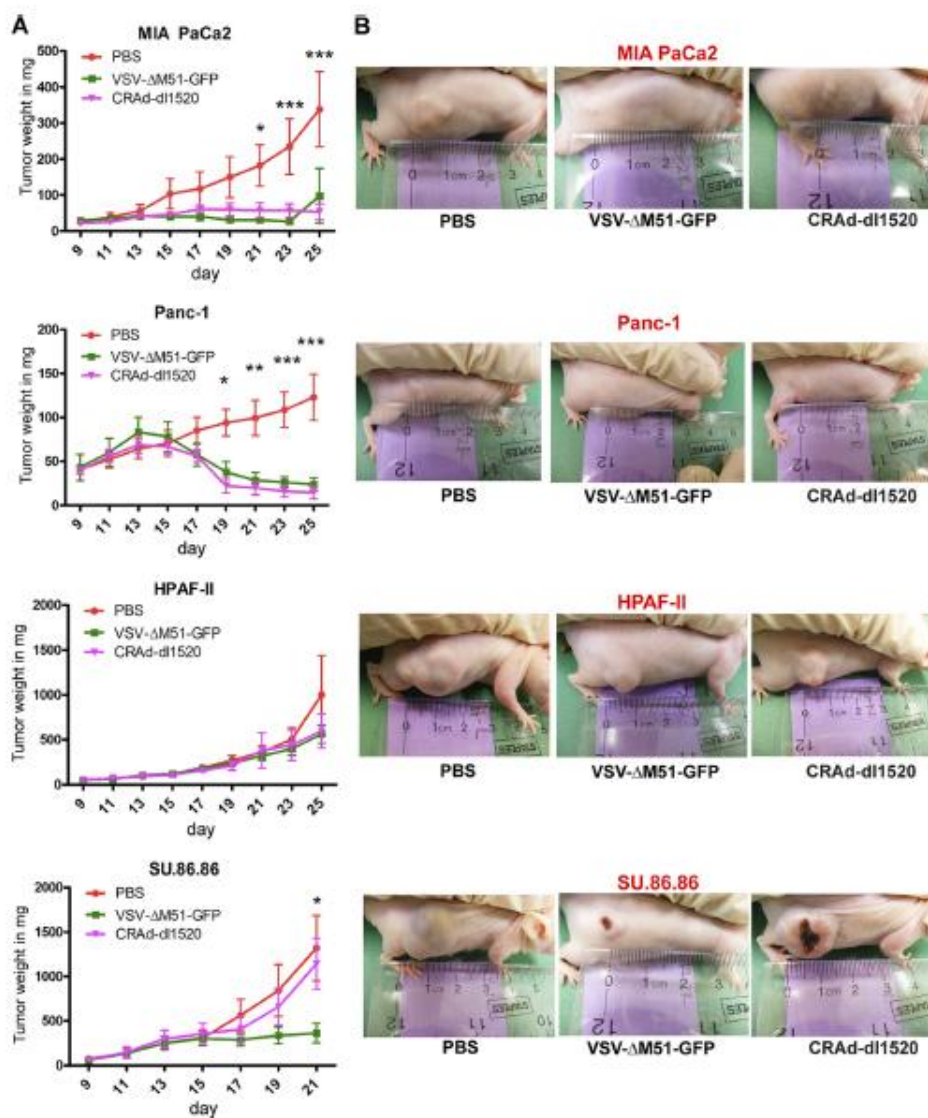


Figure 33: Efficacy of VSV-ΔM51-GFP and CRAd-dl1520 in nude mice bearing human PDA tumors. Six- to 8-week-old male athymic nude mice were subcutaneously injected with MIA PaCa2, Panc-1, HPAF-II, or Su.86.86 cells in the right flank ($n=18$ per group). Tumors were established by day 13, and the mice were randomly divided into 3 groups ($n = 6$ per group). One group served as a control and received one i.t. administration of 50 μ l PBS only. The other two groups were treated i.t. once with VSV-ΔM51-GFP or CRAd-dl1520 at a dose of 5×10^7 CIU in 50 μ l PBS. Tumor size was monitored by caliper measurements, and tumor weight was calculated according to the following formula: grams = (length in centimeters \times width²)/2. Comparison of groups was done by using 2-way ANOVA, followed by the Bonferroni posttest for multiple comparisons (*, $P < 0.05$; **, $P < 0.01$; ***, $P < 0.001$).

3.6 Tables

Table 1: Early viral RNA synthesis in cells infected with VSV-ΔM51-GFP.

Cell line	Primary TXN ^a	Total TXN ^b	Total TXN/primary TXN	Antigenome RNA ^c	Total TXN/antigenome RNA
AsPC-1	668	29,232	44	1,276	23
BxPC-3	37	1,517	41	40	38
CFPAC	172	10,911	63	230	47
Capan-1	1,728	31,394	18	2,205 ^d	14
Capan-2	249	14,807	59	1,401 ^d	11
HPAC	56	1,549	28	60 ^d	26
HPAF-II	27	899	34	18 ^d	49
Hs766T	181	3,891	22	86	45
MIA PaCa2	1,520	31,434	21	1,857	17
Panc-1	1,126	34,698	31	1,401	25
Su.86.86	5,162	46,195	9	1,428	32
SuII2	854 ^d	41,203 ^d	48	2,988 ^d	14
T3M4	378	14,363	38	1,051	14
HPDE	1,682	32,759	19	1,803	18

^a VSV N mRNA transcription (TXN) level 4 h p.i. in the presence of cycloheximide.

^b VSV N mRNA transcription level 4 h p.i. in the absence of cycloheximide.

^c VSV antigenome RNA synthesis level 4 h p.i. in the absence of cycloheximide.

^d The values are for RNA bands detected using a phosphorimager and quantitated using Image Quant software and are the averages of two independent repeats, except as indicated.

3.6 Tables continued

Table 2: Correlation between IFN sensitivity, production, and resistance of PDA cells to VSV

Cell line	IFN sensitivity (24 h p.i.) ^a	IFN- β production (18 h p.i.) ^a	<i>In vitro</i> resistance to VSV- Δ M51-GFP ^a
AsPC-1	+++	-	-
Su.86.86	-	-	-
Capan-1	+++	-	-
Panc-1	-	-	-
MIA PaCa2	-	-	-
Suit2	++	-	-
Capan-2	+	-	-
T3M4	+	-	-
CFPAC-1	++	-	++
HPDE	+	+++	+++
HPAC	-	+++	++
BxPC-3	+++	-	+++
HPAF-II	+++	+++	+++
Hs766T	+	+++	+++

^a + + +, high levels of IFN sensitivity, IFN production, or virus resistance; + +, intermediate levels of IFN sensitivity, IFN production, or virus resistance; +, low levels of IFN sensitivity, IFN production, or virus resistance; -, no detectible levels of IFN sensitivity, IFN production, or virus resistance.

CHAPTER 4: EFFICACY OF ONCOLYTIC VESICULAR STOMATITIS VIRUS IN AN IMMUNOCOMPETENT MODEL OF PANCREATIC DUCTAL ADENOCARCINOMA

4.1 Abstract

Development of new treatment strategies against pancreatic ductal adenocarcinoma (PDA) is necessary, as present therapies show little efficacy. Vesicular stomatitis virus (VSV) is a promising oncolytic virus (OV) with inherent anticancer abilities. Previously, we showed the abilities of VSV recombinants to kill a majority of tested human PDA cell lines *in vitro* and *in vivo* in athymic mice. However, VSV has never been studied in any immunocompetent PDA model where virus meets the challenge of host adaptive antiviral responses. Here we tested an oncolytic VSV recombinant VSV- Δ M51-GFP in an immunocompetent mouse system using xenografts of mouse PDA cell lines originated from mice with KRAS^{G12D}-driven PDAs either expressing human mucin 1 (MUC1, KCM cells) or null for Muc1* (KCKO cells). This system allows us to study oncolytic virotherapy in the context of MUC1 overexpression (approximately 80% PDA patients) or no expression. Our results demonstrate significant oncolytic abilities of VSV *in vitro* against both KCM and KCKO cells, although KCKO cells were more permissive to VSV- Δ M51-GFP. *In vitro* experiments with isogenic mouse PDA cells expressing human MUC1 or not demonstrates that MUC1 expression itself does not interfere with VSV- Δ M51-GFP infection or oncolysis. In agreement with our *in vitro* results, *in vivo* administration of live (but not killed) VSV- Δ M51-GFP

resulted in the significant growth reduction of KCKO or KCM tumors. However, tumor size reduction was transient and adaptive immunity may be responsible for the lack of a sustained anticancer effect as animals developed antibodies against VSV- Δ M51-GFP but not against the tumor cells. VSV- Δ M51-GFP efficacy was improved when animals were treated with the virus in combination with gemcitabine. The developed PDA system can be used to study combinational therapies involving other OVs, chemotherapeutics, and explore different routes of administration, with the goal of inducing tumor-specific immunity while preventing premature virus clearance.

*Human mucin 1 designated as MUC1 and mouse mucin 1 designated as Muc1

4.2 Introduction

Pancreatic cancer has the worst prognosis of all cancers and is estimated to be the fourth leading cause of cancer-related deaths in the United States [230]. According to the Pancreatic Cancer Action Network, It is projected that by 2015, pancreatic cancer will be the second leading cause of cancer related deaths. About 95% of pancreatic cancers are pancreatic ductal adenocarcinomas (PDAs), which are highly invasive with aggressive local growth and rapid metastases [178]. PDA is primarily driven by activating mutations in the *KRAS* proto-oncogene (most commonly a G12D point mutation), and is characterized by deregulation of several genes, including mucins [231, 232]. Mucin 1 (MUC1) is a membrane-tethered glycoprotein that is normally expressed on the apical surface of glandular epithelial cells. However, MUC1 is deregulated in a tumor setting such that it becomes overexpressed and aberrantly glycosylated in more than 80% of human PDAs and in 100% of metastatic lesions [231]. In human cancers, MUC1 has been shown to play an important role in development and progression of PDA [233].

Due to its typically late diagnosis, aggressive nature, and relatively few treatment options, PDA is designated as one of the most lethal abdominal malignancies [179, 180]. This is evidenced by an estimated 5-year survival rate of only 3 to 5%, and a median survival of only 5 to 6 months after initial diagnosis [230, 234]. To date, surgery remains the only potential cure for PDA, of which only 20% of patients are eligible due to presenting with advanced disease at time of diagnosis. Alternative therapies, such as radiation therapy and chemotherapy have shown little efficacy, as pancreatic cancer has been shown to exhibit an unusual resistance to these current treatment options. Thus, the development of new treatment strategies against PDA is of utmost importance.

Oncolytic virus (OV) therapy is an emerging therapeutic approach largely based on defects in the innate immunity of cancer cells or other abnormalities that increase cancer cell susceptibility to infection and death compared to healthy cells. Vesicular stomatitis virus (VSV), a prototypic non-segmented, negative-strand (NNS) RNA virus, has been tested against an array of cancers and is currently in a phase I clinical trial against hepatocellular carcinoma [235]. Undesirable natural neurotoxicity of wild-type (wt) VSV has been addressed by the generation of various VSV-based recombinants retaining their oncolytic activities but lacking neurotoxicity [235]. One of such oncolytic recombinants, VSV- Δ M51-GFP, has a deletion of the methionine at amino acid position 51 of the VSV matrix (M) protein, as well as the GFP ORF inserted in position 5 of the viral genome [236]. This Δ M51 mutation prevents VSV M protein's ability to shut down cellular gene expression allowing virus to evade host anti-viral response. Therefore, VSV- Δ M51-GFP is unable to successfully replicate in healthy cells with an intact type I interferon (IFN) response. However, as most cancer cells are believed to have defective type I IFN signaling, they are more susceptible to VSV infection.

Previous research from our lab analyzed several VSV recombinants in an array of human PDA cell in vitro [237, 238] and in xenografts in athymic mice [237]. While these studies provide important information regarding the abilities of OVs to infect and kill various human PDAs, the complex nature of the PDA microenvironment in immunocompetent animals is known to generate additional challenges for viruses, mainly the premature elimination of viruses before they complete their task. Here, VSV was evaluated for the first time in an immunocompetent mouse PDA model that use xenografts of murine PDA cells originated from KC mice with spontaneous KRAS^{G12D}-

driven PDAs either expressing human MUC1 (KCM cells) or MUC1 null (KCKO cells).

This system allows for study of VSV and other OVVs in the context of MUC1 overexpression (approximately 80% PDA patients) or no expression. Moreover, we examined VSV- Δ M51-GFP in combination with gemcitabine, the standard drug for pancreatic cancer.

4.3 Materials and Methods

Cell Lines and Culture.

KCM and KCKO cell lines were previously generated [239] from spontaneous PDA tumors from KCM and KCKO mice, correspondingly (Figure 34). Both cell lines were characterized previously [239]. To generate these mice, KC mice were first generated on the C57BL/6 background by mating the P48-Cre with the LSL-KRAS^{G12D} mice [159]. They were further mated to the MUC1.Tg mice to generate KCM mice or to the MUC1KO mice to generate KCKO mice. Cell lines are designated KCKO for those cells completely lacking Muc1 and KCM for those cells expressing mouse Muc1 and human MUC1. Panc02-Neo (transfected with neomycin empty vector) and Panc02-MUC1 (expressing full length human MUC1) murine pancreatic cancer cells were a gift from Dr. Tony Hollingsworth [240]. Panc02 was transfected with pH β APr-1-neo expression vector containing a human MUC1 cDNA. Cloned cells with constitutive MUC1 expression were selected for use [241]. In addition, the following cell lines were used to grow viruses and/or as controls for viral replication: CFPAC-1 (human PDA, ATCC CRL-1918), 4T1 (murine mammary carcinoma, ATCC CRL-2539), BHK-21 (Syrian golden hamster kidney fibroblasts, ATCC CCL-10) and Vero (African green monkey kidney cells, ATCC CCL-81). KCM, KCKO, Panc02-MUC1, Panc02-Neo, CFPAC-1, and 4T1 were maintained in Dulbecco's modified Eagle's medium (DMEM, Cellgro). BHK-21 and Vero were maintained in modified Eagle's medium (MEM, Cellgro). All cell growth media were supplemented with 9% fetal bovine serum (FBS, Gibco), 3.4 mM L-glutamine, 900 units (U) per ml penicillin and 900 μ g/ml streptomycin (Cellgro). MEM was further supplemented with 0.3% glucose (w/v). Cells were kept in a

5% CO₂ atmosphere at 37°C. For all experiments, cell lines were passaged no more than 10 times.

Flow Cytometry.

Single-cell suspensions were obtained by detaching cells using cell scrapers without trypsin to avoid any potential proteolytic effect of trypsin on surface proteins. The cells were then incubated with Fc block (BD Biosciences) at a concentration of 0.5 µg/ml at room temperature (RT) for 10 min. The cells were stained for the extracellular domain of human MUC1 using HMFG2, for 15 minutes (min) at 4°C, washed, and subsequently stained with goat anti-mouse IgG-phycoerythrin (PE) or isotype control (Santa Cruz; 0.5 µg/ml) for 15 min at 4°C. Expression of MUC1 was determined by flow cytometry (Beckman Coulter) using FlowJo (Treestar, Ashland, OR).

Western Blot.

Cellular lysates were prepared by scraping cells followed by centrifugation at 1,000 rpm for 10 min at 4°C. Cells were re-suspended in phosphate-buffered saline (PBS, Mediatech, Inc.) followed by centrifugation at 1,200 rpm for 5 min at RT. Cell pellets were lysed in buffer (pH 7.5) containing 1% Triton-X-100, 20 mM Hepes, 0.15 M NaCl, 2 mM EDTA and supplemented with 8% Complete Mini Protease Inhibitor Cocktail Tablets (Roche, Cat. No. 11836153001) and 1% Phosphatase Inhibitor Cocktail 2 (Sigma-Aldrich, Cat. No. P5726). Samples were sonicated then spun down in a centrifuge at 13K rpm for 10 min at 4°C. Supernatants were transferred to new tubes and total protein concentration was determined by Bradford assay (BIO-RAD). Twenty-five µg of total protein was separated by electrophoresis on 12% or 7.5% SDS-PAGE, then transferred to polyvinylidene difluoride (PVDF) membranes. Membranes were blocked

using 5% non-fat powdered milk in TBS-T [0.5 M NaCl, 20 mM Tris (pH 7.5), 0.1% Tween 20]. Membranes were incubated with 1:2000 Armenian hamster monoclonal anti-human or mouse MUC1 cytoplasmic tail (CT2) [242], or 1:2000 mouse HMFG2 monoclonal anti-human MUC1 [243] antibodies in 1% of 2% sodium azide. Detection was with 1:4000 goat antibody against Armenian hamster (Santa Cruz, Cat. No. SC-2443) or 1:4000 goat anti-mouse (Jackson-ImmunoResearch, Cat. No. 115-035-003) horseradish peroxidase-conjugated secondary antibodies using the Enhanced Chemiluminescence Plus (ECL+) protein detection system (GE Healthcare). Membranes were re-probed with mouse anti-actin antibody (clone C4) to verify sample loading {Moyer, 1986/8 #1269}.

Immunofluorescence.

Cells were seeded in borosilicate glass chamber slides (Labtek, Cat. No. 155411) as to be approximately 30% confluent in 24 h. Cells were washed with PBS then fixed with 3% paraformaldehyde (PFA) (Sigma) for 15 min. Cells were permeabilized with a solution containing 20mM HEPES (pH 7.5), 300mM sucrose, 50mM NaCl, 3mM MgCl₂, and 0.5% Triton X-100 on ice for 15 min. Cells were washed with PBS then incubated with 5% bovine serum albumin (BSA, Sigma) blocking solution in PBS for 30 min. Blocking solution was removed and cells were incubated with primary 1:100 HMFG2 antibody in BSA at 4°C overnight, rocking. Cells were washed with PBS then incubated with secondary 1:100 anti-mouse-fluorescein isothiocyanate (FITC) antibody (Santa Cruz, Cat. No. 2010) in BSA wrapped in foil for 2 h at RT. In the dark, cells were washed with PBS then stained with 1 µM Hoescht for 5 min at RT. Cells were washed with PBS then stored in PBS at 4°C or used for confocal imaging.

Viruses.

VSV- Δ M51-GFP recombinant is a gift from Jack Rose[98] (Yale University). VSV- Δ M51-GFP is a derivative of VSV (Indiana serotype) and has a deletion at amino acid position 51 of the M protein, as well as the GFP ORF inserted in position 5 of the viral genome [98]. VSV- Δ M51-GFP has been shown to retain its oncolytic activities while lacking neurotoxicity in vivo [98]. VSV- Δ M51-GFP stocks were prepared using BHK-21 cells infected at a multiplicity of infection (MOI) of 0.005 and incubated at 37°C in MEM media containing 5% FBS, 3.4 mM L-glutamine, 900 U/ml penicillin and 900 µg/ml streptomycin (Cellgro). Virus containing media was collected at 24 h post infection (p.i.) and centrifuged at 3000 x g for 10 min at RT to remove large cellular debris. Virus was purified by the method of Kalvodova et al (2009), with slight modifications[244]. In brief, clarified supernatants were underlayered with 5 ml 20% (w/v) sucrose in HEN buffer (10 mM HEPES pH 7.4, 1 mM EDTA, 100 mM NaCl) and centrifuged at 28K rpm for 3.5 h at 4°C in a Beckman SW32 Ti rotor. The resulting viral pellet was resuspended in HEPES buffered saline (HBS), pH 7.5 [21 mM HEPES, 140 mM NaCl, 45 mM KCl, 0.75 mM Na₂HPO₄, 0.1% (w/v) dextrose] and left at 4°C overnight then centrifuged in a 7.5 - 27.5% continuous gradient of Optiprep (Axis Shield) in HBS at 26.5k rpm for 30 min at 4°C using a Beckman SW40 Ti rotor. The virus containing band was collected from the gradient, diluted with ET buffer (1 mM Tris-HCl pH 7.5, 1 mM EDTA), pelleted by centrifugation at 27K rpm for 1.5 h at 4°C using a Beckman SW40 Ti rotor then resuspended in PBS.

VVT7 was created by integration of the bacteriophage T7 RNA polymerase gene into the vaccinia virus (strain Western Reserve) thymidine kinase gene [245]. VVT7 and

herpes simplex virus type 1 (HSV-1) (MacIntyre strain; ATCC, VR-539) were grown on Vero cells. HSV-1 viral stocks and infections were prepared and performed as described in [246]. VVT7 viral stocks were prepared using Vero cells infected at MOI 0.05. At 3 days p.i., cells were collected by gentle scraping, pelleted by centrifugation, resuspended in PBS, disrupted by 2 freeze/thaw cycles followed by brief sonication, and centrifuged at 1100 x g for 10 min at 4°C. The resulting supernatant was layered onto a cushion of 36% sucrose in 10 mM Tris (pH 8.0) and centrifuged at 18K rpm for 80 min at 4°C using a Beckman SW40 Ti rotor. The resulting viral pellet was resuspended in 1mM Tris (pH 8.0), homogenized using a Duall homogenizer, then centrifuged in a 25-40% continuous sucrose gradient in 10 mM Tris (pH 8.0) at 13.5K rpm for 40 min at 4°C using a Beckman SW40 Ti rotor. The virus containing band was collected by insertion of a syringe needle through the side of the tube, diluted with 1 mM Tris (pH 8.0), pelleted by centrifugation at 13.5K rpm for 40 min at 4°C using a Beckman SW40 Ti rotor then resuspended in 1 mM Tris (pH 8.0).

Cell Viability Following Infection with Different Viruses.

Cells were seeded in 96-well plates so that they reached approximately 80% confluence at 24 h then infected with VSV- Δ M51-GFP at a multiplicity of infection (MOI) of 0.001, 0.1, or 1 CIU (cell infectious units) per cell (based on their titration on 4T1 cells) or mock infected in serum free media (Hyclone, SFM4MegaVir). For HSV-1 or VVT7, cells were infected at MOI of .001, 0.1, or 1 CIU per cell (based on their titration on Vero cells) or mock infected in SFM. One h p.i., the virus containing media was aspirated and replaced with growth medium containing 5% FBS. Cell viability was analyzed every 24 h for 5 days p.i. by a 3-(4,5-dimethyl-2-thiazolyl)-2,5-diphenyl-2H-

tetrazolium bromide (MTT) cell viability assay (Biotium) in accordance with manufacturer instructions. Virus replication was measured by GFP fluorescence readings every 24 h p.i. for 5 days (CytoFluor Series 4000, filter 450/50nm, Perseptive Biosystems).

Type I Interferon Sensitivity and Production.

Cells were seeded in 24-well plates so that they reached approximately 80% confluence at 24 h. For type I interferon sensitivity, the cells were mock treated or treated with 5,000, 15,000, or 30,000 U/ml human alpha interferon (IFN- α) (Calbiochem, Cat. No. 407294) contained in growth media. Twenty-four hours post treatment, the cells were infected with serial dilutions of VSV- Δ M51-GFP, and infectious foci were analyzed 16 h p.i. by fluorescence microscopy. Treatments and infections were performed in duplicate.

One-step Virus Growth Kinetics.

Cells were seeded in 96-well plates to reach confluence at 24 h. Cells were infected for 1 h at 37°C with VSV- Δ M51-GFP at an MOI of 10 CIU/cell based on the cell line specific MOIs (KCM: 6.25×10^6 , KCKO: 1.57×10^8 , Panc02.MUC1: 6.7×10^7 , and Panc02.Neo: 1.51×10^8) (tested in duplicate). At 1 h p.i., virus was aspirated and cells were washed twice with PBS (to prevent carryover of virions) then overlaid with growth medium containing 5% FBS. At 1, 24, 50, and 72 h p.i., supernatant was collected from the wells and flash frozen at -80°C. Virus titers were later determined by plaque assay analysis. BHK-21 cells were incubated with serial dilutions of the samples for 1 h. The virus was aspirated, and a growth media with 5% FBS-1% Bacto Agar overlay was applied to limit virus spread. Infectious foci were counted by fluorescence microscopy at 16 h p.i.

Plaque Reduction Neutralization Test.

BHK-21 cells were seeded in 96-well plates to reach confluence in 24 h. Mouse sera was first diluted 1:5 then serially 1:2 to make dilutions ranging from 1:20 to 1:40960 for analysis. VSV- Δ M51-GFP stock diluted 1:32,000 (a dilution determined to produce approximately 50 infectious foci per well) was incubated with the sera dilutions for 1 h at 37°C, with rocking. Sera/virus dilutions were then used to infect cells, with rocking every 10 min for 1 h at 37°C. Sera/virus dilutions were removed and a growth media with 5% FBS and 1% Bacto Agar was overlaid to limit virus spread. Infectious foci were counted by fluorescence microscopy at 16 h p.i. Antibody dilution titers were calculated as the inverse of the sera dilution resulting in half the number of plaques when compared to VSV- Δ M51-GFP alone. All sera samples were tested in triplicate.

Detecting Antibodies Generated Against KCM cells.

KCM cells were seeded in 96-well plates to reach confluence in 24 h. Cells were washed with PBS and fixed in 3% PFA for 15 min, followed by permeabilization for 15 min on ice with a solution containing 20 mM HEPES (pH 7.5), 300 mM sucrose, 50 mM NaCl, 3mM MgCl₂, and 0.5% Triton X-100. The cells were washed then blocked with 5% BSA in PBS for 20 min at RT then incubated with mouse sera dilution as prepared in section 2.9, without incubating with virus, overnight at 4°C. Cells were washed twice with PBS, incubated with peroxidase-conjugated goat anti-mouse IgG antibodies (1:300; Jackson ImmunoResearch) for 1 h. For detection, cells were washed three times with PBS then incubated with o-Phenylenediamine (OPD, Thermo Scientific) for 15 minutes. OPD was inactivated with the addition of 2.5 M sulfuric acid. Optical density was read at 490 nm. All sera samples were tested in triplicate.

In Vivo Treatment of Tumors with VSV- Δ M51-GFP.

Mice were handled and maintained under veterinary supervision in accordance with guidelines of the University of North Carolina at Charlotte Institutional Animal Care and Use Committee (IACUC) approved protocol. All cell lines used in animal experiments tested negative for an extended panel of pathogens by Charles River Laboratories. To treat animals containing KCM tumors with VSV- Δ M51-GFP and with or without gemcitabine, 16 to 18-week-old MUC1.Tg male mice were subcutaneously injected with the KCM cell line. MUC1.Tg mice express human MUC1 under its own promoter and display T and B cell tolerance to MUC1. These mice express MUC1 in a tissue specific manner and are not a model of overexpression [247]. MUC1.Tg mice tail clipped were collected when mice were approximately 11 days old. Genomic DNA was isolated and used to genotype the mice by polymerase chain reaction. For MUC1.Tg the primers were 5'-CTTGCCAGCCATAGCACCAAG-3' and 5'-CTCCACGTCGTGGACATTGATG-3' with a 341bp amplification product that was confirmed on 1% agarose gels [157]. The MUC1.Tg mice were originally developed by Dr. Sandra Gendler (Mayo Clinic Arizona) but are now bred and maintained in Dr. Mukherjee's laboratory. Based on preceding titration experiments (data not shown), mice were injected with 1×10^6 KCM (in 100 μ L of PBS) into the right flank of mice (n=29). Mice were palpated starting on day 5 post tumor injection (p.t.i.) then were randomly divided into 5 groups: PBS, VSV- Δ M51-GFP, killed VSV- Δ M51-GFP, VSV- Δ M51-GFP + gemcitabine, and gemcitabine alone (n=6 per group, n=5 for killed VSV- Δ M51-GFP). All mice were treated 5 days p.t.i. with either 50 μ L PBS or a single intraperitoneal (IP) injection of gemcitabine (50 mg/kg dissolved in 50 μ L PBS). On days 7, 9, and 11 p.t.i.,

the PBS and gemcitabine groups received intratumoral (IT) administration of 50 μ l PBS. The other groups received intratumoral (IT) administration of either VSV- Δ M51-GFP or UV killed VSV- Δ M51-GFP on days 7, 9, and 11 p.t.i. with a dose of 1×10^8 CIU in 50 μ l PBS (based on BHK-21 titer). Tumor size was monitored by caliper measurements every day until day 12 and every other day thereafter. Body weight was measured once weekly. Tumor weight was calculated according to the formula: grams = [(length in cm) x (width in cm)²]/2. Mice were sacrificed 18 days p.t.i, at which time, mice were not yet presenting with clinical signs indicating severe morbidity. To conduct survival study using VSV- Δ M51-GFP against KCKO and KCM tumors, 8 to 11-week-old MUC1.Tg male mice were subcutaneously injected with either KCM or KCKO cell lines. Mice were subcutaneously injected with 1×10^6 KCM or KCKO cells (in 100 μ L of PBS) into the flank (n=8 each). Mice were palpated starting at 5 days p.t.i. then were randomly divided into 2 groups per cell line (n=4 per group). One group per cell line served as a control and received IT administration of 50 μ l PBS only on days 8, 10 and 12 p.t.i. The other group received IT administration of VSV- Δ M51-GFP on days 8, 10 and 12 p.t.i with an initial dose of 5×10^7 CIU in 50 μ l PBS (based on A549 titer) followed by two doses of 3×10^7 CIU in 50 μ l PBS. Tumor size was monitored by caliper measurements every other day, and body weight was measured once weekly. Tumor weight was calculated according to the formula: grams = [(length in cm) x (width in cm)²]/2. Mice were sacrificed when length or width of the tumor reached 1.5 cm, or tumors became ulcerated, or mice were presenting with clinical signs indicating severe morbidity. Data were analyzed using GraphPad software and are expressed as mean \pm standard error mean. Comparison of

groups was done by two-way ANOVA only when the groups had the same number of animals (* $p < 0.05$, ** $p < 0.01$, *** $p < 0.001$).

Statistical Analysis Software.

All statistical analyses were performed using GraphPad Prism, version 5.0c for Mac OS X (GraphPad Software, San Diego, California).

4.4 Results

Susceptibility of KCM and KCKO to Viral Oncolysis.

A successful virotherapy is dependent first of all on the ability of the OV to infect and kill cancer cells. Therefore, we tested the susceptibility of murine PDA cell lines KCM and KCKO to VSV in vitro. The tractable in vitro system allowed us to address the permissibility of cancer cells to VSV-mediated cell death in a controlled manner. As described in Materials and Methods and illustrated in Figure 34, KCM and KCKO cell lines were originated from spontaneous mouse PDAs expressing or lacking human MUC1, correspondingly[248]. Using both KCM and KCKO cells allows for testing of VSV oncolytic virotherapy in the more clinically relevant context of MUC1 overexpression (approximately 80% PDA patients) or no expression. Previous comparative studies of KCM and KCKO cell lines demonstrated that KCM cells display a much more aggressive phenotype [233]. This was evidenced by an increase in invasiveness of KCM cells, an increase in proliferation, with a deregulation of the MAPK pathway[233], and increased drug resistance (unpublished data).

KCM cells express both murine and human MUC1 while KCKO cells lack MUC1 expression from either species. Expression phenotypes of the KCM and KCKO cell lines were analyzed using the HMFG2 antibody which targets sparsely glycosylated VNTR repeats of the human MUC1 extracellular domain. Using HMFG2 antibodies in flow cytometry (Figure 35A), immunofluorescence (Figure 35B), and Western blot (Figure 35C) analyses, we confirmed that KCM cells are positive and KCKO are null for MUC1 (Figure 35).

For our studies, a VSV- Δ M51-GFP recombinant was chosen based on previous experiments that demonstrate that mutation or deletion of methionine at position 51 (Δ M51) of the VSV M protein allows the virus to retain oncolytic ability without the neurotoxicity associated with wild type (wt) VSV [237, 249, 250]. In addition, the insertion of a GFP gene at position 5 of the VSV- Δ M51-GFP genome allows for monitoring of virus replication and spread based on VSV-driven GFP expression expression [98].

To analyze the ability of VSV- Δ M51-GFP to infect and kill KCM and KCKO *in vitro*, the cells were mock infected or infected at increasing MOIs^{BHK}: low (0.001 CIU/cell), medium (0.1 CIU/cell), or high (10 CIU/cell). The values for MOIs^{BHK} were calculated based on the titration of VSV- Δ M51-GFP on BHK-21 cells, which are exceptionally susceptible to VSV infection and replication[251]. Cell viability following virus infection was calculated using an MTT cell viability assay performed at 1, 24, 48, 72, and 96 h p.i. GFP fluorescence readings were taken at the same time points as MTT analysis (Figure 36A). For VSV at medium and high MOIs there was increased infection and killing of KCM and KCKO starting at 48 hours when compared to mock. A noticeable difference between KCM and KCKO was at the lowest MOI (0.001 CIU/cell), where KCM were resistant to virus-mediated cell death, while KCKO susceptibility was comparable to medium and high MOIs (Figure 36A). The MTT results were mirrored by GFP expression as robust fluorescence readings occur at all tested MOIs in KCKO cells, but only at medium and high MOIs in KCM cells.

To determine if early stages of infection are a potential rate-limiting step of the OV treatment, kinetic testing of virus replication was done to evaluate the production of

VSV- Δ M51-GFP progeny at different MOIs. In KCM and KCKO an MOI (0.001 CIU/cell) was chosen based on the difference seen in the MTT data. MOI (5 CIU/cell) was chosen as a median between the medium and high MOIs where similar patterns of cell viability and VSV- Δ M51-GFP GFP fluorescence were shown for both cell lines. After analysis of collected supernatant by plaque assay on BHK cells, similar VSV- Δ M51-GFP replication titers were seen in both cell lines at all time points (Figure 37B). These results highlight that the differences of susceptibility to VSV- Δ M51-GFP-mediated killing between KCM and KCKO occur at an unknown step in the virus life cycle. In addition, to determine if the results showing the ability of VSV- Δ M51-GFP to cause increased levels of cell killing in KCKO when compared to KCM were virus-specific, we tested the cells with two DNA viruses unrelated to VSV- Δ M51-GFP: human herpes simplex virus 1 (HSV-1) and vaccinia virus (a poxvirus, VVT7). The strains of HSV-1 and VVT7 used in these experiments are not OV, however recombinant versions are used for OV research (Figure 36A and 36B). KCM and KCKO were infected with either HSV-1 or VVT7 at MOI of .001, 0.1, or 1 CIU/cell (based on their titration on Vero cells. MTT assays were done for both viruses at the same time points as VSV- Δ M51-GFP and used for comparison of cell killing effect. HSV-1 and VVT7 displayed similar cell killing ability at most time points and MOIs for both KCM and KCKO. VVT7 appears to have a stronger oncolytic effect than HSV-1 on KCM and KCKO at medium and high MOIs at 120 hours. When compared to VSV- Δ M51-GFP, however neither HSV-1 or VVT7 show as strong of an oncolytic effect. There is a more pronounced oncolytic effect with VSV- Δ M51-GFP at all MOIs in KCM and KCKO from 48 h and afterward. This pronounced oncolytic effect of VSV- Δ M51-GFP justifies further exploration.

Our data show that at the lowest VSV- Δ M51-GFP MOI KCM cells are more resistant to VSV- Δ M51-GFP infection and killing than KCKO. Based on the known difference of MUC1 expression between the two cell lines, as well as known functions of MUC1 within the cell, it was important to address a potential role for MUC1 in resistance to VSV- Δ M51-GFP. However, it must be noted that while KCM and KCKO are MUC1 positive or null, respectively, there is no indication that the two cell lines are isogenic. Additional mutations that may have arisen during the cell line selection process could factor into the VSV- Δ M51-GFP resistant phenotype. To analyze the ability of VSV- Δ M51-GFP to infect and kill isogenic MUC1 positive, where the human MUC1 gene was inserted into an established cell line that express low levels of Muc1, testing was done with Panc02-MUC1 and Panc02-Neo, respectively[252, 253]. Immunofluorescence and Western blot analysis using HMFG2 antibody confirmed the presence or absence of human MUC1 in these cell lines (Figure 38 A and B). Additionally, MTT cell viability showed no differences in VSV- Δ M51-GFP cell killing ability between the two cell lines at all MOIs (Figure 38C). GFP fluorescence also showed similar patterns of expression at all time points regardless of MUC1 status (data not shown). Like KCM and KCKO, virus kinetics to evaluate the production of VSV- Δ M51-GFP progeny showed similar VSV- Δ M51-GFP replication titers in both cell lines at all time points (Figure 38D). These results do not definitively eliminate a potential role for MUC1 in VSV- Δ M51-GFP. As mentioned above, the KCM and KCKO cell lines may have additional mutations that contribute to the difference in susceptibility, as different glycosylation patterns may exist between the proteins. However, analysis of MUC1 glycosylation patterns and the effect they may have on virus replication is beyond the scope of this project. In addition,

Panc02 cells endogenously express low levels of MUC1 and are not null for the MUC1. Further experiments using MUC1 specific siRNA must be performed to conclusively suggest the role of MUC1 in OV susceptibility.

Efficacy of VSV- Δ M51-GFP in Vivo in Immunocompetent Muc1.Tg Mice.

Our in vitro experiments demonstrate that VSV- Δ M51-GFP is able to infect and kill both KCM and KCKO cells, although KCKO cells were more susceptible than KCM at the lowest MOI. Next, we wanted to test the efficacy of VSV- Δ M51-GFP in an immunocompetent animal model. We conducted a pilot experiment in mice bearing KCM tumors, given that the MUC1 expressing tumors are a more clinically relevant and challenging model system. Further, the human MUC1.Tg mice used to propagate the KCM tumors are tolerant to human MUC1-expressing tumors making the model relevant for the study. In this experiment, we wanted to compare the efficacy of OV therapy to the chemotherapy using gemcitabine (the most common chemotherapeutic used to treat pancreatic cancer) [254] as well as to the combined chemovirotherapy using VSV- Δ M51-GFP and gemcitabine.

VSV has never been studied in any immunocompetent PDA model. To test the oncolytic efficacy of VSV- Δ M51-GFP in an immunocompetent mouse model of PDA, subcutaneous injections of KCM cells were used to establish tumors in the right flanks of human MUC1.Tg mice. When tumors were palpable (5 – 7 mm), mice were treated IT with VSV- Δ M51-GFP alone, VSV- Δ M51-GFP plus gemcitabine, gemcitabine alone, UV-killed VSV- Δ M51-GFP, or PBS (Figure 39A). UV-inactivated virus was used as a control to determine if the presence of viral proteins without virus replication would effect tumor progression. Palpable KCM tumors were treated every other day for a total

of three treatments: days 7, 9, and 11. Mice were monitored for signs of distress, and tumor size was measured every other day. Mice were sacrificed on day 18, at which time the animals were not yet presenting clinical signs indicative of morbidity. Results show KCM tumors injected with PBS as a control continue to grow at a steady rate (Figure 39).

Interestingly, KCM tumors injected with killed virus appear more aggressive and grow larger than the PBS control, with significantly increased tumor burden on days 16 and 18. Tumor growth with gemcitabine alone was comparable to that of PBS treatment. Treatment with VSV- Δ M51-GFP alone and VSV- Δ M51-GFP plus gemcitabine showed significant reduction in tumor burden beginning on day 12 when compared to PBS treatment (Figure 39A). This significance was maintained until day 18 at which point the mice were sacrificed. The greatest therapeutic effect, however, was seen in the combinational therapy of VSV plus gemcitabine, which showed significant reduction in tumor burden when compared to VSV- Δ M51-GFP alone at day 18 (Figure 39A).

Survival of Mice Treated with VSV- Δ M51-GFP

The above experiment demonstrated that live VSV- Δ M51-GFP significantly reduced KCM tumor burden up to 18 days following subcutaneous injections of cancer cells. However, as shown in Figure 39A, OV therapy did not abolish tumor growth. Therefore, we conducted a longevity study to determine whether VSV- Δ M51-GFP treatment could result in a sustained antitumor effect. In this experiment, in addition to a more aggressive KCM-based model, we included KCKO-based tumors. First, subcutaneous injections of KCM or KCKO cells were used to establish tumors in the right flanks of human MUC1.Tg mice. When tumors were palpable (5 – 7 mm), mice were treated IT with PBS as a control or with VSV- Δ M51-GFP every other day for three

treatments: days 8, 10, and 12 (Figure 40A). Mice were monitored for signs of distress, and tumor size was measured every other day. When tumor length reached 1.5 cm, or tumors became ulcerated, or animals presented clinical signs indicative of morbidity then mice were sacrificed. Results show that the KCM and KCKO cell lines do establish tumors and that KCM is a more aggressive form of PDA, with tumor size exceeding that of KCKO. Even more, VSV treatment of both cell lines demonstrates delayed tumor growth when compared to the control mice (Figure 40B). Specifically, for KCM tumors, delayed tumor progression was seen with virus treatment, though, only half of the VSV-treated mice outlived the control animals. For KCKO there was a significant decrease in tumor burden starting at day 12 that lasted through day 32 when significance could no longer be determined due to the need to sacrifice control animals needed for comparison (Figure 40B). A delay in tumor progression in treated animals was visible, but not sustained through the course of the experiments. In fact, by day 34 control tumors and those treated with VSV- Δ M51-GFP reached similar sizes. Regardless of treatment, most KCKO tumors never grew as large as the KCM tumors. This observation is in agreement with the previous studies where mice bearing KCKO tumors represent a less challenging, stable form of PDA disease as the cells grow at a slower rate than the more aggressive KCM cells [233].

Potential Mechanisms for Lack of a Sustained Anti-cancer Effect.

While our *in vitro* and short-term *in vivo* results show promising oncolytic abilities of VSV- Δ M51-GFP *in vivo* against both KCM and KCKO cells, there is clear indication that this treatment is not having a long-term sustained anticancer effect with the 3 OV injections. Several mechanisms (not mutually exclusive) may explain these

conflicting results: limited penetration of virus into the tumor, premature clearance of virus by adaptive immune responses, virus administration protocol (including virus titer, timing and portal of administration, etc.).

Because of an active adaptive immune system, clearance of OV treatment in an immunocompetent subject would be expected after a time. This potential adaptive immune response against virus treatment must be addressed. Samples were examined from the KCM experiments where all mice were sacrificed at the same time on day 18 post KCM cell injection.

To determine potential clearance of VSV- Δ M51-GFP, via an adaptive immune response aimed at viral proteins, it was important to look for antibodies generated against VSV- Δ M51-GFP proteins. Serial dilutions of mouse sera was incubated with a known amount of VSV- Δ M51-GFP plaque forming units and was then used to infect BHK cells for plaque assay analysis 16 h p.i.. In the VSV alone and VSV plus gemcitabine groups it is evident that a strong adaptive immune response was mounted against the virus as viral infections were almost eliminated in some samples (Figure 39B). Whether complete clearance of virus occurred within the tumor is not known.

In looking for an adaptive immune response to KCM cells, there was no indication of a T-cell response against KCM antigen in an ELISPOT assay (data not shown). To further investigate a potential adaptive immune response to KCM cells, mouse sera was analyzed for antibodies directed against KCM cells. KCM cells were fixed and permeabilized then incubated with serial dilution of mouse sera. Detection was done using an HRP-conjugated secondary and OPD read at 490nm. Results indicate that there was no significant difference in adaptive immune generation of antibodies against

KCM in any of the treatments when compared to sera from mice that were never injected with KCM (Figure 39C).

4.5 Discussion

In the present study, for the first time, VSV has been tested in an immunocompetent animal model of pancreatic cancer (specifically PDA). Importantly, we have developed a system that allows us to study oncolytic virotherapy (VSV or any other OV) in the context of MUC1 overexpression (approximately 80% PDA patients) or no expression [231, 255]. Our data show that VSV- Δ M51-GFP can infect and kill all tested mouse PDA cell lines *in vitro* and cause transient reduction in tumor (-MUC1 or +MUC1 tumors) growth *in vivo*.

Our *in vitro* studies demonstrate that, although VSV was able to infect and kill all tested murine PDA cells *in vitro*, there were clear variations in the susceptibility of different cell lines to VSV infection and VSV-induced oncolysis. This is consistent with our recent studies with an array of human PDA cell lines demonstrating that PDA cells are highly heterogeneous in their susceptibility to oncolytic virus treatment [237, 238]. Here, our particular focus was on mouse PDA cell lines, KCM and KCKO, which could be used in the immunocompetent model of PDA illustrated in Figure 34. We found that, although the cell lines were susceptible to VSV- Δ M51-GFP at both low and high MOI, KCM overexpressing human MUC1 were clearly more resistant than KCKO at a low MOI. We hypothesized that the physical presence of MUC1 might be responsible for this resistance of KCM cells to VSV at low MOI. Previous studies with other viruses showed that O-linked carbohydrates of MUC1 purified from human breast milk can inhibit poxvirus, HIV, and rotavirus and that MUC1 expression can block adeno-associated virus attachment [256-261]. Multiple attempts to remove or truncate the O-linked glycosylations of the MUC1 protein using neuraminidase, Endo- α -N-

Acetylgalactosaminidase, Exo- α -N-Acetylgalactosaminidase, or sialidase, showed no change in the infectivity of VSV (data not shown). Even more, our experiments showed no significant difference in attachment of VSV to any of the murine cell lines regardless of MUC1 expression. Together, these results suggest that even if MUC1 overexpression interferes with viral replication, the mechanism of this interference is not due to the physical prevention of virion attachment as it was shown for other viruses.

In many cancer types, including PDA, MUC1 overexpression is linked to tumor development, aggressive growth and metastasis. Beyond the physical presence of MUC1, signaling pathways are responsible for these tumorigenic results [262]. Whether MUC1 signaling can alter cellular antiviral response is unclear. Generation of the murine PDA cell lines from spontaneous murine PDA tumors allows us to study virotherapy in the presence or absence of MUC1. However, because accumulation of additional mutations cannot be ruled out during the creation of the KCM and KCKO cell lines [233], we were unable to determine if the presence of MUC1 was solely responsible for the resistance of KCM at the low MOI. Moreover, a complete knockdown of MUC1 in KCM is very challenging as this cell line also expresses murine Muc1 (Figure 34). Instead, to examine a possible role of human MUC1 overexpression on VSV infection, two isogenic PDA murine cell lines, Panc02-MUC1 and Panc02-Neo, were evaluated. The presence of MUC1 has no obvious affect on the oncolytic ability of VSV. Both Panc02-MUC1 and Panc02-Neo were similarly susceptible to VSV infection and killing at low and high MOIs. This result suggests that MUC1 expression alone may not be responsible for higher resistance of KCM cells to VSV.

Because of the involvement of MUC1 in numerous signaling pathways, we also considered a possibility that MUC1 plays an indirect antiviral role in KCM cells. We were particularly interested in a possibility that MUC1 expression could activate type I IFN antiviral responses in KCM cells. Recently, our analysis of 12 human PDA cell lines showed that resistant cell lines had active Type I IFN signaling [238]. Previous studies have demonstrated a potential link between cellular response to IFN- α and IFN- γ and upregulation of MUC1 expression [263]. Additionally, MUC1 has been shown to interact with proteins that result in activation of NF- κ B, a regulatory factor of IFN expression [264, 265]. While this potential link between MUC1 activation of an antiviral response requires more study, our data experiments show that all tested mouse PDA cell lines have defective Type I IFN pathway regardless of their MUC1 expression status (data not shown). In summary, another elusive mechanism is responsible for the difference seen between KCM and KCKO cells. Additional studies, beyond the scope of this project, will be needed to provide a detailed account of what may be responsible for the different susceptibility of KCKO and KCM cells to VSV.

We focused on KCM cells for our *in vivo* experiments as xenografts of KCM lead to more aggressive tumors than KCKO or KC and because most of the PDA patients exhibit MUC1 overexpression [233]. Our *in vivo* data demonstrated that VSV- Δ M51-GFP significantly reduced tumor burden in mice with subcutaneous KCM xenografts for 18 days. However, this effect was not sustainable when mice were monitored for survival, with all mice required to be sacrificed after 26 days. Even more, a similar result was shown in KCKO-derived tumors which exhibit much slower tumor growth when compared to KCM [233]. The transient reduction of tumor growth seen in both cell types

suggests that MUC1 may not play a role in the limitation of VSV oncolytic ability. In mice with KCM xenografts, analysis of mouse sera determined that adaptive immunity generates a robust antibody response directed at VSV. At the same time, when KCM cells were fixed and permeabilized then incubated with mouse sera from mice with KCM tumors, a modified ELISA assay, no adaptive immune responses against tumor cells could be detected in any treatment groups. Together, these data suggest that VSV- Δ M51-GFP-based monotherapy does not have a sustained antitumor response in the tested immunocompetent mice, possibly due to the strong antiviral response and absence of an effective adaptive immune response against the tumor.

Several options exist to increase the efficacy of VSV *in vivo*. First, VSV expressing a tumor (PDA) associate antigen (TAA) like MUC1 can be used. Several studies utilized recombinant VSV encoding TAAs and demonstrated the ability to generate increased numbers TAA-specific T cells when compared to control virus [266-268]. Otherwise, other recombinant VSV expressing immune system modulating cytokines, microRNA targets, tumor specific attachment proteins, or even cancer suppressors proteins [268] could be tested and compared to VSV- Δ M51-GFP. Moreover, considering future OV monotherapy may benefit from chemotherapeutic co-therapy, we utilized a commonly used PDA chemotherapeutic, gemcitabine, to test a potential co-treatment. While this therapeutic effect with a suboptimal concentration of gemcitabine showed significantly more tumor reduction when compared to VSV- Δ M51-GFP alone, ongoing experiments will study potential of other gemcitabine (or other drugs) concentrations as well as treatment schedules. Finally, the possibility remains that VSV is not an optimal virotherapy against murine PDA. Our *in vitro* experiments with herpes

simplex virus and vaccinia virus did not show improved efficacy compared to VSV- Δ M51-GFP. However, these viruses could be more effective *in vivo*. Overall, the described here immunocompetent murine system is a clinically relevant PDA model to study oncolytic virotherapy against PDA tumors (MUC1 positive or null) using oncolytic viruses as a monotherapy or in combination with other treatments.

4.6 Figures

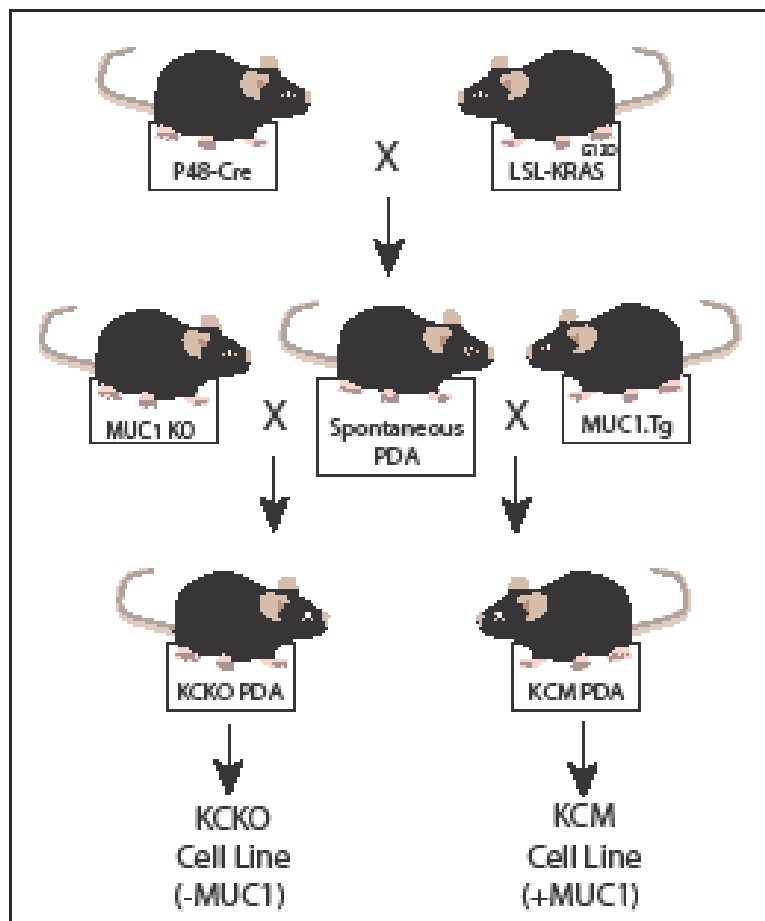


Figure 34: Generation of KCM and KCKO cell lines. C57BL/6 mice with KRAS^{G12D}-driven spontaneous PDAs were crossed with mice expressing human MUC1 (MUC1.Tg) or null (MUC1 KO) were used to generate the MUC1 positive KCM or MUC1 null KCKO cell lines, respectively.

4.6 Figures continued

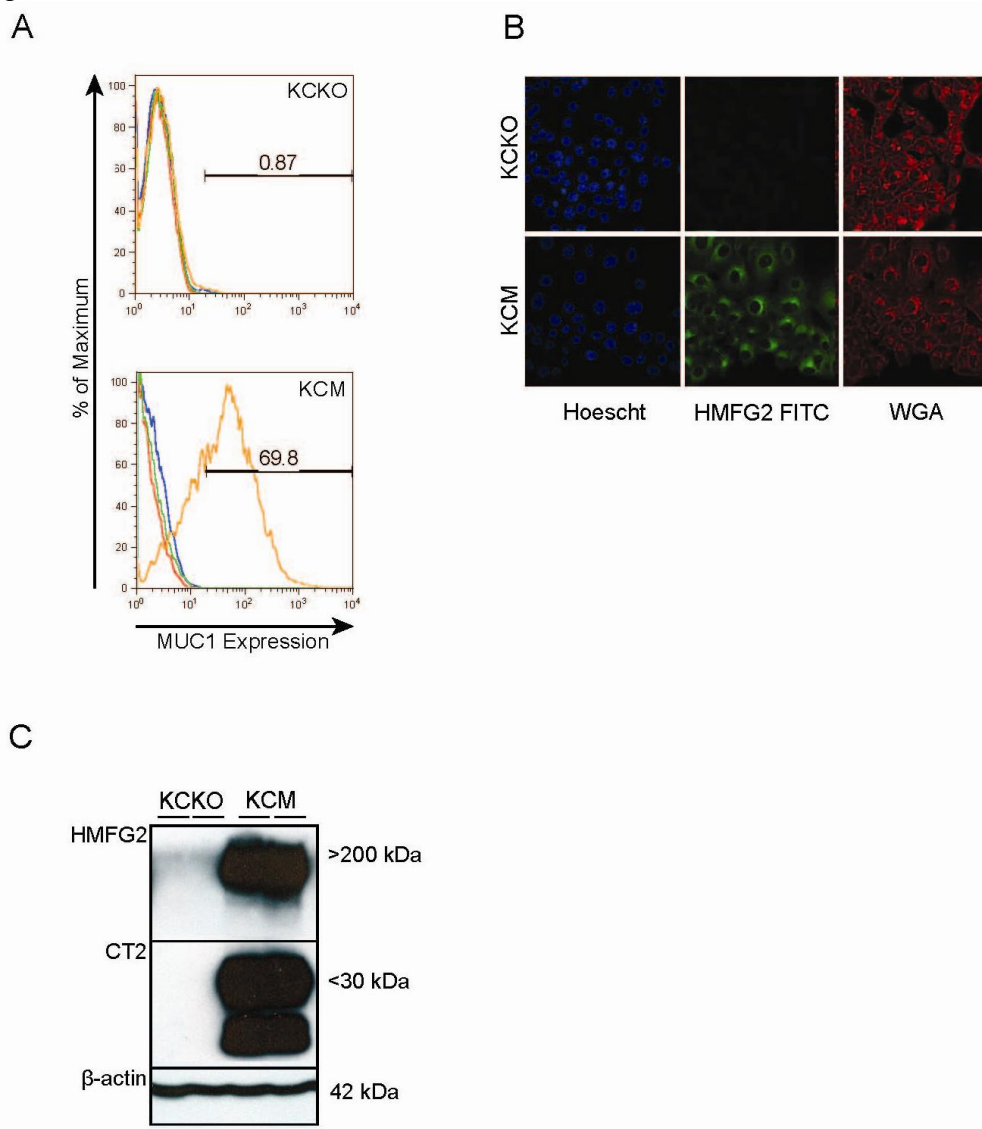


Figure 35: Characterization of human MUC1 expression of KCM and KCKO. (A) KCM and KCKO cells were collected and resuspended in PBS then incubated with Fc block and primary HMFG2 antibodies to detect surface expression of extracellular human MUC1 on KCM and KCKO cells via FACs analysis. (B) Cells were fixed and permeabilized then incubated with HMFG2 antibodies directed against the extracellular domain of human MUC1 with a FITC-conjugated secondary antibody used for immunofluorescence detection. Hoescht dye was used to stain for the nucleus while wheat germ agglutinin (WGA) was used to stain membranes. (C) KCM and KCKO total cell lysates were separated by 7.5% or 12% SDS-PAGE, respectively, then analyzed by Western blot with antibodies against extracellular human MUC1 (HMFG2 HRP-conjugated antibody) and human and murine transmembrane (CT2 HRP-conjugated antibody) MUC1 domains, respectively. β -actin antibodies were used as a marker for loading control.

4.6 Figures continued

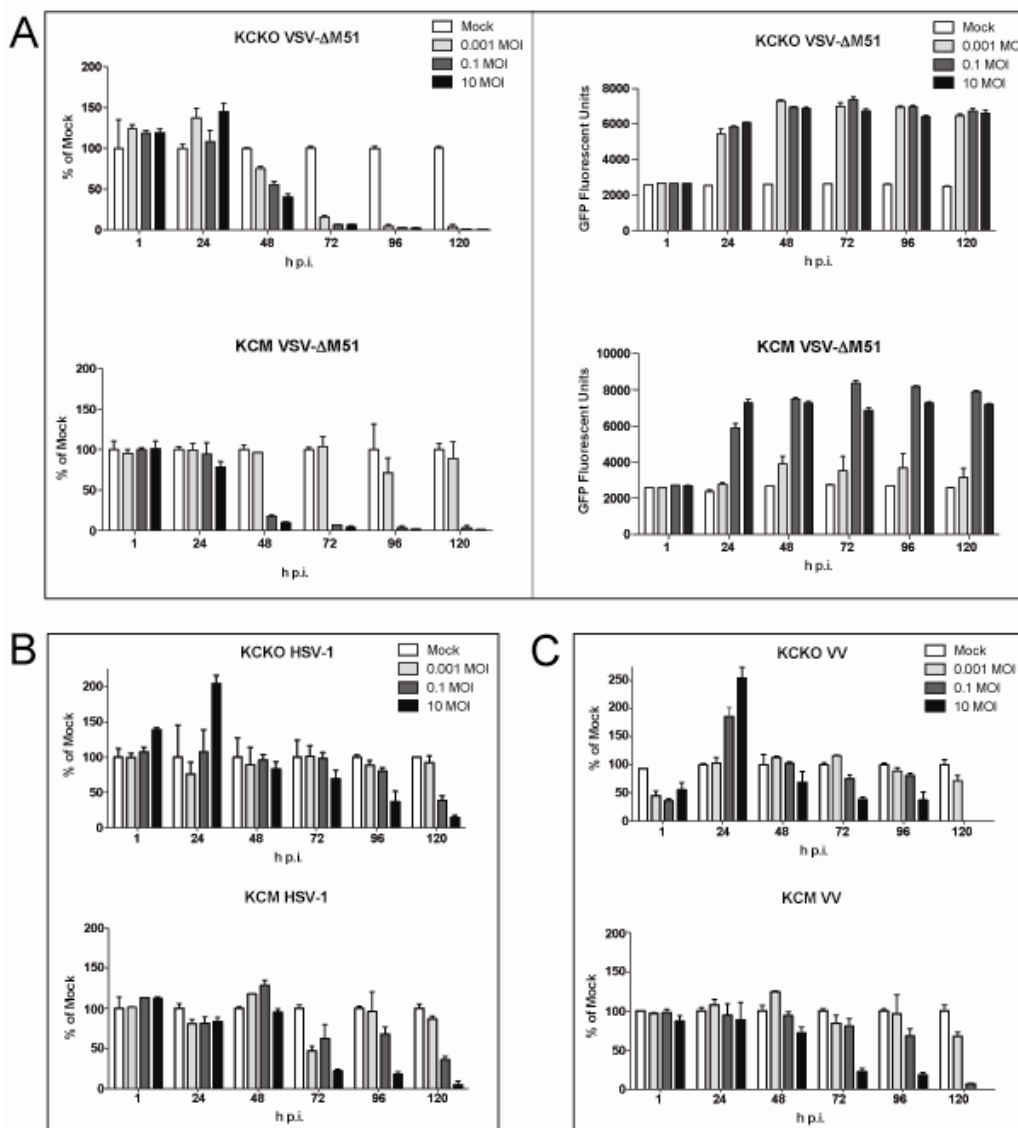


Figure 36: KCM and KCKO viability following infection with viruses. KCM and KCKO were seeded in 96-well plates so they reached approximately 80% confluence at 24 h. Cells were mock infected or infected with VSV- Δ M51-GFP (A), HSV-1 (B), or VV (C) at low (.001 CIU/cell), intermediate (0.1 CIU/cell), or high (1 CIU/cell) MOI. Cell viability was analyzed at the indicated times by an MTT cell viability assay and is expressed as a ratio of virus-infected to mock-treated cells. All MTT assays were done in triplicate and the data represent the mean and standard deviations. VSV- Δ M51-GFP replication detection as an expression of GFP in KCM and KCKO cells. (A) Cells were seeded in 96-well plates so they reached approximately 80% confluence at 24 h. Cells were mock infected or virus infected at .001, 0.1, or 10 MOI. Virus replication was measured by CytoFluor GFP fluorescence readings (485/20nm) at indicated times.

4.6 Figures continued

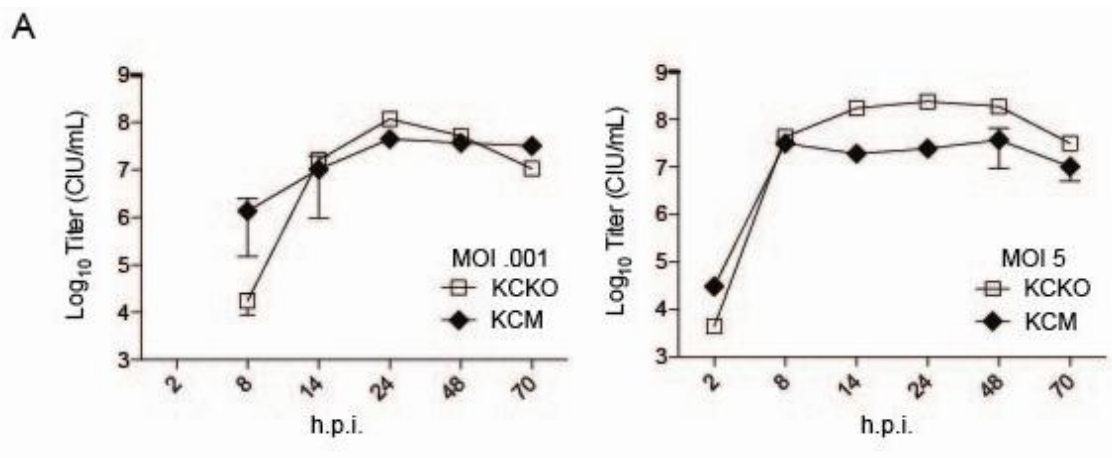


Figure 37: Cells were infected with VSV- Δ M51-GFP at cell line specific .001 or 5 MOIs. At 1 h p.i. the virus was aspirated and cells were washed and growth media with 5% FBS was applied. At the times indicated, supernatant was collected, and virus titers were determined by plaque assay on BHK-21 cells. All infections were done in triplicate, and the data represent means \pm standard deviations.

4.6 Figures continued

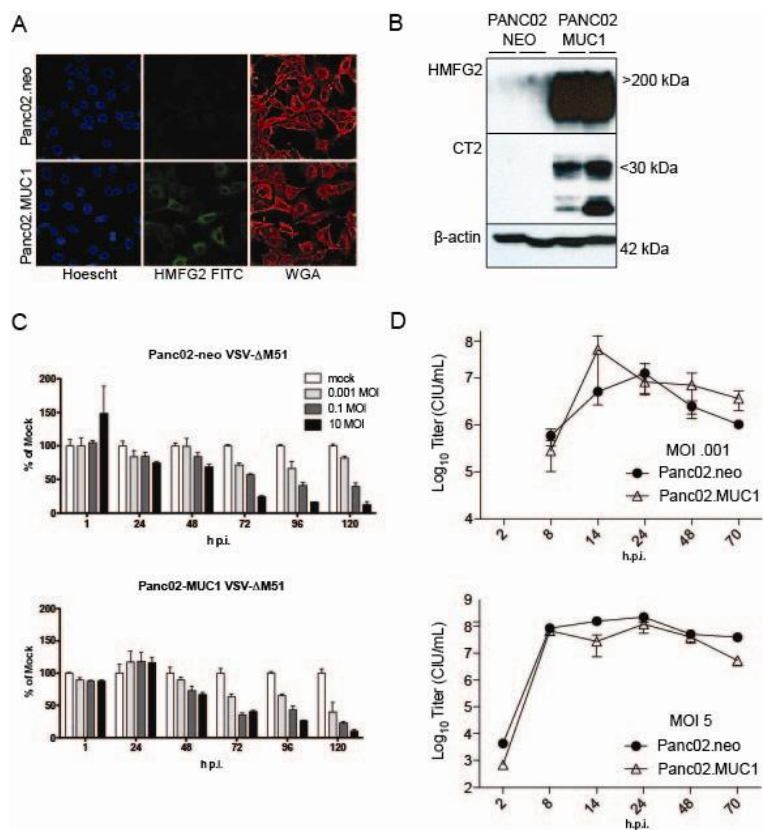


Figure 38: Panc02.MUC1 and Panc02.Neo expression of human MUC1. (A) Cells were fixed, permeabilized, and blocked with BSA before incubation with HMFG2 antibody. FITC-conjugated secondary antibody was used for immunofluorescence detection using confocal microscopy. Hoescht dye was used to stain for the nucleus and WGA was used to stain membranes. (B) Panc02.MUC1 and Panc02.Neo total cell lysates were separated by 7.5% or 12% SDS-PAGE, respectively, then analyzed by Western blot with HMFG2 antibody to detect the extracellular domain of human MUC1 or CT2 antibody to detect the transmembrane domain of human MUC1. β -actin antibodies were used as a marker for loading control. Cell viability of Panc02.MUC1 and Panc02.Neo. (C) Panc02.MUC1 and Panc02.Neo were mock infected or infected with VSV- Δ M51-GFP at .001, 0.1, or 10 MOI. Cell viability was analyzed at the indicated time points by a MTT cell viability assay and is expressed as a ratio of virus-infected to mock-treated cells. All MTT assays were done in triplicate, and the data represent the mean and standard deviations. One-step growth kinetics of VSV- Δ M51-GFP in Panc02.MUC1 and Panc02.Neo cells. (D) Cells were infected with VSV- Δ M51-GFP at cell line specific .001 or 5 MOIs. At 1 h p.i. the virus was aspirated and cells were washed and growth media with 5% FBS. was applied. At the times indicated, supernatant was collected, and virus titers were determined by plaque assay on BHK-21 cells. All infections were done in triplicate, and the data represent means \pm standard deviations.

4.6 Figures continued

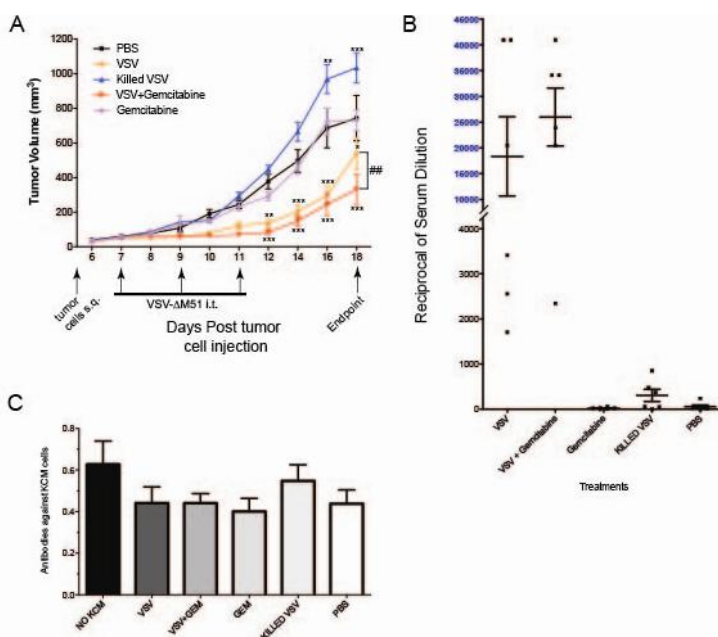


Figure 39: Efficiency of VSV- Δ M51-GFP in human MUC1 transgenic immunocompetent mice bearing KCM tumors. (A) 16 to 18 week old MUC1.Tg male mice were subcutaneously injected with KCM cells in the right flank ($n=30$). Tumors were established by day 5, and the mice were randomly divided into 2 groups ($n=6$ per group). One group served as a control and was administered 50 μ l PBS i.t on days 7, 9, and 11. The other group was treated with three doses of VSV- Δ M51-GFP at a concentration 1×10^8 CIU in 50 μ l PBS on days 7, 9, and 11. Tumor size was monitored by caliper measurements, and tumor weight was calculated according to the standard ellipsoid formula: grams = (length in cm X width²)/2. Mice were sacrificed at day 18 post tumor injection. Comparison of treatments to the PBS only control was done using a 2-way ANOVA, followed by the Bonferroni posttest to compare VSV to VSV + Gemcitabine (*, $P<.05$; ** $P<.01$; *** $P<.001$; ## $P<.01$). Virus neutralizing antibody detection in serum. (B) BHK-21 were seeded in 96-well plates so they reached approximately 80% confluence at 24 h. Growth media was removed from cells and sera/virus dilutions were added to cells. After 1 h, virus was aspirated from cells and a growth media with 5% FBS-1% Bacto Agar overlay was applied. Infectious foci were counted by fluorescence microscopy at 16 h p.i. Antibody dilution titers were determined to be the inverse of the dilution with half the number of plaques when compared to VSV- Δ M51-GFP alone. All sera samples were tested in triplicate. KCM cell-specific antibody detection in serum. (C) BHK-21 were seeded in 96-well plates so they reached approximately 80% confluence at 24 h. Cells were fixed and permeabilized then blocked in BSA. BSA was removed and sera dilutions were added to cells. Sera was removed and cells were washed with PBS. Cells were then incubated with HRP-conjugated secondary antibodies. Cells were washed and OPD substrate was added as per manufacturer instructions. The reaction was stopped and OD was read at 490nm. All sera samples were repeated in triplicate and the data represent the mean and standard deviation.

4.6 Figures continued

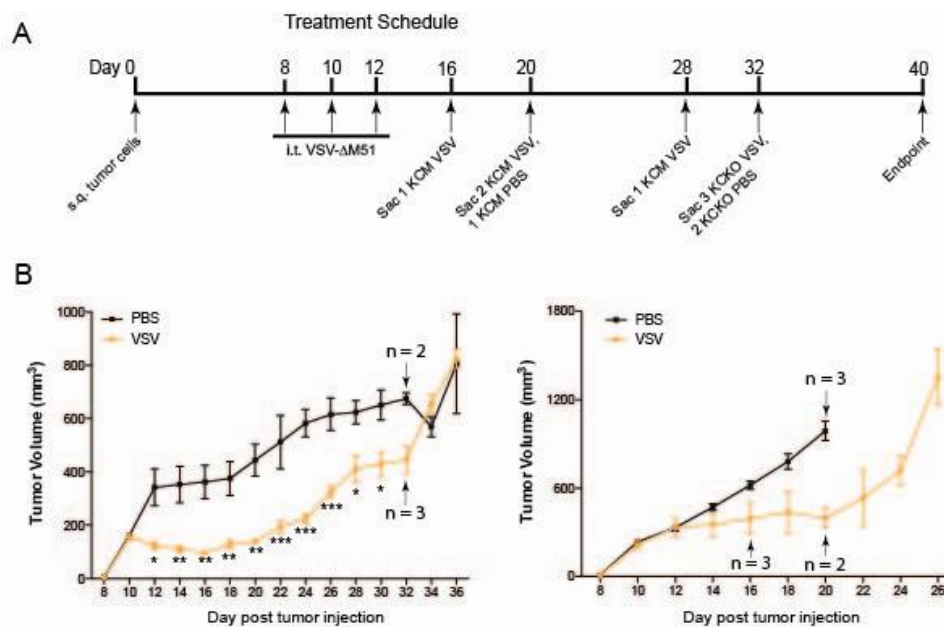


Figure 40: Treatment Schedule for human MUC1 transgenic immunocompetent mice bearing KCM or KCKO tumors (A) Efficiency of VSV-ΔM51-GFP in human MUC1 transgenic immunocompetent mice bearing KCM or KCKO tumors. (B) 8-11 week old male MUC1Tg mice were subcutaneously injected with KCM or KCKO cells in the right flank (n=8 per group). KCKO tumors are shown on the left in panel B, KCM tumors on the right. Tumors were established by day 8, then mice were randomly divided into 2 groups (n=4 per group) per cell line. One group served as a control and was administered 50μl PBS i.t on days 8, 10, and 12. The other group was treated with three doses of VSV-ΔM51-GFP at a concentration of 5×10^7 CIU in 50 μl PBS, on days 8, 10, and 12. Tumor size was monitored by caliper measurements, and tumor weight was calculated according to the standard ellipsoid formula: grams = (length in cm X width²)/2. Mice were sacrificed when length of the tumor reached 1.5cm, tumors became ulcerated, or mice were presenting with clinical signs indicating morbidity. Comparison of groups was done using a 2-way ANOVA only at the time points when the groups had the same population (*, P<.05; **P<0.01; ***P<0.001).

CHAPTER 5: ENHANCING THE EFFICACY OF A MUC1 TARGETED BREAST CANCER VACCINE

5.1 Abstract

While much advancement has been made in breast cancer treatment, metastatic breast cancer remains an incurable disease. MUC1 is a glycoprotein expressed on normal glandular epithelial cells but is over-expressed and underglycosylated in over 90% of human breast tumors and 100% of metastatic lesions, which lead to its ranking by NCI as the second most targetable antigen. Vaccines against tumor antigens have several benefits, including the chance to eliminate metastatic lesions that express the vaccinating tumor antigen. To this end, we have proposed vaccinating with peptides from the MUC1 protein core, which is only visible to the immune system on the tumor-associated form of the protein. Previous work from our lab has demonstrated that this vaccine does elicit a MUC1-specific immune response that can only be functional if the immunosuppressive tumor microenvironment is altered to allow efficient killing of tumor cells. Thus, we investigated the effectiveness of MUC1 vaccination in combination with drugs known to inhibit immunosuppression to determine which drug is the most effective. Methods: Mice that are transgenic for human MUC1 (MUC1.Tg) mice were orthotopically injected with a syngeneic breast cancer cell line expressing human MUC1 (Mtag.MUC1). Mice were vaccinated after palpable tumor formation with the vaccine cocktail, consisting of two MHC class I-restricted MUC1 tandem repeat peptides and a class II pan helper peptide mixed with GM-CSF and CpG ODN, in incomplete Freund's adjuvant. Previous work in

our lab has shown that blocking the cyclooxygenase pathway (COX) resulted in an inhibition of immunosuppression. Thus we used the following drugs in combination with the MUC1-vaccine therapy: Indomethacin (COX1 and COX2 inhibitor), Celecoxib (COX2 inhibitor), 1-methyl tryptophan (indoleamine 2,3 dioxygenase inhibitor), and AH6809 (EP2 receptor antagonist). Mice were euthanized and tissue was collected post the final vaccination. MUC1 vaccine therapy alone caused a slight reduction in tumor burden, although not significant. The combinational therapy of Vaccine+Indomethacin resulted in a significant reduction in tumor burden, whereas all other treatments resulted in no significant reduction in tumor burden, as measured by caliper measurements. The combination treatment of Vaccine +Indomethacin and Vaccine+Celecoxib both reduced PGE2 levels compared to vaccine alone. In a repeat experiment, we found that the combination of Vaccine+Indomethacin caused a significant reduction in tumor wet weight compared to vaccine alone as well as compared to control. However, Indomethacin alone did not significantly reduce tumor wet weight compared to control, indicating a synergistic effect of vaccine and indomethacin. Since Indomethacin but not Celecoxib reduced tumor burden when given in combination with the MUC1 vaccine, we are further investigating COX-independent pathways which are unique to Indomethacin involved in this mechanism.

5.2 Introduction

Breast Cancer is diagnosed in 200,000 individuals in the United States each year and contributes to approximately 40,000 deaths annually. For tumors confined within the breast, surgical removal can result in a favorable outcome. However, tumors have the ability to metastasize to distant sites, such as lymph nodes, lungs, liver or brain.

Complications from metastatic disease are the leading causes of cancer-related deaths. It is for this reason that research now focuses on the development of novel breast cancer-specific vaccines. Cancer vaccines are designed to immunize individuals to antigens present on tumors, in order to stimulate the patient's own immune system to fight metastasis. Vaccines are non-toxic therapies that have the potential to control disease and prolong survival, often with a long delay before tumor recurrence [109, 110].

MUC1 is a transmembrane mucin glycoprotein that is overexpressed in >90% of breast carcinomas [48, 50, 117-119]. MUC1 contains an extracellular domain (comprised of tandem repeats (TR) of twenty amino acids) that is extensively O-glycosylated, a transmembrane domain, and a cytoplasmic tail. MUC1 is normally expressed on the apical surface of glandular epithelial cells. However, in the case of a tumor, MUC1 is overexpressed and is no longer restricted to the apical surface, but is found across the cell membrane and in the cytoplasm with an aberrant glycosylation pattern. These attributes have long made MUC1 an interesting target molecule for immunotherapeutic strategies. Recently, MUC1 was listed as the second most targetable tumor antigen by the National Cancer Institute [269]. Our lab has demonstrated the effectiveness of MUC1-directed tumor vaccines in colorectal, pancreatic, and breast cancer models; however

immunosuppression was observed at the tumor site, hindering the immune response to the vaccine [136, 161, 270].

There are two major limitations associated with the use of cancer vaccines. The first obstacle is the existence of tumor antigen-specific immune tolerance. Most of tumor-specific antigens are non-mutated, aberrant and/or over-expressed forms of self-antigens. Thus, high avidity T cells directed against that antigen are deleted; however, low avidity T cells do exist and can be activated with the appropriate therapy [271-278]. Despite the existence of tolerance, several groups, including ours, have shown that it is possible to elicit a strong tumor-antigen targeted immune response to overcome the tolerance [47, 111, 112, 279-281]. The second obstacle is the large tumor burden itself. Most studies, to date, utilizing tumor vaccines, have been given to patients with large tumor burden. Patients with large tumor burden are well known to have defective functioning of the immune system and the tumors of these patients have many immune escape mechanisms [282]. These include down regulation of MHC expression on tumor cells, functional impairment of T cells, and secretion of immunosuppressive cytokines by tumor cells as well as immune regulatory cells [283-289]. Breast tumors also produce high levels of immunosuppressive enzymes during cancer progression. In recent clinical trials, testing of tumor vaccines strongly indicated that although immune responses were generated, these approaches failed to generate significant clinical responses [111, 114, 271, 290, 291]. Thus, tumor vaccines alone have a limited potential for the treatment of patients with large tumor burdens.

Immunotherapy by itself can elicit tumor-specific immune responses that infiltrate the spontaneously arising breast tumor. However, the effector cells become non-

functional within the tumor microenvironment. Thus, combining immunotherapy with available adjuvant treatments may sufficiently alter the tumor microenvironment such that the effector cells can function properly. Immunosuppression within the tumor microenvironment is a barrier to targeted immunotherapy because it can inhibit direct cellular cytotoxicity and prohibit the development of immunological memory.

COX-2 is an enzyme that converts arachidonic acid to prostaglandins. COX-2 is induced in breast cancer during various pathologic conditions. COX-2 affects multiple pathways of tumorigenesis including angiogenesis, invasion and tumor-induced immune suppression. It has been recognized that COX-2 induces its immunosuppressive effects through prostaglandin₂ (PGE₂), which targets both cytotoxic (CTL) and T helper lymphocyte (Th) functions [134, 135]. Celecoxib, a specific COX-2 inhibitor, has been extensively exploited as a chemoprevention strategy for colon and other cancers [292-296].

Our lab previously found that Cyclooxygenase 2 (COX2) over-expression and subsequent Prostaglandin E2 (PGE2) production, in response to vaccination, are immunosuppressive [136, 297]. They have been shown to reduce T cell and dendritic cell function in patients with breast cancer. As a result of the immunosuppression observed in response to the MUC1 vaccine, our lab previously combined vaccine therapy with COX-2 inhibitor treatment in a spontaneous mouse model of breast cancer. This combination did indeed increase the clinical efficacy of the vaccine [136]. Further, COX-2 inhibition, via the use of Celecoxib, reduced breast tumor levels of indolamine 2, 3-dioxygenase (IDO).

The enzyme IDO is an enzyme that catabolizes L-tryptophan to L-kynurenine and its activity is increased during tumor development [137, 138]. IDO was first identified in

maintaining maternal tolerance towards the antigenically foreign fetus during pregnancy [139]. IDO is over expressed in many types of tumors including breast cancer, as well as in tumor-associated antigen presenting cells (APCs) [137, 142-144]. Tumor cells exploit this unusual system to prevent rejection by tumor-specific T cells [298]. Depletion of tryptophan within the tumor microenvironment can lead to T-cell anergy and apoptosis, thus IDO expression inhibits T cell functions [299-301]. The Inhibitor of IDO, 1-methyl-tryptophan (1MT) has shown strong anti-tumor effects *in vitro* and in *in vivo* models of cancer [145]. Moreover, PGE₂ has been shown to regulate IDO function.

COX-2, PGE₂, and IDO have been linked with the presence of T regulator (T-regs) and myeloid-derived suppressor cells (MDSCs) in the tumor microenvironment [136]. Therefore, we sought to determine whether a newly developed, orthotopic breast cancer model could achieve enhanced clinical efficacy when treated with a MUC1 specific vaccine in combination with COX2 inhibitors or inhibitors of molecules downstream of COX2. In the present study, we tested the MUC1 specific tumor vaccine with targeted inhibition of immune suppression in an effort to achieve a maximum clinical response. We tested the MUC1 vaccine in combination with a COX1 and COX2 inhibitor (Indomethacin), a COX2 inhibitor (Celecoxib), an indoleamine 2,3 dioxygenase (IDO) inhibitor (1-MT; 1-methyl tryptophan) as well as in combination with a PGE₂ antagonist (AH6809). AH-6809 is a relatively nonselective PGE₂ antagonist, which can bind with EP1, EP2, EP3 and DP receptors. Both 1MT and EP1/EP2 receptor antagonists have previously shown clinical efficacy in reducing tumor metastases. Our results indicate that Indomethacin in combination with the MUC1 vaccine resulted in a significant reduction in tumor burden. All other drug combinations tested were unable to

significantly reduce tumor burden at the dosages tested. While further studies are needed to better understand the molecular mechanisms of this reduction in tumor burden, this data clearly indicate that an enhanced clinical response can be achieved when the MUC1 vaccine is combined with the COX1 and COX2 inhibitor, Indomethacin. [302]

5.3 Materials and Methods

Cell Lines and Culture.

MTAG cell lines were previously generated in our lab from PyVMT (Polyoma virus middle T antigen) spontaneous breast cancer mouse model [303]. In the PyV MT mice, mammary gland tumors are induced by the action of tyrosine kinase activity associated with the polyoma virus middle T Ag driven by the mouse mammary tumor virus long terminal repeat (MMTV). Briefly, PyVMT male mice were mated to C57BL/6 mice to maintain the MTag mice as heterozygous. PCR was used to routinely identify the MTag oncogene. PCR was carried out as described previously [304]. Primer pairs for MTag transgene are 5'-AGTCACTGCTACTGCACCCAG-3' (282-302 bp) and 5'-CTCTCCTCAGTTCCTCGCTCC-3' (817-837 bp). The PCR product was analyzed by size fractionation through a 1% agarose gel. Heterozygous female PyVMT mice developed tumors, and tumors were dissected at pre-determined time points. Tumors were dissociated using collagenase IV (Worthington Biochemical) and the cell line was generated in our laboratory and designated as MTAG cells. The cells were maintained in complete DMEM (Invitrogen) supplemented with 10% FBS (HyClone), 1% glutamax (Invitrogen), and 1% penicillin/streptomycin.

Retroviral Infection.

For retroviral infection, GP2–293 packaging cells (stably expressing the *gag* and *pol* proteins) were co-transfected with the full-length MUC1 construct expressing the VSV-G envelope protein as previously described [305]. Cells were selected with 300 ug/mL G418, beginning 48 hours post infection. Expression of the constructs was stable throughout the span of experiments. MUC1 positive cells were

sorted using the FACS Aria to achieve 88% purity. MTAG cells retrovirally infected with full length MUC1 plasmid are referred to as MTAG.MUC1 cells.

Flow cytometry.

Single-cell suspensions were obtained by detaching cells using cell scrapers without trypsin to avoid any potential proteolytic effect of trypsin on surface proteins. The cells were then incubated with Fc block (BD Biosciences) at a concentration of 0.5 µg/ml at room temperature (RT) for 10 min. The cells were stained for the extracellular domain of human MUC1 using human milk fat globule antigen (HMFG2) antibody [243], for 15 minutes (min) at 4°C, washed, and subsequently stained with goat anti-mouse IgG-phycoerythrin (PE) or isotype control (Santa Cruz; 0.5 µg/ml) for 15 min at 4°C. Expression of MUC1 was determined by flow cytometry (Beckman Coulter) using FlowJo (Treestar, Ashland, OR).

³H-Thymidine Incorporation.

MTAG.MUC1 cells were serum-starved for 24hrs and treated for 24 or 48 hours with 0µM, 12.5µM, 25 µM, 50µM, 100µM, 200µM, and 400µM of Celecoxib, 1-MT, AH6809, Indomethacin or corresponding vehicle controls. Cell proliferation was determined by using [³H]-thymidine incorporation, in which 1 µCi of [³H]-thymidine was added per well for 24hrs prior to harvesting. Incorporated thymidine was evaluated using the Topcount micro-scintillation counter. All determinations were performed in triplicate.

Vaccine Formulation.

The vaccine consists of 100µg each of two MHC class I-restricted MUC1 peptides, APGSTAPPA and SAPDTRPAP, 140µg of one MHC class II helper peptide TPPAYRPPNAPIL (Hepatitis B virus core antigen sequence 128-140); 100µg of mouse

unmethylated CpG oligodeoxynucleotide constructs (CpG ODN); and 10,000 Units (2 μ g) GM-CSF, all emulsified in IFA.

Drug Preparations.

To prepare 1-MT for oral gavage, 1 g of 1-dl-MT (Sigma) was added to a 15 ml conical tube with 7.8 ml Methocel/Tween [0.5% Tween/0.5% Methylcellulose (v/v in water; Sigma)]. The following day, the 1-MT concentration was adjusted to 85mg/ml by adding an additional 4 ml Methocel/Tween and mixing again briefly. The 1MT was administered by oral gavage at 400 mg/kg/dose (0.1 cc/20 g mouse) using a curved feeding needle (20 G x 1 1/2 in; Fisher). 1-MT was administered once in the morning and once in the evening. For in vitro use, 1-MT was prepared as a 20 mmol/L stock in 0.1 N NaOH, adjusted to pH 7.4 and stored at -20°C protected from light. To prepare Indomethacin, a stock of Indomethacin was made at a concentration of 50mg/mL in 100% ethanol (heating to dissolve). Afterwards, indomethacin was diluted 1:10 in 25% Solutol. Indomethacin was administered by oral gavage at a dose of 3mg/kg/dose (0.1 cc/20 g mouse). Celecoxib was prepared by dissolving 100mg in 0.5mL of DMSO for 2-3hours at 37°C, creating a stock solution of 200ug/uL. Stock celecoxib was diluted 1:100 in water. Celecoxib was administered by oral gavage at 10mg/kg/dose. AH6809 was prepared by dissolving 1mg into 500uL of solutol (heating at 60°C in order to get into solution). Mice were then injected intraperitoneally with 100uL of AH6809 solution (200 μ g per day).

In Vivo Treatment of Tumors.

Mice were handled and maintained under veterinary supervision in accordance with guidelines of the University of North Carolina at Charlotte Institutional Animal Care

and Use Committee (IACUC) approved protocol. The MTAG.MUC1 cell line used in animal experiments tested negative for an extended panel of pathogens by Charles River Laboratories. Female MUC1.Tg mice aged 8-12 weeks old were orthotopically injected with MTAG.MUC1 tumor cells. MUC1.Tg mice tail clips were collected when mice were approximately 11 days old. Genomic DNA was isolated and used to genotype the mice by polymerase chain reaction. For MUC1.Tg the primers were 5'-CTTGCCAGCCATAGCACCAAG-3' and 5'-CTCCACGTCGTGGACATTGATG-3' with a 341bp amplification product that was confirmed on 1% agarose gels [157].

Based on preceding titration experiments (data not shown), mice were injected with 1×10^6 MTAG.MUC1 cells (in 100 μ L of PBS/Matrigel) into the mammary fat pad (n=24). Mice were palpated starting on day 8 post tumor injection (p.t.i.) then were randomly divided into 5 groups: vaccine only, vaccine + celecoxib, vaccine + indomethacin, vaccine + AH6809, vaccine + 1-MT (n=5 per group, n=4 for vaccine). All mice were vaccinated on days 8, 19, 34, and 35 p.t.i. and treated with Celecoxib, AH6809, Indomethacin once daily, and 1-MT twice daily, five days a week. Tumor size was monitored by caliper measurements every other day until sacrifice. Body weight was measured every other day. Tumor weight was calculated according to the formula: grams = [(length in cm) x (width in cm)²]/2. Mice were sacrificed 34 and 35 days p.t.i, at which time, mice were not yet presenting with clinical signs indicating severe morbidity. To conduct experiments with Indomethacin, 8 to 12-week-old MUC1.Tg female mice were orthotopically injected with the MTAG.MUC1 cell line. Mice were injected with 1×10^6 MTAG.MUC1 cells (in 100 μ L of PBS/Matrigel) into the mammary fat pad (n=23). Mice were palpated starting at 6 days p.t.i. then were randomly divided into 4

groups per cell line (n=6 per group, n=5 for Indomethacin alone). One group served as a control, the indomethacin group was gavaged three times weekly with 3mg/kg, all vaccine groups were vaccinated on days 6, 15, 24, 27, and 28 p.t.i, whereas the vaccine + indomethacin in addition to vaccination, received three times weekly gavage treatment of indomethacin at 3mg/kg. Tumor size was monitored by caliper measurements three times per week and body weight was measured twice weekly. Tumor weight was calculated according to the formula: grams = [(length in cm) x (width in cm)²]/2. Mice were sacrificed on day 27 and 28 p.t.i. Data were analyzed using GraphPad software and are expressed as mean ± standard error mean. Comparison of groups was done by two-way ANOVA (*p<0.05, **p<0.01, ***p<0.001).

PGEM ELISA.

PGE₂ levels in the tumor lysate were determined using a specific ELISA kit for PGE₂ metabolite (PGE-M) (Cayman Chemical Co., Ann Arbor, MI for PGE₂ and Oncogene Research Products, La Jolla, CA for VEGF) from treated and control mice. All tumor lysates were made in tissue lysis buffer containing 20 mmol/L HEPES, 0.15 mol/L NaCl, and 1% Triton X-100 supplemented with 80 μL/mL phosphatase inhibitor cocktail II (Sigma P-5726, St. Louis, MO) and 10 μL/mL complete protease inhibitor cocktail (Boehringer Mannheim GmbH, Indianapolis, IN). The PGE₂ assays were done according to the manufacturer's recommendation. Lysates were diluted appropriately to ensure that readings were within the limits of accurate detection. Results are expressed as picogram of PGE₂ per mL.

Flow Cytometry.

Single cell suspensions of splenocytes in PBS were harvested in 15mL conicals. Cells were centrifuged at 2000 rpm for 2 min to obtain a cell pellet. The cell pellet was re-suspended in 1mL of RBC lysis buffer for 1 min, and then diluted with 5mL of cDMEM. Cells were washed in staining buffer (1 X PBS with 1% FBS and 0.1% sodium azide), filtered and counted and plated for staining. Cells were centrifuged at 2000 rpm for 2 min to obtain a cell pellet. The cell pellet was re-suspended in staining buffer and Fc block (anti-CD16/CD32 anti-body) for 10 min on ice. Cells were washed once with staining buffer. Cells were then labeled with an 1) MDSC panel: anti-CD11b-PECy7, anti-Gr1-APC, 2) a T-Regulatory cell panel: anti-CD25-V450, anti-CD4-FITC, anti-FoxP3-APC, anti-CD62L-V450, and 3) a T cell panel: anti-CD8-FITC, anti-CD11b-PECy7 and anti-CD44-APC, or their corresponding isotype controls and incubated on ice for 15 min. Cells were then washed twice, and the MDSC panel, as well as the T cell panel were fixed with 2% paraformaldehyde and stored at 4°C till further use. For intracellular staining, in the T-Regulatory panel, the cells were fixed and simultaneously permeabilized with BD Cytfix/Cytoperm for 20 min on ice. The cells were then washed with staining buffer twice and stained with anti-FoxP3-APC, and washed with staining buffer twice. Cells were then fixed with 2% paraformaldehyde and stored at 4°C till further use. For the T cell panel, Naïve T cells were defined as CD8+CD62L+CD11b-CD44-, Effector T cells were defined as CD8+CD62L-CD11b+CD44+ and Memory T cells were defined as CD8+CD62L-CD11b-CD44+.

Statistical Analysis.

Data were analyzed using GraphPad software. Results are expressed as mean±SEM. Comparison of groups was performed using one-way or two-way ANOVA followed by post-test for multiple comparisons (* p <0.05, ** p <0.01, *** p <0.001).

5.4 Results

Generation and Characterization of the MTAG.MUC1 Cell Line.

PyVMT mice were dissected and dissociated using collagenase IV. The cell line generated from these tumors was designated as MTAG cells. In order to test the human MUC1 vaccine in vivo, we transfected the MTAG cells with the full length human MUC1 plasmid. In order to insure a high purity of MUC1 expressing MTAG.MUC1 cells, the transfected cell line was sorted for MUC1 expression using FACS Aria. Expression of the MUC1 was analyzed using the TAB004 antibody which targets sparsely glycosylated VNTR repeats of the human MUC1 extracellular domain. Using TAB004 antibodies for flow cytometry, we confirmed that MTAG.MUC1 cells are highly positive for MUC1 (Figure 41). Cox-1 and Cox-2 expression was confirmed in both the cell lysate and tumor lysate, using β -actin as a loading control (Figure 41).

Efficacy of Vaccine Therapy in Combination with Inhibitors of Immune Suppression.

In order to test the efficacy of the vaccine in combination with a variety of COX inhibitors, and inhibitors of downstream molecules, 24 female MUC1.Tg mice were orthotopically injected with MTAG.MUC1 cells in the mammary fat pad. When tumors were palpable, approximately day 8 post tumor cell injection (p.t.i.), mice were randomly assigned to five different treatment groups: vaccine alone, vaccine + indomethacin, vaccine + 1-MT, vaccine + celecoxib, vaccine + AH6809. Unfortunately, in this pilot experiment, we did not have MUC1.Tg female mice available to include all appropriate controls. Therefore, in this pilot experiment, we merely included the five treatment groups above in order to determine which drug would enhance the efficacy of the

vaccine. As the appropriate controls were not included in this experiment, any interpretation of the data must be made with this fact in mind. In future experiments, this pilot experiment will be repeated with the appropriate controls included.

All treatment groups were administered the MUC1 vaccine subcutaneously on day 8 p.t.i. In addition to vaccine administration, mice were treated with either indomethacin (3mg/kg), 1-MT (400mg/kg), Celecoxib (10mg/kg), or AH6809 (200ug) on a five day on, two day off, schedule. All drugs were administered once per day with the exception of 1-MT which was administered twice per day. Mice were again administered the MUC1 vaccine on days 19, 34 and 35 p.t.i. Mice were monitored for signs of distress, and tumor burden was measured three times per week. Mice were euthanized on day 35 p.t.i. Results demonstrate that MTAG.MUC1 tumors treated with a combination of vaccine + indomethacin significantly reduced tumor burden beginning on day 30 p.t.i. as compared to vaccine alone. This significance was maintained until mice were euthanized on day 35 (Figure 42). All other treatment combinations did not display a significant reduction in tumor burden compared to vaccine alone. Upon euthanasia, the tumors were weighed, prepared for lysates, and fixed for immunohistochemistry. Analysis of the tumor wet weight displayed similar trends, suggesting that the only group in which there was a reduced tumor wet weight was the vaccine + indomethacin group; however, this reduction was not significant (Figure 43).

COX-2 derived PGE-2 is the major prostaglandin produced by breast cancer cells. Production of PGE2 in the tumor lysate is an appropriate measure of COX-2 activity in this orthotopic mouse model of breast cancer; however, PGE2 is unstable in vivo. Therefore, we measured PGEM, the PGE2 metabolite (namely, 13,14-dihydro-15-keto-

PGA2) in order to provide a reliable estimate of PGE2 production. PGEM levels were measured in the tumor lysates of all treatment groups by ELISA. A significant reduction in tumor PGEM was observed in mice treated with vaccine + celecoxib, as well as vaccine + indomethacin, as compared to vaccine alone ($p < 0.05$, Figure 44).

Immune Status of Treated Mice.

As stated previously, COX-2, PGE2, and IDO have been linked with T regulator (T-regs) and myeloid-derived suppressor cells (MDSCs) presence in the tumor microenvironment. Tregs play a key role in the maintenance of immune tolerance to both self-and foreign antigens and are reviewed in [306]. Upon antigen stimulation, Tregs potently suppresses the activation/proliferation of CD4⁺ or CD8⁺ cells *in vitro*. It is well established that Tregs are present in the tumor microenvironment and hamper efficient anti-tumor immune responses. Several reports have documented the potential role of Treg removal for the induction of tumor rejection. Although Tregs are well known as suppressor cells there are other types of suppressor cells like MDSCs, also known as immature myeloid cells [307-309]. MDSCs can suppress the activation of CD4⁺ and CD8⁺ T cells, inhibiting the generation of an antitumor response [310-314]. MDSCs are thought to be induced by a variety of cytokines and growth factors (TGF- β , VEGF) which are produced within the tumor microenvironment [315, 316]. MDSCs have poor antigen-presenting capability, and produce factors that suppress T cell proliferation and activity, and promote angiogenesis [317]. This phenotype contrasts markedly with the phenotype of classically activated type I or M1 macrophages that are efficient immune effector cells able to kill microorganisms and tumor cells, present antigens, and produce high levels of T cell stimulatory cytokines.

Therefore, in order to determine the underlying mechanism of enhanced vaccine efficacy in combination with indomethacin, we isolated splenocytes from MTAG.MUC1 tumors bearing mice, pooled the splenocytes, stained, and assessed a number of immune parameters. Levels of myeloid-derived suppressor cells were assessed, characterized by the co-expression of Gr1 and CD11b. There was no significant difference observed in MDSC levels in mice treated with any of the combinational treatments tested (Figure 45A). Helper T cells were defined as CD4⁺, whereas T regulatory cells (Tregs) were characterized by the coexpression of CD4 and FoxP3. No significant difference was observed in the percentage of helper T cells or Tregs in any of the combinational treatments tested (Figure 45 B, C). However, there was a slight increase in the percentage of Tregs in the mice treated with the combination of vaccine +AH6809, although this increase was not significant.

Functionally distinct phenotypes of CD8⁺ T cells spanning from naïve (CD8⁺CD62L⁺CD11b⁻CD44⁻) to an effector and/or memory stage of differentiation have been described [318]. Effector CD8⁺ T cells (CD8⁺CD62L⁻CD11b⁺CD44⁺), are terminally differentiated and are known to release an array of cytokines upon stimulation (IFN- γ and TNF- α), as well as display strong cytolytic activity with high expression of perforin and granzyme. Memory T cells were defined as CD8⁺CD62L⁻CD11b⁻CD44⁺. Therefore, in order to determine the nature of the cells induced by this treatment, we assessed levels of naïve, memory and effector T cells, as well as CD8⁺ T cells. No significant differences were observed among the different treatment groups in overall CD8⁺ T cells (Figure 46A). The Naïve T cell population was significantly reduced in the vaccine + celecoxib treatment group (Figure 46B). The combinational treatment of

vaccine + AH6809 significantly reduced effector T cell populations (Figure 46 C), while there was no significant difference observed among any of the combinational treatment groups with respect to memory T cells (Figure 46 D).

Efficacy of Combinational Treatment of MUC1 Vaccine + Indomethacin.

In order to further examine the enhanced efficacy of vaccine + indomethacin combination, female MUC1.Tg mice were orthotopically injected with MTAG.MUC1 cells in the mammary fat pad. By day 6 p.t.i. tumors were palpable, and mice were divided into four different treatment groups. One group served as a control, whereas the other three groups were treated with indomethacin alone, vaccine alone, or vaccine + indomethacin. The treatment groups receiving the MUC1 vaccine were vaccinated on days 6, 15, 24, 27, and 28 p.t.i. Mice receiving indomethacin treatment were gavaged three days per week (3mg/kg). Tumor burden was monitored three times per week, while body weight was measured twice weekly. Mice were sacrificed on days 27 and 28 p.t.i. Results demonstrate that MTAG.MUC1 tumors treated with the combination of vaccine + indomethacin resulted in a significantly reduced tumor burden beginning at day 17. This significant reduction in tumor burden was maintained until mice were sacrificed (Figure 47 A). Indomethacin alone, as well as vaccine alone, resulted in a significant reduction in tumor burden, as compared to control, beginning at 24 days p.t.i (Figure 47 B). Results also demonstrated that tumor burden of mice treated with vaccine + indomethacin was significantly lower than either indomethacin alone or vaccine alone. This significance was noted at day 20 p.t.i and remained until mice were sacrificed (Figure 47B). This is suggestive of a synergistic effect between vaccine and indomethacin treatment.

Upon euthanasia, the tumors were weighed, prepared for lysates, and fixed for immunohistochemistry. Analysis of the tumor wet weight displayed similar trends, specifically, mice receiving the combination treatment of vaccine + indomethacin had significantly decreased tumor wet weight as compared to control ($p < 0.01$). Moreover, the combination treatment also resulted in a significantly reduced tumor burden compared to vaccine alone ($p < 0.05$, Figure 48). However, no significant difference was observed between mice treated with indomethacin alone and control mice (Figure 48). In order to insure that the treatment was indeed effective in reducing PGE2 levels, Prostaglandin E2 Metabolite (PGEM) was again measured in the tumor lysate of treated mice as a read out for PGE2 levels. The combination of vaccine + indomethacin as well as indomethacin alone, significantly decreased levels of PGEM in the tumor lysate of treated mice as compared to control mice (Figure 49). Additionally, the mice treated with the combination treatment of vaccine + indomethacin resulted in significantly decreased PGEM levels as compared to vaccine alone ($p < 0.05$, Figure 49). Thus, we suggest that this combinational treatment is immunologically relevant and warrants further investigation.

5.5 Discussion

Previously, our lab has made use of the oncogenic mice that carry the polyoma virus middle T antigen driven by the MMTV promoter (PyV MT mice). These mice developed spontaneous tumors of the breast, which metastasize to the lungs and bone marrow. We have previously shown that celecoxib, a specific cyclooxygenase-2 (COX-2) inhibitor when administered in combination with a dendritic cell (DC)-based breast cancer vaccine (DCs pulsed with PyV MT tumor lysate) significantly augments the effectiveness of the vaccine in reducing primary tumor burden, preventing metastasis, and increasing survival. In that study, it was found that tumor-associated COX-2 activity *in vivo* can regulate IDO expression within the tumor microenvironment [136].

In this study, we generated a breast cancer cell line from the tumors of PyVMT mice and retrovirally infected the cells with the full length MUC1 plasmid (Figure 41). Using these cell lines, tumors were generated in MUC1.Tg mice and we tested the MUC1 specific tumor vaccine in combination with four different drugs, each with targeted inhibition of immune suppression in an effort to achieve maximal vaccine efficacy. The four drugs used in this study targeted different aspects of the COX pathway. In an effort to compare what had previously shown efficacy in combination with a dendritic cell vaccine in the spontaneous model, we included the use of celecoxib, a specific COX-2 inhibitor, in our studies. In the current study, we utilized a different vaccine, a MUC1 peptide vaccine that consists of two MHC class-I restricted peptides, an MHC class-II restricted helper peptide, as well as CpG-ODN and GM-CSF. This peptide vaccine was tested in combination with not only celecoxib, but also in combination with

a non-selective, COX-1 and COX-2 inhibitor, indomethacin, as well as the IDO inhibitor 1-MT, and the EP2 receptor antagonist, AH6809 (Figure 42).

The results clearly indicated that, compared to vaccine alone, the only combinational therapy that significantly reduced tumor burden, was the combination of indomethacin + vaccine (Figure 42). In future experiments, this will be conducted again with all proper controls included in the study. We observed very little change in immune cell levels measured in the spleen of combinational treated mice (Figure 45, Figure 46). When this experiment is repeated in the future, we plan to analyze immune cell status in the tumor draining lymph nodes, as well as in the tumor itself, via immunohistochemistry (IHC) as those parameters would be a more relevant assessment of the immunological changes that are occurring within and around the tumor.

Interestingly, the previously effective COX-2 inhibitor, celecoxib, did not significantly reduce tumor burden in combination with the vaccine, as seen in the spontaneous model. There are a number of reasons that the celecoxib + vaccine combination may be less efficacious than expected: 1) Although the cells we are using in this orthotopic injection model originally arose from the spontaneous model referred to above, it is important to note that tumors are a heterogeneous population of cells. Therefore, the cells that were isolated from the tumor, and used to generate the MTAG cell line may in fact be more aggressive than the spontaneous tumors in which they arose from. 2) The two models, orthotopic vs. spontaneous, are inherently different tumor models, and as such, may display differential results. 3) the dose used for celecoxib is a very low dose (10mg/kg). Perhaps the cells we are using are not as sensitive to this low dose, as their spontaneous model counterparts. In future experiments we will increase the

dose of celecoxib to determine if we can achieve enhanced efficacy with a more potent dose. However, it seems as though celecoxib is effective and functional, as evidenced by the significant reduction in PGEM levels in the tumor lysate of mice treated with vaccine + celecoxib (Figure 44).

Interestingly, IDO inhibition as well as mediating the actions of PGE2 with the use of the PGE2 antagonist, AH6809, seemed to be ineffective treatment options in combination with the vaccine regimen. It has been shown previously that administration of 1-MT in tumor bearing mice enhanced the potency of a DC-based vaccine [319]. Although the same dosage of 1-MT was administered to those mice, the mice were given the 1-MT treatment prior to tumor implantation. Given that the mice used in our study had a large tumor burden before any drugs were administered, it is not surprising that a similar effect could not be seen. Moreover, it has been shown by a number of groups that the PGE2 antagonist, AH6809 is able to reduce tumor cell proliferation [320]. However, we did not demonstrate a similar effect with this drug possibly due to a different tumor model. In fact, the only treatment that seemed to be efficacious was the vaccine + indomethacin treatment.

The results clearly suggest that combining indomethacin with a MUC1 based tumor vaccine increased the efficacy of the vaccine treatment compared with either treatment alone. Mice treated with the combinational therapy of vaccine + indomethacin displayed a significant clinical response with significant reduction in tumor burden and tumor wet weight (Figure 47, Figure 48). This reduction in tumor burden was associated with a decrease in PGEM levels (Figure 49), indicating that indomethacin was indeed functional. Preliminary data suggests that MAPK and β -catenin pathways may be

involved in the enhanced efficacy of the vaccine in combination with Indomethacin (Figure 50). In future experiments, we will continue to investigate these and other pathways.

While further studies are necessary to identify the molecular mechanisms underlying the reduced tumor burden associated with treatment, the data clearly indicate that an enhanced vaccine efficacy can be achieved with a combination of MUC1 peptide vaccine + non-selective, COX-1 and COX-2 inhibitor, indomethacin. Our preclinical studies offer us an opportunity to assess the feasibility of inhibition of COX pathway in combination with immunotherapy for the treatment of breast cancer. This is especially relevant at a time when clinical trials with COX-2 inhibitors are under debate and safer alternative agents are desired.

5.6 Figures

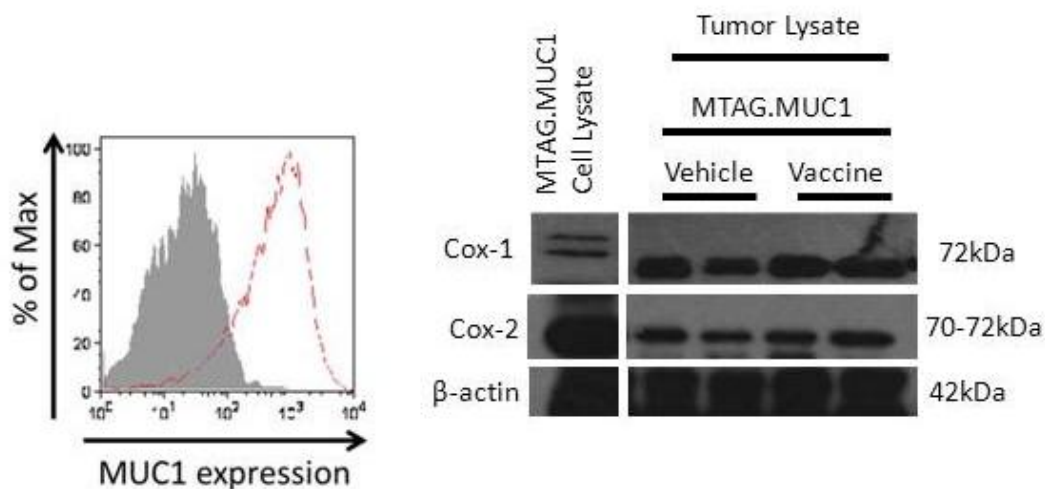


Figure 41: Characterization of the MTAG.MUC1 cell line. MUC1 expression was confirmed by flow cytometry. The gray histogram represents isotype control stained, and the red dashed line represents MUC1 staining. Cox-1 and Cox-2 expression was confirmed by western blot analysis. β -actin was used as a loading control

5.6 Figures continued

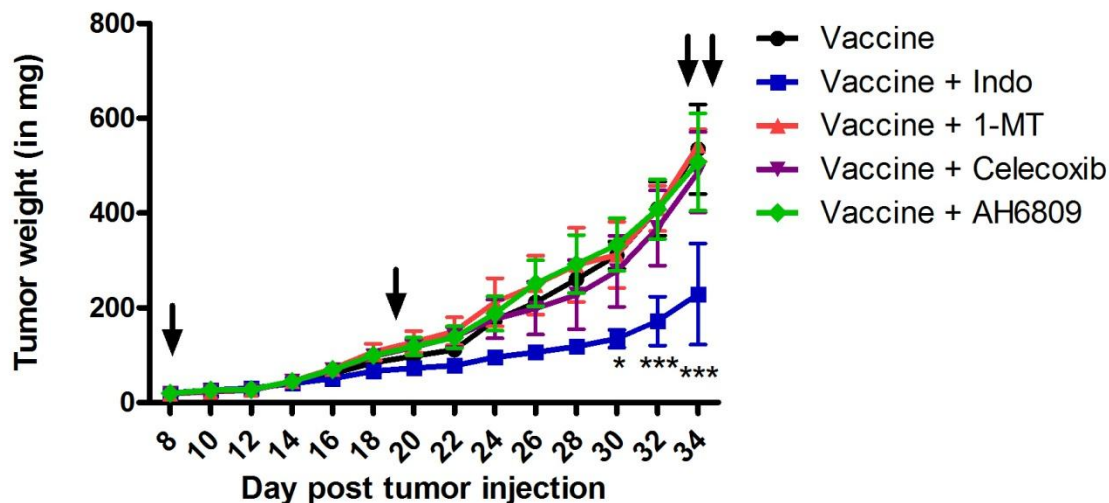


Figure 42: Indomethacin treatment with vaccination is the only combination that reduces tumor burden. Female MUC1.Tg mice, aged 8-12 weeks old were orthotopically injected with MTAG.MUC1 cells in the mammary fat pad (n=24). Tumors were palpable by day 8, and mice were randomly divided into 5 groups (n=5 per group, n=4 for vaccine). All mice were vaccinated on days 8, 19, 34, and 35 p.t.i.(as indicated by arrows) and treated with Celecoxib (10mg/kg), AH6809 (200ug), Indomethacin (3mg/kg) once daily, and 1-MT (400mg/kg) twice daily, five days a week. Tumor size was monitored by caliper measurements every other day until sacrifice. Body weight was measured every other day. Tumor weight was calculated according to the formula: grams = [(length in cm) x (width in cm)²]/2. Mice were sacrificed 35 days p.t.i, at which time, mice were not yet presenting with clinical signs indicating severe morbidity. Comparison of groups was done using a two-way ANOVA with a bonferoni post-hoc test (*, p<.05; **p<0.01; ***p<0.001 compared to control).

5.6 Figures continued

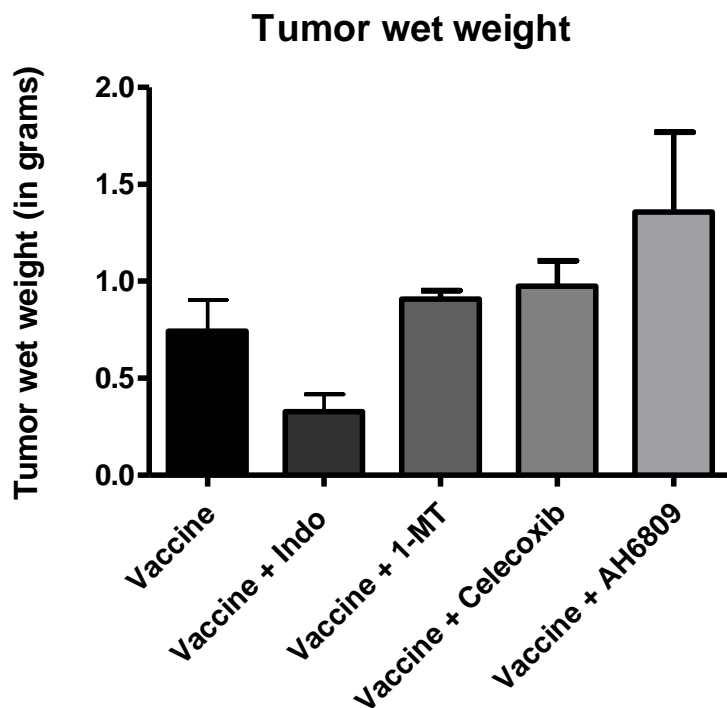


Figure 43: Indomethacin treatment with vaccination is the only combination that has a trend indicating reduced tumor burden. Female MUC1.Tg mice, aged 8-12 weeks old were orthotopically injected with MTAG.MUC1 cells in the mammary fat pad (n=24). Tumors were palpable by day 8, and mice were randomly divided into 5 groups (n=5 per group, n=4 for vaccine). All mice were vaccinated on days 8, 19, 34, and 35p.t.i. and treated with Celecoxib (10mg/kg), AH6809 (200ug), Indomethacin once daily (3mg/kg), and 1-MT (400mg/kg) twice daily, five days a week. Mice were sacrificed 35 days p.t.i, at which time tumors were excised and weighed. Comparison of groups was done using a one-way ANOVA with a Dunnetts multiple comparisons post hoc test. Although significance was not reached, there was a trend toward reduced tumor burden in the vaccine + indomethacin treatment group.

5.6 Figures continued

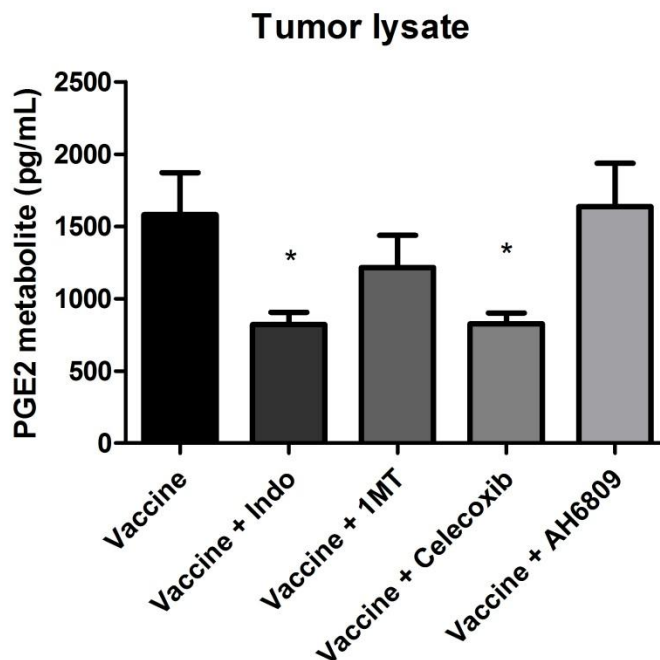


Figure 44: Celecoxib and Indomethacin both reduce PGE2 metabolite levels in combination with vaccination. Prostaglandin E2 Metabolite (PGEM) was measured in tumor lysate as a read out for PGE2 levels. Combinational treatment of vaccine + Indomethacin as well as vaccine + celecoxib significantly reduced tumor PGEM levels compared to vaccine treatment alone. Comparison of groups was done using a one-way ANOVA with a Dunnetts multiple comparisons post hoc test (*, $p < 0.05$ vs. vaccine alone).

5.6 Figures continued

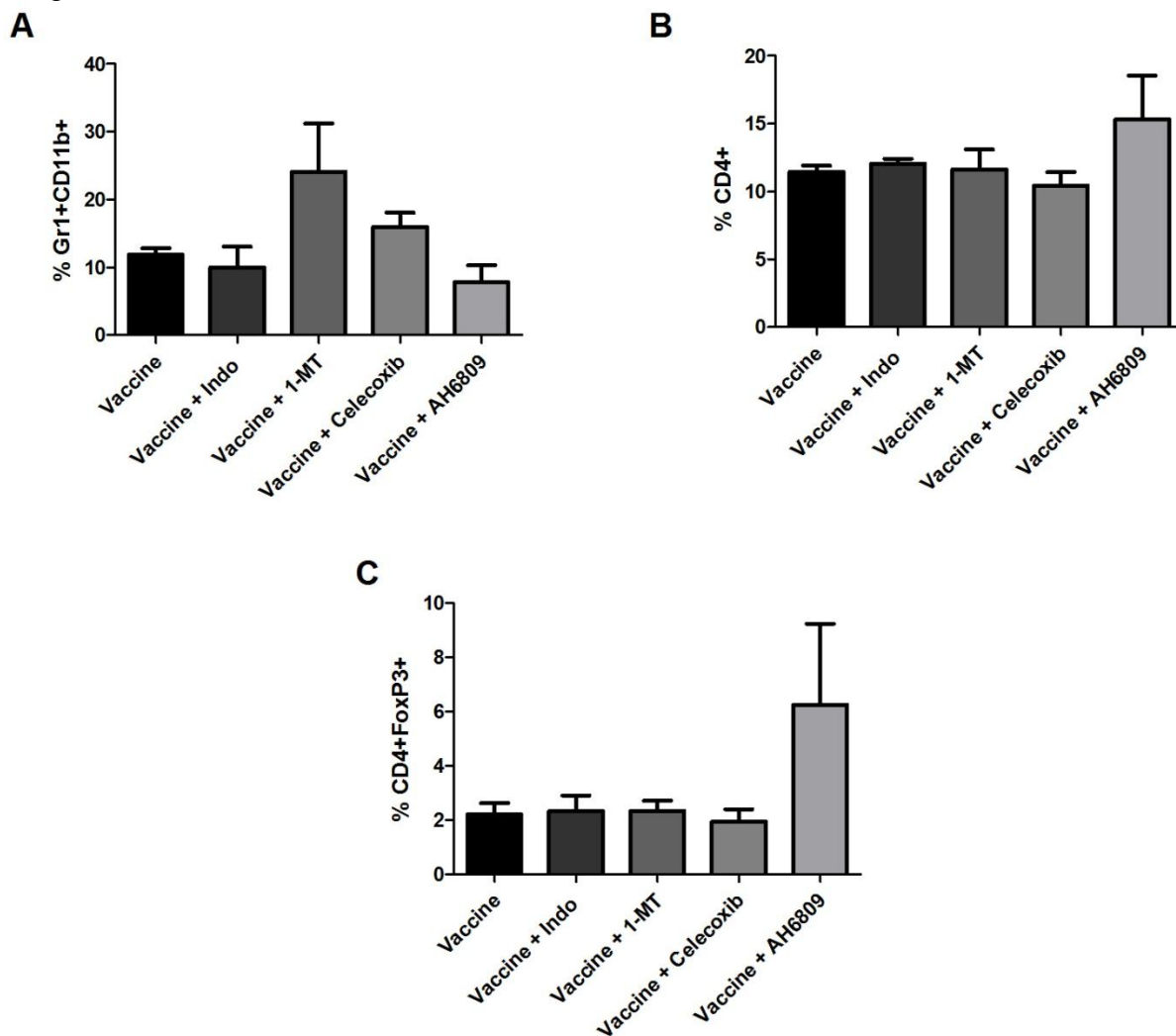


Figure 45: Immune analysis (MDSCs and Tregs) of combinational MUC1 vaccine therapy. Splenocytes from mice bearing MTAG.MUC1 tumors treated with vaccine therapy were assessed. A) Myeloid-derived suppressor cells (MDSCs) were characterized as Gr1+CD11b+ splenocytes. There was no significant difference in MDSC levels in mice treated with any of the combinational treatments. Vaccine in combination with 1-MT was the only group that seemed to increase MDSC levels, although the increase was not significant. B) Helper T cells were defined as CD4+ splenocytes. No significant difference was observed in the levels of T helper cells in any of the combinational treatment groups. C) Levels of T regulatory cells were measured in splenocytes, as defined by the co-expression of CD4 and FoxP3. No significant difference was observed in the levels of T regulatory cells in any of the treatment groups; however, the combination of Vaccine+AH6809 seems to increase percentage of T regulatory cells, although this increase was not significant. Comparison of groups was done using a one-way ANOVA with a Dunnetts multiple comparisons post hoc test (*, $p < 0.05$ vs. vaccine alone).

5.6 Figures continued

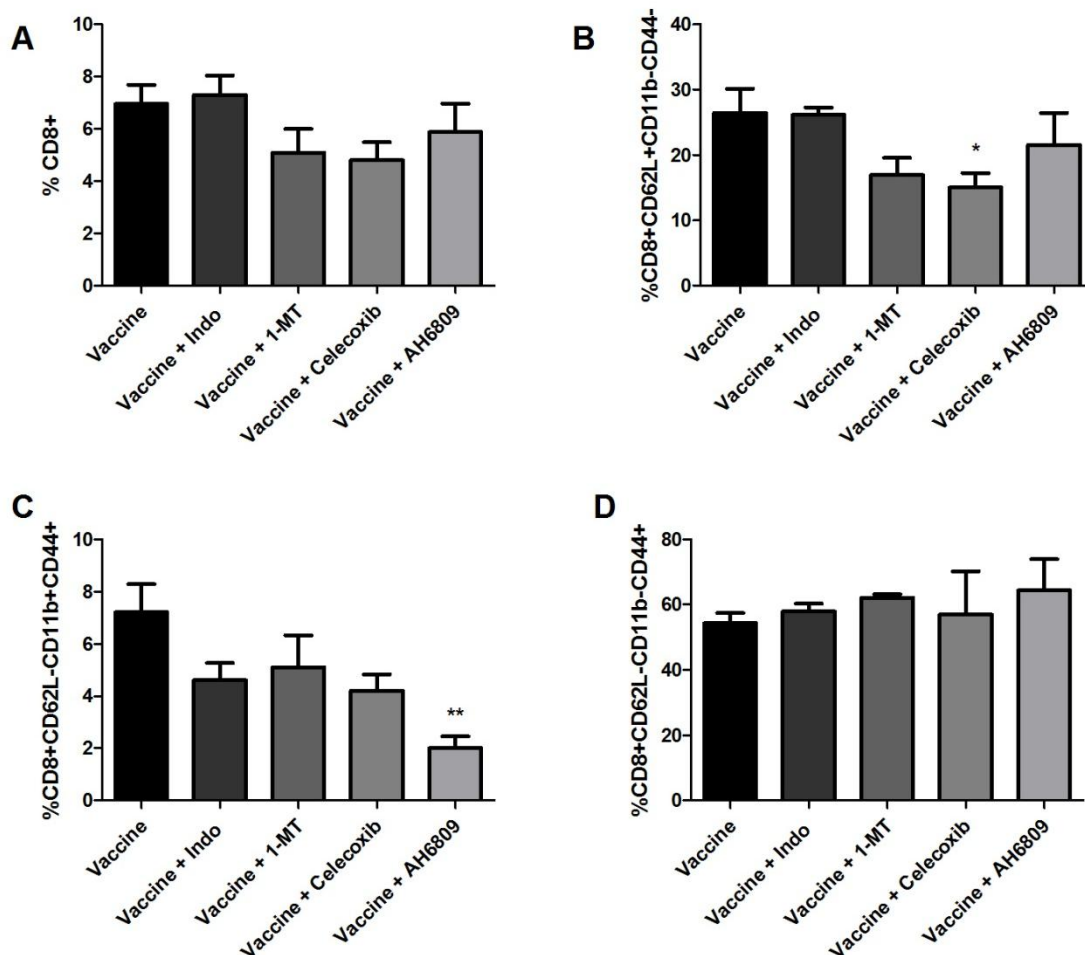


Figure 46: Immune analysis (T cells) of combinational MUC1 vaccine therapy. Splenocytes from MTAG.MUC1 tumor bearing mice treated with MUC1 vaccine therapy were analyzed for T cell flow panels. For the T cell panel, Naïve T cells were defined as CD8+CD62L+CD11b-CD44-, Effector T cells were defined as CD8+CD62L-CD11b+CD44+ and Memory T cells were defined as CD8+CD62L-CD11b-CD44+. A) No significant changes were observed among the different treatment groups in overall CD8+ T cells. B) The combinational treatment of Vaccine+Celecoxib significantly reduced levels of Naïve T cell populations. C) The combinational treatment of Vaccine+AH6809 significantly decreased the percentage of effector T cells. D) No significant changes were observed among the different treatment groups in reference to memory T cells. Comparison of groups was done using a one-way ANOVA with a Dunnetts multiple comparisons post hoc test (*, $p < 0.05$, **, $p > 0.01$ vs. vaccine alone).

5.6 Figures continued

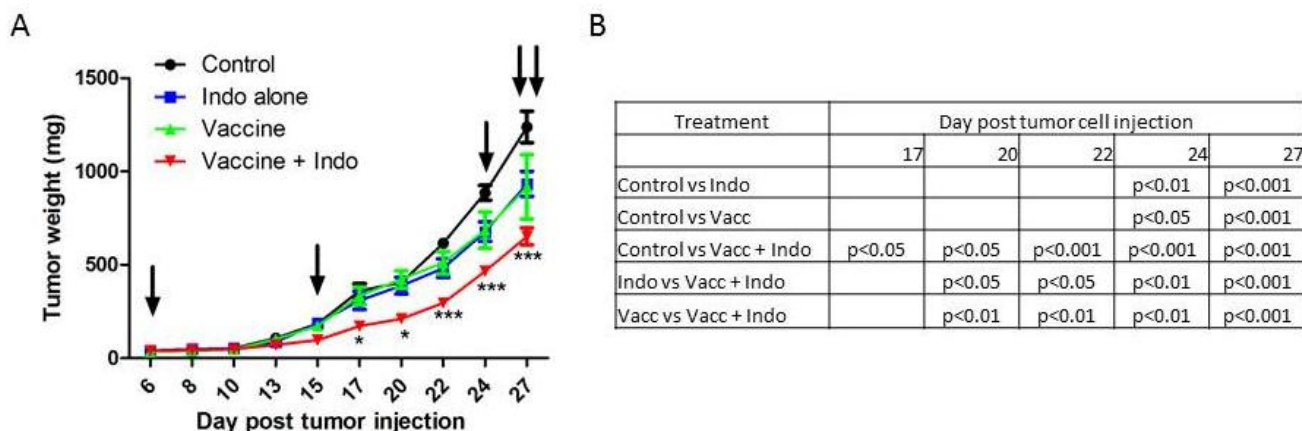


Figure 47: Combinational treatment of Vaccine + Indomethacin significantly reduces tumor burden. Female MUC1.Tg mice, aged 8-12 weeks old were orthotopically injected with MTAG.MUC1 cells in the mammary fat pad (n=23). Tumors were palpable by day 6, and mice were randomly divided into 4 groups (n=6 per group, n=5 for indomethacin alone). One group served as a control, the indomethacin group was gavaged daily with 3mg/kg. The vaccine groups were vaccinated on days 6, 15, 24, 27, and 28 (as indicated by arrows). The combinational treatment group received both vaccination as well as three times a week treatment of indomethacin (3mg/kg) by gavage. Tumor size was monitored by caliper measurements three times a week, and body weight was measured twice weekly. Tumor weight was calculated according to the formula: grams = [(length in cm) x (width in cm)²]/2. Mice were sacrificed on day 27 and 28 days p.t.i. A) Treatment with vaccine + indomethacin resulted in a significant decrease in tumor burden vs. control beginning at day 17. B) Table displaying significant decreases in tumor burden. Data were analyzed using GraphPad software and are expressed as mean \pm standard error mean. Comparison of groups was done by two-way ANOVA (*p<0.05, **p<0.01, ***p<0.001).

5.6 Figures continued

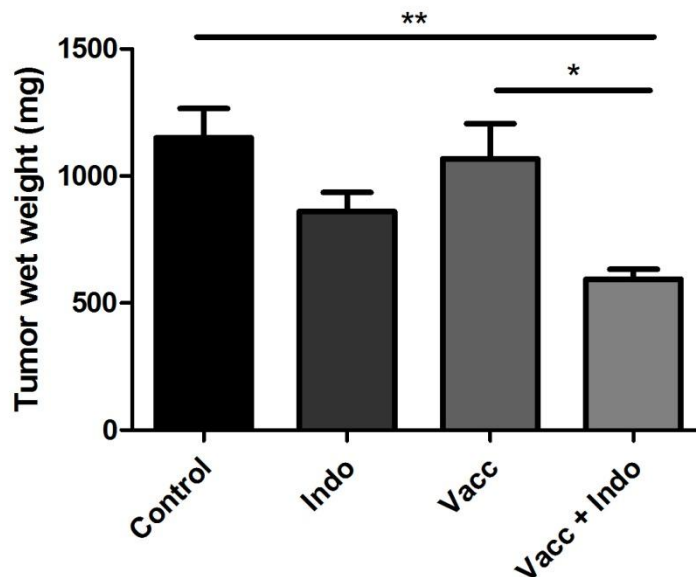


Figure 48: Combinational treatment of Vaccine + Indomethacin significantly reduces tumor wet weight. Female MUC1.Tg mice, aged 8-12 weeks old were orthotopically injected with MTAG.MUC1 cells in the mammary fat pad (n=23). Tumors were palpable by day 6, and mice were randomly divided into 4 groups (n=6 per group, n=5 for indomethacin alone). One group served as a control, the indomethacin group was gavaged daily with 3mg/kg. The vaccine groups were vaccinated on days 6, 15, 24, 27, and 28. The combinational treatment group received both vaccination as well as three times a week treatment of indomethacin (3mg/kg) by gavage. Mice were sacrificed on day 27 and 28 days p.t.i. Tumors were excised and weighed. Mice receiving the combinational treatment vaccine+indomethacin had significantly reduced tumor wet weight as compared to vaccine alone as well as control. Data were analyzed using GraphPad software and are expressed as mean \pm standard error mean. Comparison of groups was done by one-way ANOVA with Tukey's post hoc test (*p<0.05, **p<0.01, ***p<0.001).

5.6 Figures continued

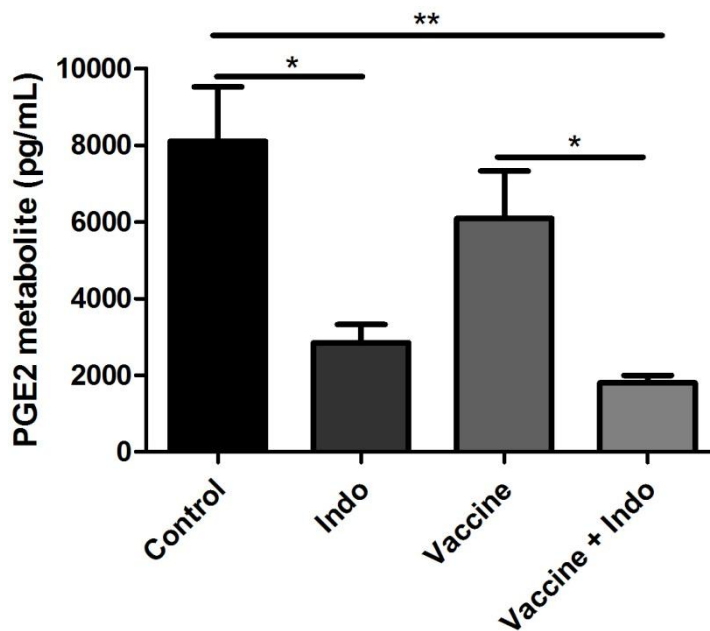


Figure 49: Indomethacin reduces PGE2 metabolite levels alone and in combination with vaccination. Prostaglandin E2 Metabolite (PGEM) was measured in tumor lysate as a read out for PGE2 levels. Indomethacin alone as well as the combinational treatment of vaccine + Indomethacin significantly reduced tumor PGEM levels compared to control. Additionally, the combinational treatment resulted in significantly reduced tumor PGEM levels as compared to vaccine alone. Comparison of groups was done using a one-way ANOVA with a Tukey's multiple comparisons post hoc test (*, $p < 0.05$ vs. vaccine alone)

5.6 Figures continued

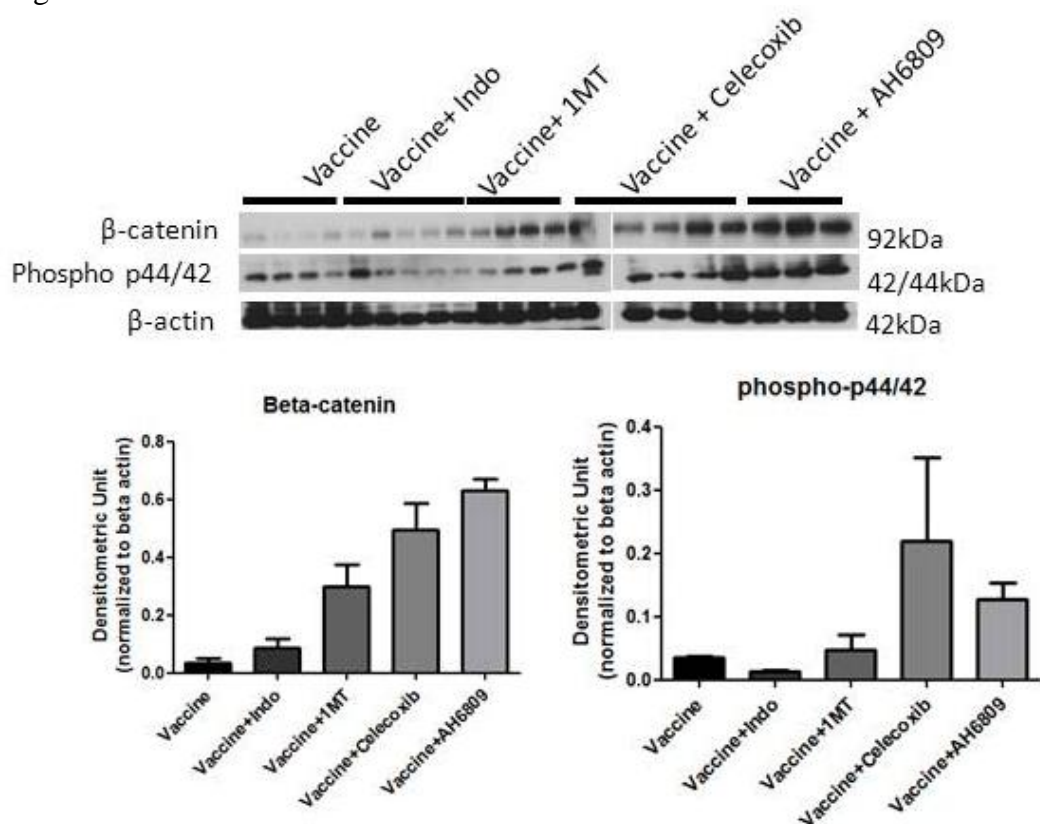


Figure 50: Potential pathways involved in the enhanced efficacy of Vaccine + Indomethacin. β -catenin and MAPK pathway status was assessed using western blot analysis. β -actin was used as a loading control.

CHAPTER 6: CONCLUSIONS AND FUTURE DIRECTIONS

The aim of this dissertation was to evaluate the role of MUC1 in the progression of pancreatic cancer, as well as to develop, enhance and evaluate novel therapeutic treatment options for pancreatic and breast cancers. In the first section, we evaluated the role of MUC1 in the progression of pancreatic cancer, utilizing a number of in vitro techniques as well as two different mouse models of pancreatic cancer: a subcutaneous xenograft model and a spontaneous model. We determined that spontaneous mice that are null for Muc1 (designated as KCKO), have significantly slower tumor progression and rates of secondary metastasis, as compared to PDA mice (designated as KC) or mice that express both human and mouse MUC1 (designated as KCM). This was evidenced by a significant increase in survival benefit and decreased levels of PGE₂M and VEGF levels (Figure 1).

Cells were extracted from the tumors of these spontaneous mouse models, and subsequently cultured in vitro, and utilized in xenograft mouse models. Mice challenged with KCKO cells displayed significantly lower tumor burden with a much more stable disease process, correlating with increased survival rates, as compared to their MUC1 expressing counterparts (Figure 2). In vitro analysis of KCKO and KCM cell lines indicated that Muc1 null cells have reduced rates of proliferation as well as alterations in the cell cycle (Figure 3-6). KCKO cells treated with MEK1/2 inhibitor displayed minimal decreases in proliferative rates; whereas the enhanced proliferative rate of KCM cells was

completely abrogated with the same treatment. This indicated that MUC1 expression is necessary for enhanced MAPK activity and oncogenic signaling.

Preliminary data from our lab, and others, has indicated that the oncogenic signaling associated with MUC1 is attributed to the cytoplasmic tail of MUC1 [54]. The MUC1 cytoplasmic tail (CT) contains 7 tyrosines that have been implicated in the oncogenic signaling of MUC1. Specifically, phosphorylated YNTP leads to activation of the MAPK pathway. Moreover, we have previously shown that the MUC1 CT is essential for epithelial to mesenchymal transition (a process associated with metastatic spread of cancer cells) [173]. Therefore, MUC1 CT appears to be a valid target. Our lab, and others, have found MUC1 to be a likely druggable target for small molecule inhibitors [321]. This also creates the possibility of utilizing a MUC1 CT inhibitor in combination with other chemotherapeutic options as an effective treatment against pancreatic cancer. Some researchers have already begun testing MUC1 peptide inhibitors in preclinical models, and have found that it can be efficiently targeted with limited toxicity of the treatment [322, 323]. A MUC1 peptide inhibitor could then be used to assess cell proliferation and tumor cell viability both *in vitro* and *in vivo*.

In the second study, in an effort to develop and test a novel therapeutic option for pancreatic cancer, we tested the potential of vesicular stomatitis virus (VSV) as an oncolytic agent. VSV has already been tested in a variety of pre-clinical models including prostate [84-86], breast [87-90], melanoma [88, 91], colorectal [92-94], liver [95-97], glioblastoma [98-100] and other cancers [101]; however, it had never been tested as an oncolytic agent against pancreatic cancer. In this study, we analyzed the oncolytic ability of VSV in a panel of 13 human PDA cell lines. We compared the oncolytic ability of

VSV to conditionally replicative adenoviruses (CRAds), Sendai virus, and respiratory syncytial virus. Among the viruses tested, VSV demonstrated superior oncolytic ability. *In vitro* data suggested that there was great variability in PDA cell lines susceptibility to viral oncolysis. Suggesting that there are key cellular factors present, making certain cell types more resistant to viral oncolysis. We also assessed the PDA cells abilities to produce and respond to Type I IFN. Responsiveness of cancer cells to IFN could be an important factor *in vivo*, where VSV infection would induce IFN production in surrounding healthy tissues, thus limiting oncolytic potential towards cancer cells sensitive to IFN. Results indicated that IFN sensitivity and production may be used to predict responsiveness of PDA cells to oncolytic virotherapy. VSV has been shown to cause cell death via apoptosis [99, 194, 226, 227]. The variability in susceptibility of cancer cells to viral oncolysis, could very well be attributed to differences in their mechanisms of cell death induction. While our preliminary studies indicate increases in caspase-3 activation, additional studies are needed to determine whether there is a delay in induction of apoptosis or a reduced level of apoptotic response.

Moreover, we tested the oncolytic ability of VSV in an immunodeficient xenograft mouse model. We selected four cell lines that displayed varying permissiveness to VSV in our *in vitro* studies. The induced tumors in the nude mice showed similar permissiveness as was observed *in vitro*. Future studies could focus on understanding the underlying mechanisms and identifying potential biomarkers of resistance. Follow-up studies have already identified MxA and OAS as potential biomarkers for PDA resistance to VSV and other OV's sensitive to type I IFN responses [324]. This study also allows for potential pre-screening of cancer cells, in order to assess which OV would be the best

treatment options for that specific tumor. Furthermore, future studies could focus on using VSV virotherapy in a combinational treatment in order to obtain a maximal anti-tumor effect.

In the third section, we evaluate VSV as an oncolytic agent, in an immunocompetent mouse model. In this study, we utilized the cell lines generated from the spontaneous PDA mouse models either expressing human MUC1 (KCM) or null for Muc1 (KCKO). We included another mouse cell line that was retrovirally infected with empty vector (Panc02.NEO) or full length MUC1 (Panc02.MUC1). With the use of these cell lines, we were able to study the application of VSV as an oncolytic virotherapy within the context of MUC1 expression. We first compared the oncolytic potential of VSV with herpes simplex virus (HSV-1) and vaccinis virus (VVT7) on these cell lines *in vitro*. Our results indicated that HSV-1 and VVT7 displayed a similar cell killing effect, but neither had as pronounced an effect as VSV. VSV had a significant oncolytic effect on both KCM and KCKO cells; however, KCKO cells were more permissive to VSV mediated viral oncolysis than KCM cells. However, the same was not true when in Panc02.NEO and Panc02.MUC1 cells were used, VSV showed similar oncolysis in Panc02 NEO and Panc02 MUC1 cells. These results indicate that MUC1 may not be the only factor contributing to the differential effect of VSV oncolysis observed in KCM and KCKO cells.

VSV was then tested for the first time in an immunocompetent MUC1 immune tolerant mouse model. Xenografts of KCM and KCKO tumors were used to test the ability of VSV *in vivo*. Administration of live VSV resulted in a significant reduction in tumor burden in both cell lines tested. However, the tumor burden reduction was not

sustained. Moreover, in agreement with our *in vitro* data, KCKO tumors seemed to be more susceptible to viral oncolysis. The lack of sustained tumor reduction once VSV treatment was terminated was attributed to an antibody response against VSV. There was no antibody or cell mediated immune response against the tumor itself. Moreover, VSV efficacy was improved when combined with a chemotherapeutic option, gemcitabine. Future studies will focus on using VSV as an oncolytic therapy in combination with other traditional therapies including vaccination and chemotherapeutic administration. Furthermore, future studies would need to optimize the treatment schema, titer of virus, as well as route of administration in order to achieve a maximal, sustained response, while preventing premature clearance of the virus.

In the fourth section, we focused on enhancing the efficacy of a breast cancer vaccine. Previous work from our lab indicated that the MUC1 vaccine can elicit a MUC1 specific immune response, but can only be functional and efficacious if the immune suppression within the tumor microenvironment is altered [136, 297]. Our lab previously found that administration of a COX-2 inhibitor, celecoxib, enhanced the efficacy of the MUC1 vaccine by reducing overall tumor burden in a spontaneous mouse model of breast cancer [136]. In this study, we isolated cells from the spontaneous tumors, and generated a cell line (designated MTAG) and retrovirally infected with full length MUC1 plasmid (then designated as MTAG.MUC1). This cell line was orthotopically injected into the mammary fat pad of MUC1.Tg mice. These mice were then treated with vaccine alone or a combination of vaccine with COX1/2 inhibitors or inhibitors of molecules downstream of COX2. Our results indicate that the combination of vaccine and indomethacin is the only drug combination that was able to significantly reduce tumor

burden. Moreover, this reduction in tumor burden was associated with a decrease in PGEM levels. Interestingly, the combination that was effective in the spontaneous model, vaccine and celecoxib, did not seem to have the same affect when tested in an orthotopic model, highlighting the heterogeneity of breast tumors themselves. Since Indomethacin but not Celecoxib reduced tumor burden when given in combination with the MUC1 vaccine, we are further investigating pathways that may be unique to Indomethacin involved in this mechanism. Therefore, future studies will focus on reconfirming some of the data shown here, as well as identifying the molecular mechanisms underlying the reduced tumor burden associated with the combinational treatment of vaccine and indomethacin.

REFERENCES

1. Jemal, A., et al., *Cancer statistics, 2010*. CA Cancer J Clin, 2010. **60**(5): p. 277-300.
2. Jemal, A., et al., *Cancer statistics, 2005*. CA Cancer J Clin, 2005. **55**(1): p. 10-30.
3. Greenlee, R.H.-H., MB; Murray, T; Thun, M., *Cancer Statistics, 2001*. CA Cancer J Clin., 2001. **51**(2): p. 144.
4. Jaffee, E.M., et al., *Focus on pancreas cancer*. Cancer Cell, 2002. **2**(1): p. 25-8.
5. Institute, N.C., *Annual Cancer Statistics Review 1973-1988*. NIH Publication No. 91-27891991, [Bethesda, MD].
6. Stolzenberg-Solomon, R.Z., et al., *Dietary and other methyl-group availability factors and pancreatic cancer risk in a cohort of male smokers*. Am J Epidemiol, 2001. **153**(7): p. 680-7.
7. Lowenfels, A.B. and P. Maisonneuve, *Epidemiology and risk factors for pancreatic cancer*. Best Pract Res Clin Gastroenterol, 2006. **20**(2): p. 197-209.
8. Villeneuve, P.J., et al., *Alcohol, tobacco and coffee consumption and the risk of pancreatic cancer: results from the Canadian Enhanced Surveillance System case-control project*. Canadian Cancer Registries Epidemiology Research Group. Eur J Cancer Prev, 2000. **9**(1): p. 49-58.
9. Everhart J., W.D., *Diabetes mellitus as a risk factor for pancreatic cancer. A meta-analysis*. JAMA, 1995. **273**(1605-1609).
10. C.S, F., *Physical activity, obesity, height, and the risk of pancreatic cancer*. JAMA, 2001. **286**(921-929).
11. Virtamo J., A.D., *Insulin, glucose, insulin resistance, and pancreatic cancer in male smokers*. JAMA 2005. **294**
p. 2872-2878.
12. Fryzek J.P., Y.G.S., Garabrant D.H, *Familial risk of pancreatic cancer*. J. Natl. Cancer Inst, 2001. **93**: p. 640-644.
13. Whitcomb D.C., G.M.C., Preston R.A., Furey W., Sossenheimer M.J., Ulrich C.D., Martin S.P., Gates L.K., Jr., Amann S.T., Toskes P.P, *Hereditary*

- pancreatitis is caused by a mutation in the cationic trypsinogen gene.* Nat. Genet, 1996. **14**: p. 141-145.
14. Jaffee E.M., H.R.H., Canto M., Kern S.E, *Focus on pancreas cancer.* Cancer Cell, 2002. **2**(25-28).
 15. Thompson D., E.D.F., *Cancer incidence in BRCA1 mutation carriers.* J. Natl. Cancer Inst, 2002. **94**: p. 1358-1365.
 16. Klimstra D.S., L.D.S., *K-ras mutations in pancreatic ductal proliferative lesions.* Am. J. Pathol, 1994. **145**: p. 1547-1550.
 17. Rozenblum E., S.M., Goggins M., Hahn S.A., Panzer S., Zahurak M., Goodman S.N., Sohn T.A., Hruban R.H., Yeo C.J, *Tumor-suppressive pathways in pancreatic carcinoma.* Cancer Res, 1997. **57**: p. 1731-1734.
 18. Almoguera C., S.D., Forrester K., Martin J., Arnheim N., Perucho M, *Most human carcinomas of the exocrine pancreas contain mutant c-K-ras genes.* Cell Cycle, 1988. **53**(549-554).
 19. Haglund, C., et al., *CA 242, a new tumour marker for pancreatic cancer: a comparison with CA 19-9, CA 50 and CEA.* Br J Cancer, 1994. **70**(3): p. 487-92.
 20. Stefanidis, D., et al., *The current role of staging laparoscopy for adenocarcinoma of the pancreas: a review.* Ann Oncol, 2005.
 21. Sener, S.F., et al., *Pancreatic cancer: a report of treatment and survival trends for 100,313 patients diagnosed from 1985-1995, using the National Cancer Database.* J Am Coll Surg, 1999. **189**(1): p. 1-7.
 22. Beger, H.G., F. Gansauge, and G. Leder, *Pancreatic cancer: who benefits from curative resection?* Can J Gastroenterol, 2002. **16**(2): p. 117-20.
 23. Roldan, G.E., et al., *External beam versus intraoperative and external beam irradiation for locally advanced pancreatic cancer.* Cancer, 1988. **61**(6): p. 1110-6.
 24. Conroy, T., et al., *Quality-of-life findings from a randomised phase-III study of XELOX vs FOLFOX-6 in metastatic colorectal cancer.* Br J Cancer, 2010. **102**(1): p. 59-67.

25. Cunningham, D., et al., *Phase III randomized comparison of gemcitabine versus gemcitabine plus capecitabine in patients with advanced pancreatic cancer*. J Clin Oncol, 2009. **27**(33): p. 5513-8.
26. Poplin, E., et al., *Phase III, randomized study of gemcitabine and oxaliplatin versus gemcitabine (fixed-dose rate infusion) compared with gemcitabine (30-minute infusion) in patients with pancreatic carcinoma E6201: a trial of the Eastern Cooperative Oncology Group*. J Clin Oncol, 2009. **27**(23): p. 3778-85.
27. Kindler, H.L., et al., *Gemcitabine plus bevacizumab compared with gemcitabine plus placebo in patients with advanced pancreatic cancer: phase III trial of the Cancer and Leukemia Group B (CALGB 80303)*. J Clin Oncol, 2010. **28**(22): p. 3617-22.
28. Philip, P.A., et al., *Phase III study comparing gemcitabine plus cetuximab versus gemcitabine in patients with advanced pancreatic adenocarcinoma: Southwest Oncology Group-directed intergroup trial S0205*. J Clin Oncol, 2010. **28**(22): p. 3605-10.
29. Hezel, A.F., et al., *Genetics and biology of pancreatic ductal adenocarcinoma*. Genes Dev, 2006. **20**(10): p. 1218-49.
30. Santini, D., F. Poli, and S. Lega, *Solid-papillary tumors of the pancreas: histopathology*. JOP, 2006. **7**(1): p. 131-6.
31. Hruban, R.H., et al., *An illustrated consensus on the classification of pancreatic intraepithelial neoplasia and intraductal papillary mucinous neoplasms*. Am J Surg Pathol, 2004. **28**(8): p. 977-87.
32. Hruban, R.H., et al., *Pancreatic intraepithelial neoplasia: a new nomenclature and classification system for pancreatic duct lesions*. Am J Surg Pathol, 2001. **25**(5): p. 579-86.
33. Maitra, A., S.E. Kern, and R.H. Hruban, *Molecular pathogenesis of pancreatic cancer*. Best Pract Res Clin Gastroenterol, 2006. **20**(2): p. 211-26.
34. Maitra, A., et al., *Precursors to invasive pancreatic cancer*. Adv Anat Pathol, 2005. **12**(2): p. 81-91.
35. van Heek, N.T., et al., *Telomere shortening is nearly universal in pancreatic intraepithelial neoplasia*. Am J Pathol, 2002. **161**(5): p. 1541-7.

36. Adsay, N.V., et al., *Ductal neoplasia of the pancreas: nosologic, clinicopathologic, and biologic aspects*. Semin Radiat Oncol, 2005. **15**(4): p. 254-64.
37. Gendler, S.J., *MUC1, the renaissance molecule*. J Mammary Gland Biol Neoplasia, 2001. **6**: p. 339-53
38. Gendler, S.J., et al., *Molecular cloning and expression of human tumor-associated polymorphic epithelial mucin*. J. Biol. Chem., 1990. **265**: p. 15286-15293.
39. Spicer, A.P., et al., *Analysis of mammalian MUC1 genes reveals potential functionally important domains*. Mamm Genome, 1995. **6**(12): p. 885-8.
40. Zrihan-Licht S., V.H.L., Baruch A., Elroy-Stein O., Sagiv D., Keydar I., Hilkens J., Wreschner D. H, *Characterization and molecular cloning of a novel MUC1 protein, devoid of tandem repeats, expressed in human breast cancer tissue*. Eur. J. Biochem, 1994. **224**: p. 787-795.
41. Baruch A., H.M., Yoeli M., Adereth Y., Greenstein S., Stadler Y., Skornik Y., Zaretsky J., Smorodinsky N. I., Keydar I., Wreschner D. H, *The breast cancer-associated MUC1 gene generates both a receptor and its cognate binding protein*. Cancer Res, 1999. **59**: p. 1552-1561.
42. Oosterkamp H. M., S.L., Stefanova M. C., Lloyd K. O., Finstad C. L, *Comparison of MUC-1 mucin expression in epithelial and non-epithelial cancer cell lines and demonstration of a new short variant form (MUC-1/Z)*. Int. J. Cancer, 1997. **72**: p. 87-94.
43. Smorodinsky N., W.M., Hartmann M. L., Baruch A., Harness E., Yaakovovitz M., Keydar I., Wreschner D. H, *Detection of a secreted MUC1/SEC protein by MUC1 isoform specific monoclonal antibodies*. Biochem. Biophys. Res. Commun, 1996. **228**: p. 115-121.
44. Baeckström D, N.O., Price MR, Lindholm L, Hansson GC, *Discrimination of MUC1 mucins from other sialyl-Le(a)-carrying glycoproteins produced by colon carcinoma cells using a novel monoclonal antibody*. Cancer Res, 1993 **53**(4): p. 755-61.
45. Peat N, G.S., Lalani N, Duhig T, Taylor-Papadimitriou J, *Tissue-specific expression of a human polymorphic epithelial mucin (MUC1) in transgenic mice*. Cancer Res, 1992 **52**(7): p. 1954-60.

46. Gendler, S.J., *MUC1, the renaissance molecule*. J Mammary Gland Biol Neoplasia, 2001. **6**(3): p. 339-53.
47. Mukherjee, P., et al., *Mice with spontaneous pancreatic cancer naturally develop MUC1-specific CTLs that eradicate tumors when adoptively transferred*. J Immunol, 2000. **165**(6): p. 3451-3460.
48. Zotter, S., et al., *Tissue and tumor distribution of human polymorphic epithelial mucin*. Cancer Reviews, 1988. **11-12**: p. 55-101.
49. Rahn, J.J., et al., *The importance of MUC1 cellular localization in patients with breast carcinoma*. Cancer, 2001. **91**(11): p. 1973-82.
50. Croce, M.V., et al., *Patterns of MUC1 tissue expression defined by an anti-MUC1 cytoplasmic tail monoclonal antibody in breast cancer*. J Histochem Cytochem, 2003. **51**(6): p. 781-8.
51. Levi, E., et al., *MUC1 and MUC2 in pancreatic neoplasia*. J Clin Pathol, 2004. **57**(5): p. 456-62.
52. Gendler, S.J. and P. Mukherjee, *Spontaneous adenocarcinoma mouse models for immunotherapy*. Trends Mol Med, 2001. **7**(10): p. 471-5.
53. Chhieng, D.C., et al., *MUC1 and MUC2 expression in pancreatic ductal carcinoma obtained by fine-needle aspiration*. Cancer, 2003. **99**(6): p. 365-71.
54. Kufe, D.W., *Functional targeting of the MUC1 oncogene in human cancers*. Cancer Biol Ther, 2009. **8**(13): p. 1197-203.
55. Gold, D.V., et al., *PAM4-reactive MUC1 is a biomarker for early pancreatic adenocarcinoma*. Clin Cancer Res, 2007. **13**(24): p. 7380-7.
56. Chauhan, S.C., et al., *Aberrant expression of MUC4 in ovarian carcinoma: diagnostic significance alone and in combination with MUC1 and MUC16 (CA125)*. Mod Pathol, 2006. **19**(10): p. 1386-94.
57. Kawamoto, T., et al., *Expression of MUC1 recognized by a monoclonal antibody MY.1E12 is a useful biomarker for tumor aggressiveness of carcinoma of the gallbladder*. Clin Exp Metastasis, 2004. **21**(4): p. 353-62.
58. Cozzi, P.J., et al., *MUC1, MUC2, MUC4, MUC5AC and MUC6 expression in the progression of prostate cancer*. Clin Exp Metastasis, 2005. **22**(7): p. 565-73.

59. Li Y, C.W., Ren J, Yu WH, Li Q, Yoshida K, Kufe D, *DF3/MUC1 signaling in multiple myeloma cells is regulated by interleukin-7*. *Cancer Biol Ther*, 2003. **2**(2): p. 187-93.
60. Al Masri A, G.S., *Muc1 affects c-Src signaling in PyV MT-induced mammary tumorigenesis*. *Oncogene*, 2005. **24**(38): p. 5799-808.
61. Mukherjee P, T.T., Basu GD, Gendler SJ, *MUC1 (CD227) interacts with lck tyrosine kinase in Jurkat lymphoma cells and normal T cells*. *J Leukoc Biol*, 2005. **77**(1): p. 90-9.
62. Yamamoto, M., et al., *Interaction of the DF3/MUC1 breast carcinoma-associated antigen and beta-catenin in cell adhesion*. *J Biol Chem*, 1997. **272**(19): p. 12492-4.
63. Wen, Y., et al., *Nuclear association of the cytoplasmic tail of MUC1 and beta-catenin*. *J Biol Chem*, 2003. **278**(39): p. 38029-39.
64. Li, Y., et al., *Heregulin targets gamma-catenin to the nucleolus by a mechanism dependent on the DF3/MUC1 oncoprotein*. *Mol Cancer Res*, 2003. **1**(10): p. 765-75.
65. Li, Y.Q., et al., *Interaction of glycogen synthase kinase-3 beta with the DF3/MUC1 carcinoma-associated antigen and beta-catenin*. *Mol Cell Biol*, 1998. **18**(12): p. 7216-7224.
66. Pandey, P., S. Kharbanda, and D. Kufe, *Association of the DF3/MUC1 breast cancer antigen with Grb2 and the Sos/Ras exchange protein*. *Cancer Res*, 1995. **55**(18): p. 4000-3.
67. Schroeder, J.A., et al., *Transgenic MUC1 interacts with EGFR and correlates with MAP kinase activation in the mouse mammary gland*. *J. Biol. Chem.*, 2001. **276**: p. 13057-13064.
68. Alroy, I. and Y. Yarden, *The ErbB signaling network in embryogenesis and oncogenesis: signal diversification through combinatorial ligand-receptor interactions*. *FEBS Lett*, 1997. **410**(1): p. 83-6.
69. Sporn, M.B., *The war on cancer*. *Lancet*, 1996. **347**(9012): p. 1377-81.
70. Kalluri, R. and M. Zeisberg, *Fibroblasts in cancer*. *Nat Rev Cancer*, 2006. **6**(5): p. 392-401.

71. Mbeunkui, F. and D.J. Johann, Jr., *Cancer and the tumor microenvironment: a review of an essential relationship*. *Cancer Chemother Pharmacol*, 2009. **63**(4): p. 571-82.
72. Nieto, M.A., *The snail superfamily of zinc-finger transcription factors*. *Nat Rev Mol Cell Biol*, 2002. **3**(3): p. 155-66.
73. Thiery, J.P., *Epithelial-mesenchymal transitions in tumour progression*. *Nat Rev Cancer*, 2002. **2**(6): p. 442-54.
74. Battle, E., et al., *The transcription factor snail is a repressor of E-cadherin gene expression in epithelial tumour cells*. *Nat Cell Biol*, 2000. **2**(2): p. 84-9.
75. Cano, A., et al., *The transcription factor snail controls epithelial-mesenchymal transitions by repressing E-cadherin expression*. *Nat Cell Biol*, 2000. **2**(2): p. 76-83.
76. Guaita, S., et al., *Snail induction of epithelial to mesenchymal transition in tumor cells is accompanied by MUC1 repression and ZEB1 expression*. *J Biol Chem*, 2002. **277**(42): p. 39209-16.
77. Roy LD, S.M., Subramani DB, Besmer D, Nath S, Tinder TL, Bajaj E, Shanmugam K, Lee YY, Hwang SI, Gendler SJ, Mukherjee P, *MUC1 enhances invasiveness of pancreatic cancer cells by inducing epithelial to mesenchymal transition*. *Oncogene*, 2010. **Epub ahead of print**.
78. Sahraei, M.C., J.Roy LD, Tinder TL, Nath, S. Dalia, R. Gendler SJ, Mukherjee P, *MUC1 regulates PDGFA expression during Pancreatic Cancer progression*. *Oncogene*, 2011. **online-submission**
79. Ornitz, D.M., et al., *Pancreatic neoplasia induced by SV40 T-antigen expression in acinar cells of transgenic mice*. *Science*, 1987. **238**(4824): p. 188-93.
80. Hingorani, S.R., et al., *Preinvasive and invasive ductal pancreatic cancer and its early detection in the mouse*. *Cancer Cell*, 2003. **4**: p. 437-450.
81. Cartwright T, R.D., Boehm KA., *Cancer of the pancreas: are we making progress? A review of studies in the US Oncology Research Network*. *Cancer Control*, 2008. **15**(4): p. 308-313.
82. Vähä-Koskela MJ, Heikkilä JE, and A.E. and Hinkkanen, *Oncolytic viruses in cancer therapy*. *Cancer Letters*, 2007. **254**(2): p. 178-216.

83. Liu TC, Galanis E, and D. and Kirn, *Clinical trial results with oncolytic virotherapy: a century of promise, a decade of progress*. Nature Clinical Practice: Oncology, 2007. **4**(2): p. 101-117.
84. Ahmed M, Cramer SD, and D.S. and Lyles, *Sensitivity of prostate tumors to wild type and M protein mutant vesicular stomatitis viruses*. Virology, 2004. **330**(1): p. 34-49.
85. Chang, G., et al., *Enhanced oncolytic activity of vesicular stomatitis virus encoding SV5-F protein against prostate cancer*. J Urol, 2010. **183**(4): p. 1611-8.
86. Moussavi, M., et al., *Oncolysis of prostate cancers induced by vesicular stomatitis virus in PTEN knockout mice*. Cancer Research, 2010. **70**(4): p. 1367-76.
87. Obuchi M, Fernandez M, and G.N. and Barber, *Development of recombinant vesicular stomatitis viruses that exploit defects in host defense to augment specific oncolytic activity*. Journal of Virology, 2003. **77**(16): p. 8843-8856.
88. Fernandez M, et al., *Genetically engineered vesicular stomatitis virus in gene therapy: application for treatment of malignant disease*. Journal of Virology, 2002. **76**(2): p. 895-904.
89. Ahmed, M., S. Puckett, and D.S. Lyles, *Susceptibility of breast cancer cells to an oncolytic matrix (M) protein mutant of vesicular stomatitis virus*. Cancer Gene Ther, 2010. **17**(12): p. 883-92.
90. Shi, W., et al., *Antitumor and antimetastatic activities of vesicular stomatitis virus matrix protein in a murine model of breast cancer*. J Mol Med, 2009. **87**(5): p. 493-506.
91. Galivo F, et al., *Interference of CD40L-mediated Tumor Immunotherapy by Oncolytic VSV*. Human Gene Therapy, 2010.
92. Edge RE, et al., *A let-7 MicroRNA-sensitive vesicular stomatitis virus demonstrates tumor-specific replication*. Molecular Therapy, 2008. **16**(8): p. 1437-1443.
93. Huang, T.G., et al., *Oncolysis of hepatic metastasis of colorectal cancer by recombinant vesicular stomatitis virus in immune-competent mice*. Mol Ther, 2003. **8**(3): p. 434-40.
94. Shinozaki, K., O. Ebert, and S.L. Woo, *Treatment of multi-focal colorectal carcinoma metastatic to the liver of immune-competent and syngeneic rats by*

- hepatic artery infusion of oncolytic vesicular stomatitis virus*. International Journal of Cancer. Journal International Du Cancer, 2005. **114**(4): p. 659-64.
95. Wu L, H.T., Meseck M, Altomonte J, Ebert O, Shinozaki K, García-Sastre A, Fallon J, Mandeli J, Woo SL., *rVSV(M Delta 51)-M3 is an effective and safe oncolytic virus for cancer therapy*. Human Gene Therapy, 2008. **19**(6): p. 635-647.
96. Altomonte, J., et al., *Enhanced oncolytic potency of vesicular stomatitis virus through vector-mediated inhibition of NK and NKT cells*. Cancer Gene Ther, 2009. **16**(3): p. 266-78.
97. Ausubel, L.J., et al., *Current good manufacturing practice production of an oncolytic recombinant vesicular stomatitis viral vector for cancer treatment*. Hum Gene Ther, 2011. **22**(4): p. 489-97.
98. Wollmann G, R.V., Simon I, Rose JK, van den Pol AN., *Some attenuated variants of vesicular stomatitis virus show enhanced oncolytic activity against human glioblastoma cells relative to normal brain cells*. Journal of Virology, 2010. **84**(3): p. 1563-1573.
99. Cary, Z.D., M.C. Willingham, and D.S. Lyles, *Oncolytic Vesicular Stomatitis Virus Induces Apoptosis in U87 Glioblastoma Cells by a Type II Death Receptor Mechanism and Induces Cell Death and Tumor Clearance In Vivo*. J Virol, 2011. **85**(12): p. 5708-17.
100. Ozduman, K., et al., *Systemic vesicular stomatitis virus selectively destroys multifocal glioma and metastatic carcinoma in brain*. The Journal of Neuroscience : the Official Journal of the Society For Neuroscience, 2008. **28**(8): p. 1882-93.
101. Barber, G.N., *Vesicular stomatitis virus as an oncolytic vector*. Viral Immunology, 2004. **17**(4): p. 516-527.
102. Lyles, D., Rupprecht, CE., *Rhabdoviridae*, in *Fields Virology*, e. In: DM Knipe and PM Howley, Editor 2007, Lippincott Williams & Wilkins, Philadelphia, 5th edition. p. 1363-1408.
103. Adsay, N.V., et al., *The dichotomy in the preinvasive neoplasia to invasive carcinoma sequence in the pancreas: differential expression of MUC1 and MUC2 supports the existence of two separate pathways of carcinogenesis*. Mod Pathol, 2002. **15**(10): p. 1087-95.

104. Moniaux, N., et al., *Multiple roles of mucins in pancreatic cancer, a lethal and challenging malignancy*. Br J Cancer, 2004. **91**(9): p. 1633-8.
105. Tirona, M.T., R. Sehgal, and O. Ballester, *Prevention of breast cancer (Part II): risk reduction strategies*. Cancer Invest, 2010. **28**(10): p. 1070-7.
106. Althuis, M.D., et al., *Etiology of hormone receptor-defined breast cancer: a systematic review of the literature*. Cancer Epidemiol Biomarkers Prev, 2004. **13**(10): p. 1558-68.
107. Pelekanou, V. and G. Leclercq, *Recent insights into the effect of natural and environmental estrogens on mammary development and carcinogenesis*. Int J Dev Biol, 2011. **55**(7-9): p. 869-78.
108. Carey, L.A., et al., *Race, breast cancer subtypes, and survival in the Carolina Breast Cancer Study*. JAMA, 2006. **295**(21): p. 2492-502.
109. Antonia, S., J.J. Mule, and J.S. Weber, *Current developments of immunotherapy in the clinic*. Curr Opin Immunol, 2004. **16**(2): p. 130-6.
110. Avigan, D., et al., *Fusion cell vaccination of patients with metastatic breast and renal cancer induces immunological and clinical responses*. Clin Cancer Res, 2004. **10**(14): p. 4699-708.
111. Jaffee, E.M., et al., *A phase I clinical trial of lethally irradiated allogeneic pancreatic tumor cells transfected with the GM-CSF gene for the treatment of pancreatic adenocarcinoma*. Hum Gene Ther, 1998. **9**(13): p. 1951-71.
112. Jaffee, E.M., et al., *Novel allogeneic granulocyte-macrophage colony-stimulating factor-secreting tumor vaccine for pancreatic cancer: a phase I trial of safety and immune activation*. J Clin Oncol, 2001. **19**(1): p. 145-56.
113. Mukherjee, P., et al., *MUC1-specific CTLs are non-functional within a pancreatic tumor microenvironment*. Glycoconj J, 2001 (published in 2003). **18**: p. 931-942.
114. Laheru, D., B. Biedrzycki, and E.M. Jaffee, *Immunologic approaches to the management of pancreatic cancer*. Cancer J, 2001. **7**(4): p. 324-37.
115. Finn, O.J., et al., *MUC-1 epithelial tumor mucin-based immunity and cancer vaccines*. Immunological Reviews, 1995. **145**: p. 61-89.

116. Ramanathan, R.K., et al., *Phase I study of a MUC1 vaccine composed of different doses of MUC1 peptide with SB-AS2 adjuvant in resected and locally advanced pancreatic cancer*. *Cancer Immunol Immunother*, 2005. **54**(3): p. 254-64.
117. Girling, A., et al., *A core protein epitope of the polymorphic epithelial mucin detected by the monoclonal antibody SM-3 is selectively exposed in a range of primary carcinomas*. *Int J Cancer*, 1989. **43**: p. 1072-1076.
118. Treon, S.P., et al., *MUC1 core protein is expressed on multiple myeloma cells and is induced by dexamethasone*. *Blood*, 1999. **93**(4): p. 1287-1298.
119. Brossart, P., et al., *The epithelial tumor antigen MUC1 is expressed in hematological malignancies and is recognized by MUC1-specific cytotoxic T-lymphocytes*. *Cancer Res*, 2001. **61**(18): p. 6846-50.
120. Barnd, D.L., et al., *Specific, major histocompatibility complex-unrestricted recognition of tumor-associated mucins by human cytotoxic T cells*. *Proc Natl Acad Sci U S A*, 1989. **86**(18): p. 7159-63.
121. Ioannides, C.G., et al., *Cytotoxic T cells from ovarian malignant tumors can recognize polymorphic epithelial mucin core peptides*. *J Immunol*, 1993. **151**(7): p. 3693-703.
122. Jerome, K.R., N. Domenech, and O.J. Finn, *Tumor-specific cytotoxic T cell clones from patients with breast and pancreatic adenocarcinoma recognize EBV-immortalized B cells transfected with polymorphic epithelial mucin complementary DNA*. *J Immunol*, 1993. **151**(3): p. 1654-62.
123. Rughetti, A., et al., *Human B-cell immune response to the polymorphic epithelial mucin*. *Cancer Res*, 1993. **53**(11): p. 2457-9.
124. Kotera, Y., et al., *Humoral immunity against a tandem repeat epitope of human mucin MUC-1 in sera from breast, pancreatic, and colon cancer patients*. *Cancer Res*, 1994. **54**(11): p. 2856-60.
125. Hanisch, F.G. and S. Muller, *MUC1: the polymorphic appearance of a human mucin*. *Glycobiology*, 2000. **10**(5): p. 439-49.
126. Agrawal, B., M.A. Reddish, and B.M. Longenecker, *In vitro induction of MUC-1 peptide-specific type 1 T lymphocyte and cytotoxic T lymphocyte responses from healthy multiparous donors*. *J Immunol*, 1996. **157**(5): p. 2089-95.

127. Reddish, M., et al., *Anti-MUC1 class I restricted CTLs in metastatic breast cancer patients immunized with a synthetic MUC1 peptide*. *Int J Cancer*, 1998. **76**(6): p. 817-23.
128. Singh, R. and D. Bandyopadhyay, *MUC1: a target molecule for cancer therapy*. *Cancer Biol Ther*, 2007. **6**(4): p. 481-6.
129. Mukherjee, P., et al., *MUC1-specific CTLs are non-functional within a pancreatic tumor microenvironment*. *Glycoconj J*, 2001. **18**(11-12): p. 931-42.
130. Mukherjee, P., et al., *Therapeutic efficacy of MUC1-specific cytotoxic T lymphocytes and CD137 co-stimulation in a spontaneous breast cancer model*. *Breast Dis*, 2004. **20**: p. 53-63.
131. Minn, A.J., et al., *Genes that mediate breast cancer metastasis to lung*. *Nature*, 2005. **436**(7050): p. 518-24.
132. Eberhart, C.E. and R.N. Dubois, *Eicosanoids and the gastrointestinal tract*. *Gastroenterology*, 1995. **109**(1): p. 285-301.
133. O'Neill, G.P. and A.W. Ford-Hutchinson, *Expression of mRNA for cyclooxygenase-1 and cyclooxygenase-2 in human tissues*. *FEBS Lett*, 1993. **330**(2): p. 156-60.
134. Okuno, K., et al., *A high level of prostaglandin E2 (PGE2) in the portal vein suppresses liver-associated immunity and promotes liver metastases*. *Surg Today*, 1995. **25**(11): p. 954-8.
135. Takayama, K., et al., *Prostaglandin E2 suppresses chemokine production in human macrophages through the EP4 receptor*. *J Biol Chem*, 2002. **277**(46): p. 44147-54.
136. Basu, G.D., et al., *Cyclooxygenase-2 inhibitor enhances the efficacy of a breast cancer vaccine: role of IDO*. *J Immunol*, 2006. **177**(4): p. 2391-402.
137. Kai, S., et al., *Inhibition of indoleamine 2,3-dioxygenase suppresses NK cell activity and accelerates tumor growth*. *J Exp Ther Oncol*, 2003. **3**(6): p. 336-45.
138. Takikawa, O., et al., *Tryptophan degradation in mice initiated by indoleamine 2,3-dioxygenase*. *J Biol Chem*, 1986. **261**(8): p. 3648-53.
139. Munn, D.H., et al., *Prevention of allogeneic fetal rejection by tryptophan catabolism*. *Science*, 1998. **281**(5380): p. 1191-3.

140. Miki, T., et al., *Blockade of tryptophan catabolism prevents spontaneous tolerogenicity of liver allografts*. *Transplant Proc*, 2001. **33**(1-2): p. 129-30.
141. Mellor, A.L. and D.H. Munn, *Tryptophan catabolism and T-cell tolerance: immunosuppression by starvation?* *Immunol Today*, 1999. **20**(10): p. 469-73.
142. Yoshida, R., et al., *Tryptophan degradation in transplanted tumor cells undergoing rejection*. *J Immunol*, 1988. **141**(8): p. 2819-23.
143. Takikawa, O., A. Habara-Ohkubo, and R. Yoshida, *IFN-gamma is the inducer of indoleamine 2,3-dioxygenase in allografted tumor cells undergoing rejection*. *J Immunol*, 1990. **145**(4): p. 1246-50.
144. Hwu, P., et al., *Indoleamine 2,3-dioxygenase production by human dendritic cells results in the inhibition of T cell proliferation*. *J Immunol*, 2000. **164**(7): p. 3596-9.
145. Uyttenhove, C., et al., *Evidence for a tumoral immune resistance mechanism based on tryptophan degradation by indoleamine 2,3-dioxygenase*. *Nat Med*, 2003. **9**(10): p. 1269-74.
146. Munn, D.H. and A.L. Mellor, *IDO and tolerance to tumors*. *Trends Mol Med*, 2004. **10**(1): p. 15-8.
147. Mellor, A.L. and D.H. Munn, *IDO expression by dendritic cells: tolerance and tryptophan catabolism*. *Nat Rev Immunol*, 2004. **4**(10): p. 762-74.
148. Fallarino, F., et al., *T cell apoptosis by tryptophan catabolism*. *Cell Death Differ*, 2002. **9**(10): p. 1069-77.
149. Grohmann, U., et al., *A defect in tryptophan catabolism impairs tolerance in nonobese diabetic mice*. *J Exp Med*, 2003. **198**(1): p. 153-60.
150. Munn, D.H., et al., *GCN2 kinase in T cells mediates proliferative arrest and anergy induction in response to indoleamine 2,3-dioxygenase*. *Immunity*, 2005. **22**(5): p. 633-42.
151. Mellor, A.L., et al., *Cells expressing indoleamine 2,3-dioxygenase inhibit T cell responses*. *J Immunol*, 2002. **168**(8): p. 3771-6.
152. Otto, J.C. and W.L. Smith, *Prostaglandin endoperoxide synthases-1 and -2*. *J Lipid Mediat Cell Signal*, 1995. **12**(2-3): p. 139-56.

153. Narumiya, S. and G.A. FitzGerald, *Genetic and pharmacological analysis of prostanoid receptor function*. J Clin Invest, 2001. **108**(1): p. 25-30.
154. Rowse, G.J., et al., *Tolerance and immunity to MUC1 in a human MUC1 transgenic murine model*. Cancer Res, 1998. **58**(2): p. 315-21.
155. Saif, M.W., *Pancreatic cancer: highlights from the 42nd annual meeting of the American Society of Clinical Oncology, 2006*. JOP, 2006. **7**(4): p. 337-48.
156. Acres, B. and J.M. Limacher, *MUC1 as a target antigen for cancer immunotherapy*. Expert Rev Vaccines, 2005. **4**(4): p. 493-502.
157. Tinder, T.L., et al., *MUC1 enhances tumor progression and contributes toward immunosuppression in a mouse model of spontaneous pancreatic adenocarcinoma*. J Immunol, 2008. **181**(5): p. 3116-25.
158. Kohlgraf, K.G., et al., *Contribution of the MUC1 tandem repeat and cytoplasmic tail to invasive and metastatic properties of a pancreatic cancer cell line*. Cancer Research, 2003. **63**(16): p. 5011-20.
159. Hingorani, S.R., et al., *Preinvasive and invasive ductal pancreatic cancer and its early detection in the mouse*. Cancer Cell, 2003. **4**(6): p. 437-50.
160. Adhikary, R., et al., *Fluorescence spectroscopy of the retina for diagnosis of transmissible spongiform encephalopathies*. Anal Chem, 2010. **82**(10): p. 4097-101.
161. Mukherjee, P., et al., *Progression of pancreatic adenocarcinoma is significantly impeded with a combination of vaccine and COX-2 inhibition*. J Immunol, 2009. **182**(1): p. 216-24.
162. Spicer, A.P., et al., *Delayed mammary tumor progression in Muc-1 null mice*. J Biol Chem, 1995. **270**(50): p. 30093-101.
163. Roy, L.D., et al., *MUC1 enhances invasiveness of pancreatic cancer cells by inducing epithelial to mesenchymal transition*. Oncogene, 2010. **10.1038/onc.2010.526** 2010/11/26(Nov 22): p. 10.1038/onc.2010.526.
164. Hoang, M.V., J.A. Nagy, and D.R. Senger, *Cdc42-mediated inhibition of GSK-3beta improves angio-architecture and lumen formation during VEGF-driven pathological angiogenesis*. Microvasc Res, 2010.

165. Sheng, H., et al., *Modulation of apoptosis and Bcl-2 expression by prostaglandin E2 in human colon cancer cells*. Cancer Res, 1998. **58**(2): p. 362-6.
166. Sheng, H., et al., *Prostaglandin E2 increases growth and motility of colorectal carcinoma cells*. J Biol Chem, 2001. **276**(21): p. 18075-81.
167. Wang, R., et al., *Regulation of Cdc25C by ERK-MAP kinases during the G2/M transition*. Cell, 2007. **128**(6): p. 1119-32.
168. Kalluri, H.S., R. Vemuganti, and R.J. Dempsey, *Mechanism of insulin-like growth factor I-mediated proliferation of adult neural progenitor cells: role of Akt*. Eur J Neurosci, 2007. **25**(4): p. 1041-8.
169. Wiese, C., et al., *Nestin expression--a property of multi-lineage progenitor cells?* Cell Mol Life Sci, 2004. **61**(19-20): p. 2510-22.
170. Beckers, T., et al., *2-aryloxyindoles, a novel class of potent, orally active small molecule tubulin inhibitors*. Cancer Res, 2002. **62**(11): p. 3113-9.
171. Kufe, D.W., *Mucins in cancer: function, prognosis and therapy*. Nat Rev Cancer, 2009. **9**(12): p. 874-85.
172. Schroeder, J.A., et al., *MUC1 overexpression results in mammary gland tumorigenesis and prolonged alveolar differentiation*. Oncogene, 2004. **23**: p. 5739-5747.
173. Roy, L.D., et al., *MUC1 enhances invasiveness of pancreatic cancer cells by inducing epithelial to mesenchymal transition*. Oncogene, 2010.
174. Russell, S.J. and K.W. Peng, *Viruses as anticancer drugs*. Trends Pharmacol Sci, 2007. **28**(7): p. 326-33.
175. Breitbach, C.J., et al., *Navigating the clinical development landscape for oncolytic viruses and other cancer therapeutics: no shortcuts on the road to approval*. Cytokine Growth Factor Rev, 2010. **21**(2-3): p. 85-9.
176. Naik, S. and S.J. Russell, *Engineering oncolytic viruses to exploit tumor specific defects in innate immune signaling pathways*. Expert Opin Biol Ther, 2009. **9**(9): p. 1163-76.
177. Stojdl DF, et al., *Exploiting tumor-specific defects in the interferon pathway with a previously unknown oncolytic virus*. Nature Medicine, 2000. **6**(7): p. 821-825.

178. Stathis A and M.J. Moore, *Advanced pancreatic carcinoma: current treatment and future challenges*. Nature Reviews in Clinical Oncology, 2010. **7**: p. 163-172.
179. Lindsay TH, et al., *Pancreatic cancer pain and its correlation with changes in tumor vasculature, macrophage infiltration, neuronal innervation, body weight and disease progression*. Pain, 2005. **119**(1-3): p. 233-246.
180. Farrow B, Albo D, and D.H. and Berger, *The role of the tumor microenvironment in the progression of pancreatic cancer*. Journal of Surgical Research, 2008. **149**(2): p. 319-328.
181. Huch M, G.A., José A, González JR, Alemany R, Fillat C., *Urokinase-type plasminogen activator receptor transcriptionally controlled adenoviruses eradicate pancreatic tumors and liver metastasis in mouse models*. . Neoplasia, 2009. **11**(6): p. 518-528.
182. He, X., et al., *E1B-55kD-deleted oncolytic adenovirus armed with canstatin gene yields an enhanced anti-tumor efficacy on pancreatic cancer*. Cancer Letters, 2009. **285**: p. 89-98.
183. Kuhlmann, K.F., D.J. Gouma, and J.G. Wesseling, *Adenoviral gene therapy for pancreatic cancer: where do we stand?* Dig Surg, 2008. **25**(4): p. 278-92.
184. Eisenberg, D.P., et al., *Hyperthermia potentiates oncolytic herpes viral killing of pancreatic cancer through a heat shock protein pathway*. Surgery, 2010. **148**(2): p. 325-34.
185. Kasuya, H., et al., *Suitability of a US3-inactivated HSV mutant (LIBR1) as an oncolytic virus for pancreatic cancer therapy*. Cancer Gene Ther, 2007. **14**(6): p. 533-42.
186. Nakao, A., et al., *Clinical experiment of mutant herpes simplex virus HF10 therapy for cancer*. Curr Cancer Drug Targets, 2007. **7**(2): p. 169-74.
187. Sarinella, F., et al., *Oncolysis of pancreatic tumour cells by a gamma34.5-deleted HSV-1 does not rely upon Ras-activation, but on the PI 3-kinase pathway*. Gene Therapy, 2006. **13**(14): p. 1080-7.
188. Watanabe, I., et al., *Effects of tumor selective replication-competent herpes viruses in combination with gemcitabine on pancreatic cancer*. Cancer Chemother Pharmacol, 2008. **61**(5): p. 875-82.

189. Etoh, T., et al., *Oncolytic viral therapy for human pancreatic cancer cells by reovirus*. Clin Cancer Res, 2003. **9**(3): p. 1218-23.
190. Himeno, Y., et al., *Efficacy of oncolytic reovirus against liver metastasis from pancreatic cancer in immunocompetent models*. Int J Oncol, 2005. **27**(4): p. 901-6.
191. Hirano, S., et al., *Reovirus inhibits the peritoneal dissemination of pancreatic cancer cells in an immunocompetent animal model*. Oncol Rep, 2009. **21**(6): p. 1381-4.
192. von Messling, V. and R. Cattaneo, *Toward novel vaccines and therapies based on negative-strand RNA viruses*. Curr Top Microbiol Immunol, 2004. **283**: p. 281-312.
193. Lichty BD, et al., *Vesicular stomatitis virus: re-inventing the bullet*. TRENDS in Molecular Medicine, 2004. **10**(5): p. 210-216.
194. Gaddy DF and D.S. and Lyles, *Oncolytic vesicular stomatitis virus induces apoptosis via signaling through PKR, Fas, and Daxx*. Journal of Virology, 2007. **81**(6): p. 2792-2804.
195. Quiroz E, et al., *A human case of encephalitis associated with vesicular stomatitis virus (Indiana serotype) infection*. The American Journal of Tropical Medicine and Hygiene, 1988. **39**(3): p. 312-314.
196. Kelly EJ, et al., *Attenuation of vesicular stomatitis virus encephalitis through microRNA targeting*. Journal of Virology, 2010. **84**(3): p. 1550-1562.
197. Ahmed M, M.T., Puckett S, Kock ND, Lyles DS., *Immune response in the absence of neurovirulence in mice infected with m protein mutant vesicular stomatitis virus*. Journal of Virology, 2008. **82**(18): p. 9273-9277.
198. Okabe T, Yamaguchi N, and O. N., *Establishment and characterization of a carcinoembryonic antigen (CEA)-producing cell line from a human carcinoma of the exocrine pancreas*. Cancer, 1983. **51**(4): p. 662-668.
199. Iwamura T, Katsuki T, and I. K., *Establishment and characterization of a human pancreatic cancer cell line (SUIT-2) producing carcinoembryonic antigen and carbohydrate antigen 19-9*. Jpn J Cancer Res., 1987. **78**(1): p. 54-62.
200. Furukawa T, et al., *Long-term culture and immortalization of epithelial cells from normal adult human pancreatic ducts transfected by the E6E7 gene of human*

- papilloma virus 16*. The American Journal of Pathology, 1996. **148**(6): p. 1763-1770.
201. Lawson, N.D., et al., *Recombinant vesicular stomatitis viruses from DNA*. Proc.Natl.Acad.Sci.U.S.A, 1995. **92**(10): p. 4477-4481.
 202. Bischoff, J.R., et al., *An adenovirus mutant that replicates selectively in p53-deficient human tumor cells*. Science, 1996. **274**(5286): p. 373-6.
 203. Crompton, A.M. and D.H. Kirn, *From ONYX-015 to armed vaccinia viruses: the education and evolution of oncolytic virus development*. Curr Cancer Drug Targets, 2007. **7**(2): p. 133-9.
 204. Huang TG, et al., *Telomerase-dependent oncolytic adenovirus for cancer treatment*. Gene Therapy, 2003. **10**(15): p. 1241-1247.
 205. Wiegand, M.A., et al., *De novo synthesis of N and P proteins as a key step in Sendai virus gene expression*. J Virol, 2007. **81**(24): p. 13835-44.
 206. Hallak LK, et al., *Iduronic acid-containing glycosaminoglycans on target cells are required for efficient respiratory syncytial virus infection*. Virology, 2000. **271**(2): p. 264-275.
 207. Moyer, S.A., S.C. Baker, and J.L. Lessard, *Tubulin: a factor necessary for the synthesis of both Sendai virus and vesicular stomatitis virus RNAs*. Proc.Natl.Acad.Sci.U.S.A, 1986/8. **83**(15): p. 5405-5409.
 208. Goel, A., et al., *Radioiodide imaging and radiovirotherapy of multiple myeloma using VSV(Delta51)-NIS, an attenuated vesicular stomatitis virus encoding the sodium iodide symporter gene*. Blood, 2007. **110**(7): p. 2342-50.
 209. Stojdl DF, L.B., tenOever BR, Paterson JM, Power AT, Knowles S, Marius R, Reynard J, Poliquin L, Atkins H, Brown EG, Durbin RK, Durbin JE, Hiscott J, Bell JC., *VSV strains with defects in their ability to shutdown innate immunity are potent systemic anti-cancer agents*. Cancer Cell, 2003. **4**(4): p. 263-275.
 210. Ebert O, et al., *Systemic therapy of experimental breast cancer metastases by mutant vesicular stomatitis virus in immune-competent mice*. Cancer Gene Therapy, 2005. **12**(4): p. 350-358.
 211. Kinoh H, I.M., Washizawa K, Yamamoto T, Fujikawa S, Tokusumi Y, Iida A, Nagai Y, Hasegawa M., *Generation of a recombinant Sendai virus that is*

- selectively activated and lyses human tumor cells expressing matrix metalloproteinases.* Gene Therapy, 2004. **11**(14): p. 1137-1145.
212. Kinoh H, I.M., *New cancer therapy using genetically-engineered oncolytic Sendai virus vector.* Frontiers in Bioscience, 2008. **13**: p. 2327-2334.
213. Yonemitsu Y, U.Y., Kinoh H, Hasegawa M., *Immunostimulatory virotherapy using recombinant Sendai virus as a new cancer therapeutic regimen.* Frontiers in Bioscience, 2008. **13**: p. 4953-4959.
214. Komaru A, U.Y., Furuya A, Tanaka S, Yoshida K, Kato T, Kinoh H, Harada Y, Suzuki H, Inoue M, Hasegawa M, Ichikawa T, Yonemitsu Y., *Sustained and NK/CD4+ T cell-dependent efficient prevention of lung metastasis induced by dendritic cells harboring recombinant Sendai virus.* Journal of Immunology, 2009. **183**(7): p. 421dd1-4219.
215. Echchgadda I, et al., *Anticancer oncolytic activity of respiratory syncytial virus.* Cancer Gene Ther, 2009. **16**(12): p. 923-935.
216. Echchgadda I, et al., *Oncolytic targeting of androgen-sensitive prostate tumor by the respiratory syncytial virus (RSV): consequences of deficient interferon-dependent antiviral defense.* BMC Cancer, 2011. **28**(11): p. 43.
217. Barber, G.N., *VSV-tumor selective replication and protein translation.* Oncogene, 2005. **24**(52): p. 7710-7719.
218. Kasuya H, et al., *The potential of oncolytic virus therapy for pancreatic cancer.* Cancer Gene Therapy, 2005. **12**(9): p. 725-736.
219. Saloura, V., et al., *Evaluation of an attenuated vesicular stomatitis virus vector expressing interferon-beta for use in malignant pleural mesothelioma: heterogeneity in interferon responsiveness defines potential efficacy.* Hum Gene Ther, 2010. **21**(1): p. 51-64.
220. Linge, C., et al., *Interferon system defects in human malignant melanoma.* Cancer Research, 1995. **55**(18): p. 4099-104.
221. Wong, L.H., et al., *Interferon-resistant human melanoma cells are deficient in ISGF3 components, STAT1, STAT2, and p48-ISGF3gamma.* J Biol Chem, 1997. **272**(45): p. 28779-85.
222. Sun, W.H., et al., *Interferon-alpha resistance in a cutaneous T-cell lymphoma cell line is associated with lack of STAT1 expression.* Blood, 1998. **91**(2): p. 570-6.

223. Matin, S.F., et al., *Impaired alpha-interferon signaling in transitional cell carcinoma: lack of p48 expression in 5637 cells*. Cancer Research, 2001. **61**(5): p. 2261-6.
224. Pfeffer, L.M., et al., *Human renal cancers resistant to IFN's antiproliferative action exhibit sensitivity to IFN's gene-inducing and antiviral actions*. J Urol, 1996. **156**(5): p. 1867-71.
225. Hamacher, R., et al., *Apoptotic pathways in pancreatic ductal adenocarcinoma*. Mol Cancer, 2008. **7**: p. 64.
226. Gaddy DF and D.S. and Lyles, *Vesicular stomatitis viruses expressing wild-type or mutant M proteins activate apoptosis through distinct pathways*. Journal of Virology, 2005. **79**(7): p. 4170-4179.
227. Sharif-Askari, E., et al., *Bax-dependent mitochondrial membrane permeabilization enhances IRF3-mediated innate immune response during VSV infection*. Virology, 2007. **365**(1): p. 20-33.
228. Ottolino-Perry, K., et al., *Intelligent design: combination therapy with oncolytic viruses*. Mol Ther, 2010. **18**(2): p. 251-63.
229. Le Boeuf, F., et al., *Synergistic interaction between oncolytic viruses augments tumor killing*. Mol Ther, 2010. **18**(5): p. 888-95.
230. Parker, S.L., et al., *Cancer statistics, 1997*. CA Cancer J Clin, 1997. **47**(1): p. 5-27.
231. Jonckheere, N. and I. Van Seuningen, *The membrane-bound mucins: From cell signalling to transcriptional regulation and expression in epithelial cancers*. Biochimie, 2010. **92**(1): p. 1-11.
232. Reichert, M. and A.K. Rustgi, *Pancreatic ductal cells in development, regeneration, and neoplasia*. J Clin Invest, 2011. **121**(12): p. 4572-8.
233. Besmer, D.M., et al., *Pancreatic Ductal Adenocarcinoma (PDA) mice lacking Mucin 1 have a profound defect in tumor growth and metastasis*. Cancer Research, 2011.
234. Gudjonsson, B., *Cancer of the pancreas. 50 years of surgery*. Cancer, 1987. **60**(9): p. 2284-303.

235. Hastie, E. and V.Z. Grdzlishvili, *Vesicular stomatitis virus as a flexible platform for oncolytic virotherapy against cancer*. J Gen Virol, 2012. **93**(Pt 12): p. 2529-45.
236. Wollmann, G., et al., *Some attenuated variants of vesicular stomatitis virus show enhanced oncolytic activity against human glioblastoma cells relative to normal brain cells*. J Virol, 2010. **84**(3): p. 1563-73.
237. Murphy, A.M., et al., *Vesicular stomatitis virus as an oncolytic agent against pancreatic ductal adenocarcinoma*. J Virol, 2012. **86**(6): p. 3073-87.
238. Moerdyk-Schauwecker, M., et al., *Resistance of pancreatic cancer cells to oncolytic vesicular stomatitis virus: Role of type I interferon signaling*. Virology, 2012.
239. Besmer, D.M., et al., *Pancreatic ductal adenocarcinoma mice lacking mucin 1 have a profound defect in tumor growth and metastasis*. Cancer Res, 2011. **71**(13): p. 4432-42.
240. Morikane, K., et al., *Organ-specific pancreatic tumor growth properties and tumor immunity*. Cancer immunology, immunotherapy : CII, 1999. **47**(5): p. 287-96.
241. Burdick, M.D., et al., *Oligosaccharides expressed on MUC1 produced by pancreatic and colon tumor cell lines*. J Biol Chem, 1997. **272**(39): p. 24198-202.
242. Schroeder, J.A., et al., *Transgenic MUC1 interacts with epidermal growth factor receptor and correlates with mitogen-activated protein kinase activation in the mouse mammary gland*. J Biol Chem, 2001. **276**(16): p. 13057-64.
243. Taylor-Papadimitriou, J., et al., *Monoclonal antibodies to epithelium-specific components of the human milk fat globule membrane: production and reaction with cells in culture*. International journal of cancer. Journal international du cancer, 1981. **28**(1): p. 17-21.
244. Kalvodova L, S.J., Cordo S, Ejsing CS, Shevchenko A, Simons K., *The lipidomes of vesicular stomatitis virus, semliki forest virus, and the host plasma membrane analyzed by quantitative shotgun mass spectrometry*. Journal of Virology, 2009. **83**(16): p. 7996-8003.
245. Fuerst, T.R. and B. Moss, *Structure and stability of mRNA synthesized by vaccinia virus-encoded bacteriophage T7 RNA polymerase in mammalian cells*.

- Importance of the 5' untranslated leader.* J.Mol.Biol., 1989/3/20. **206**(2): p. 333-348.
246. Furr, S.R., et al., *A role for DNA-dependent activator of interferon regulatory factor in the recognition of herpes simplex virus type 1 by glial cells.* Journal of neuroinflammation, 2011. **8**: p. 99.
247. Akporiaye ET, B.-D.D., Gendler SJ, Mukherjee P, Madsen CS, Hahn T, Besselsen DG, Dial SM, Cui H, Trevor K., *Characterization of the MUC1.Tg/MIN transgenic mouse as a model for studying antigen-specific immunotherapy of adenomas.* Vaccine, 2007. **25**(39-40): p. 6965-6974.
248. Tinder TL, et al., *MUC1 enhances tumor progression and contributes toward immunosuppression in a mouse model of spontaneous pancreatic adenocarcinoma.* The Journal of Immunology, 2008. **181**(5): p. 3116-3125.
249. Black, B.L., et al., *The role of vesicular stomatitis virus matrix protein in inhibition of host-directed gene expression is genetically separable from its function in virus assembly.* J.Virol., 1993. **67**(8): p. 4814-4821.
250. Coulon, P., et al., *Genetic evidence for multiple functions of the matrix protein of vesicular stomatitis virus.* The Journal of general virology, 1990. **71** (Pt 4): p. 991-6.
251. Grdzlishvili, V.Z., et al., *Mutual interference between genomic RNA replication and subgenomic mRNA transcription in brome mosaic virus.* J Virol, 2005. **79**(3): p. 1438-51.
252. Corbett, T.H., et al., *Induction and chemotherapeutic response of two transplantable ductal adenocarcinomas of the pancreas in C57BL/6 mice.* Cancer Res, 1984. **44**(2): p. 717-26.
253. Morikane, K., et al., *Organ-specific pancreatic tumor growth properties and tumor immunity.* Cancer Immunol Immunother, 1999. **47**(5): p. 287-96.
254. Brunner, T., *[Gemcitabine in the chemoradiotherapy for locally advanced pancreatic cancer: a meta-analysis].* Strahlenther Onkol, 2012. **188**(4): p. 366-7.
255. Kim, G.E., et al., *Aberrant expression of MUC5AC and MUC6 gastric mucins and sialyl Tn antigen in intraepithelial neoplasms of the pancreas.* Gastroenterology, 2002. **123**(4): p. 1052-60.

256. Habte, H.H., et al., *Inhibition of human immunodeficiency virus type 1 activity by purified human breast milk mucin (MUC1) in an inhibition assay*. Neonatology, 2008. **93**(3): p. 162-70.
257. Habte, H.H., et al., *Antiviral activity of purified human breast milk mucin*. Neonatology, 2007. **92**(2): p. 96-104.
258. Saeland, E., et al., *MUC1 in human milk blocks transmission of human immunodeficiency virus from dendritic cells to T cells*. Mol Immunol, 2009. **46**(11-12): p. 2309-16.
259. Arcasoy, S.M., et al., *MUC1 and other sialoglycoconjugates inhibit adenovirus-mediated gene transfer to epithelial cells*. Am J Respir Cell Mol Biol, 1997. **17**(4): p. 422-35.
260. Stonebraker, J.R., et al., *Glycocalyx restricts adenoviral vector access to apical receptors expressed on respiratory epithelium in vitro and in vivo: role for tethered mucins as barriers to luminal infection*. J Virol, 2004. **78**(24): p. 13755-68.
261. Walters, R.W., et al., *Secreted and transmembrane mucins inhibit gene transfer with AAV4 more efficiently than AAV5*. The Journal of biological chemistry, 2002. **277**(26): p. 23709-13.
262. Horm, T.M. and J.A. Schroeder, *MUC1 and metastatic cancer: Expression, function and therapeutic targeting*. Cell adhesion & migration, 2013. **7**(2).
263. Reddy, P.K., et al., *Interferon-gamma upregulates MUC1 expression in haematopoietic and epithelial cancer cell lines, an effect associated with MUC1 mRNA induction*. European journal of cancer, 2003. **39**(3): p. 397-404.
264. Ahmad, R., et al., *MUC1 oncoprotein activates the IkappaB kinase beta complex and constitutive NF-kappaB signalling*. Nature cell biology, 2007. **9**(12): p. 1419-27.
265. Thompson, E.J., et al., *Tyrosines in the MUC1 cytoplasmic tail modulate transcription via the extracellular signal-regulated kinase 1/2 and nuclear factor-kappaB pathways*. Molecular cancer research : MCR, 2006. **4**(7): p. 489-97.
266. Diaz RM, G.F., Kottke T, Wongthida P, Qiao J, Thompson J, Valdes M, Barber G, Vile RG., *Oncolytic immunovirotherapy for melanoma using vesicular stomatitis virus*. Cancer Research, 2007. **67**(6): p. 2840-2848.

267. Wongthida, P., et al., *Activating systemic T-cell immunity against self tumor antigens to support oncolytic virotherapy with vesicular stomatitis virus*. Hum Gene Ther, 2011. **22**(11): p. 1343-53.
268. Hastie, E. and V. Grdzlishvili, *Vesicular stomatitis virus as a flexible platform for oncolytic virotherapy against cancer*. Journal of General Virology, 2012.
269. Cheever, M.A., et al., *The prioritization of cancer antigens: a national cancer institute pilot project for the acceleration of translational research*. Clin Cancer Res, 2009. **15**(17): p. 5323-37.
270. Mukherjee, P., et al., *MUC1-specific immune therapy generates a strong anti-tumor response in a MUC1-tolerant colon cancer model*. Vaccine, 2007. **25**(9): p. 1607-18.
271. Simons, J.W., et al., *Induction of immunity to prostate cancer antigens: results of a clinical trial of vaccination with irradiated autologous prostate tumor cells engineered to secrete granulocyte-macrophage colony-stimulating factor using ex vivo gene transfer*. Cancer Res, 1999. **59**(20): p. 5160-8.
272. Matzinger, P., *Tolerance, danger, and the extended family*. Annu Rev Immunol, 1994. **12**: p. 991-1045.
273. Marincola, F.M., et al., *Escape of human solid tumors from T-cell recognition: molecular mechanisms and functional significance*. Adv Immunol, 2000. **74**: p. 181-273.
274. Kruisbeek, A.M. and D. Amsen, *Mechanisms underlying T-cell tolerance*. Curr Opin Immunol, 1996. **8**(2): p. 233-44.
275. Sotomayor, E.M., I. Borrello, and H.I. Levitsky, *Tolerance and cancer: a critical issue in tumor immunology*. Crit Rev Oncog, 1996. **7**(5-6): p. 433-56.
276. Brichard, V., et al., *The tyrosinase gene codes for an antigen recognized by autologous cytolytic T lymphocytes on HLA-A2 melanomas*. J Exp Med, 1993. **178**(2): p. 489-95.
277. Kawakami, Y., et al., *Identification of a human melanoma antigen recognized by tumor-infiltrating lymphocytes associated with in vivo tumor rejection*. Proc Natl Acad Sci U S A, 1994. **91**(14): p. 6458-62.
278. Disis, M.L., et al., *Existent T-cell and antibody immunity to HER-2/neu protein in patients with breast cancer*. Cancer Res, 1994. **54**(1): p. 16-20.

279. Mukherjee, P., et al., *MUC1-specific CTLs eradicate tumors when adoptively transferred in vivo*. Clin Can Res, 2001. **7**: p. 848s-855s.
280. Mukherjee, P., et al., *MUC1-specific CTLs are non-functional within a pancreatic tumor microenvironment*. Glycobiology, 2002: p. in press.
281. Mukherjee, P., et al., *MUC1-specific immunotherapy in a mouse model of spontaneous breast cancer*. J. Immunotherapy, 2002: p. in press.
282. Staveley-O'Carroll, K., et al., *Induction of antigen-specific T cell anergy: An early event in the course of tumor progression*. Proc Natl Acad Sci U S A, 1998. **95**(3): p. 1178-83.
283. Pardoll, D., *Does the immune system see tumors as foreign or self?* Annu Rev Immunol, 2003. **21**: p. 807-39.
284. Finke, J., et al., *Where have all the T cells gone? Mechanisms of immune evasion by tumors*. Immunol Today, 1999. **20**(4): p. 158-60.
285. Goto, S., et al., *Analysis of Th1 and Th2 cytokine production by peripheral blood mononuclear cells as a parameter of immunological dysfunction in advanced cancer patients*. Cancer Immunol Immunother, 1999. **48**(8): p. 435-42.
286. Enk, A.H., et al., *Dendritic cells as mediators of tumor-induced tolerance in metastatic melanoma*. Int J Cancer, 1997. **73**(3): p. 309-16.
287. Gabrilovich, D.I., et al., *Decreased antigen presentation by dendritic cells in patients with breast cancer*. Clin Cancer Res, 1997. **3**(3): p. 483-90.
288. Almand, B., et al., *Clinical significance of defective dendritic cell differentiation in cancer*. Clin Cancer Res, 2000. **6**(5): p. 1755-66.
289. Restifo, N.P., et al., *Identification of human cancers deficient in antigen processing*. J Exp Med, 1993. **177**(2): p. 265-72.
290. Simons, J.W., et al., *Bioactivity of autologous irradiated renal cell carcinoma vaccines generated by ex vivo granulocyte-macrophage colony-stimulating factor gene transfer*. Cancer Res, 1997. **57**(8): p. 1537-46.
291. Soiffer, R., et al., *Vaccination with irradiated autologous melanoma cells engineered to secrete human granulocyte-macrophage colony-stimulating factor generates potent antitumor immunity in patients with metastatic melanoma*. Proc Natl Acad Sci U S A, 1998. **95**(22): p. 13141-6.

292. Gupta, R.A. and R.N. Dubois, *Colorectal cancer prevention and treatment by inhibition of cyclooxygenase-2*. Nat Rev Cancer, 2001. **1**(1): p. 11-21.
293. Gupta, R.A. and R.N. DuBois, *Translational studies on Cox-2 inhibitors in the prevention and treatment of colon cancer*. Ann N Y Acad Sci, 2000. **910**: p. 196-204; discussion 204-6.
294. Basu, G.D., et al., *COX-2 inhibitor induces apoptosis in breast cancer cells in an in vivo model of spontaneous metastatic breast cancer*. Molecular Cancer Research, 2004. **2**: p. 632-642.
295. Basu, G.D., et al., *Mechanisms underlying the growth inhibitory effects of COX-2 inhibitor in human breast cancer cells*. Breast Cancer Res, 2005. **7**(4): p. 422-435.
296. Basu, G.D., et al., *A novel role for cyclooxygenase-2 in regulating vascular channel formation by human breast cancer cells*. Breast Cancer Res, 2006. **8**(6): p. R69.
297. Basu, G.D., et al., *Cyclooxygenase-2 inhibitor induces apoptosis in breast cancer cells in an in vivo model of spontaneous metastatic breast cancer*. Mol Cancer Res, 2004. **2**(11): p. 632-42.
298. !!! INVALID CITATION !!!
299. Muller, A.J. and G.C. Prendergast, *Indoleamine 2,3-dioxygenase in immune suppression and cancer*. Curr Cancer Drug Targets, 2007. **7**(1): p. 31-40.
300. Muller, A.J., W.P. Malachowski, and G.C. Prendergast, *Indoleamine 2,3-dioxygenase in cancer: targeting pathological immune tolerance with small-molecule inhibitors*. Expert Opin Ther Targets, 2005. **9**(4): p. 831-49.
301. Muller, A.J., et al., *Inhibition of indoleamine 2,3-dioxygenase, an immunoregulatory target of the cancer suppression gene Bin1, potentiates cancer chemotherapy*. Nat Med, 2005. **11**(3): p. 312-9.
302. Helmersson, J., et al., *Cyclooxygenase-mediated prostaglandin F2alpha is decreased in an elderly population treated with low-dose aspirin*. Prostaglandins Leukot Essent Fatty Acids, 2005. **72**(4): p. 227-33.
303. Basu, G.D., et al., *Mechanisms underlying the growth inhibitory effects of the cyclo-oxygenase-2 inhibitor celecoxib in human breast cancer cells*. Breast Cancer Res, 2005. **7**(4): p. R422-35.

304. Mukherjee, P., et al., *Mucin 1-specific immunotherapy in a mouse model of spontaneous breast cancer*. *J Immunother*, 2003. **26**(1): p. 47-62.
305. Thompson, E.J., et al., *Tyrosines in the MUC1 cytoplasmic tail modulate transcription via the extracellular signal-regulated kinase 1/2 and nuclear factor-kappaB pathways*. *Mol Cancer Res*, 2006. **4**(7): p. 489-97.
306. Shevach, E.M., *CD4+ CD25+ suppressor T cells: more questions than answers*. *Nat Rev Immunol*, 2002. **2**(6): p. 389-400.
307. Sinha, P., et al., *Tumor immunity: a balancing act between T cell activation, macrophage activation and tumor-induced immune suppression*. *Cancer Immunol Immunother*, 2005. **54**(11): p. 1137-42.
308. Lewis, C.E. and J.W. Pollard, *Distinct role of macrophages in different tumor microenvironments*. *Cancer Res*, 2006. **66**(2): p. 605-12.
309. Serafini, P., I. Borrello, and V. Bronte, *Myeloid suppressor cells in cancer: recruitment, phenotype, properties, and mechanisms of immune suppression*. *Semin Cancer Biol*, 2006. **16**(1): p. 53-65.
310. Kusmartsev, S.A., Y. Li, and S.H. Chen, *Gr-1+ myeloid cells derived from tumor-bearing mice inhibit primary T cell activation induced through CD3/CD28 costimulation*. *J Immunol*, 2000. **165**(2): p. 779-85.
311. Almand, B., et al., *Increased production of immature myeloid cells in cancer patients: a mechanism of immunosuppression in cancer*. *J Immunol*, 2001. **166**(1): p. 678-89.
312. Serafini, P., et al., *Derangement of immune responses by myeloid suppressor cells*. *Cancer Immunol Immunother*, 2004. **53**(2): p. 64-72.
313. Gabrilovich, D.I., et al., *Mechanism of immune dysfunction in cancer mediated by immature Gr-1+ myeloid cells*. *J Immunol*, 2001. **166**(9): p. 5398-406.
314. Mazoni, A., et al., *Myeloid suppressor lines inhibit T cell responses by an NO-dependent mechanism*. *J Immunol*, 2002. **168**(2): p. 689-95.
315. Gabrilovich, D., et al., *Vascular endothelial growth factor inhibits the development of dendritic cells and dramatically affects the differentiation of multiple hematopoietic lineages in vivo*. *Blood*, 1998. **92**(11): p. 4150-66.

316. Young, M.R., et al., *Human squamous cell carcinomas of the head and neck chemoattract immune suppressive CD34(+) progenitor cells*. Hum Immunol, 2001. **62**(4): p. 332-41.
317. Kusmartsev, S. and D.I. Gabrilovich, *Immature myeloid cells and cancer-associated immune suppression*. Cancer Immunol Immunother, 2002. **51**(6): p. 293-8.
318. Yu, X.Z. and C. Anasetti, *Memory stem cells sustain disease*. Nat Med, 2005. **11**(12): p. 1282-3.
319. Li, Y., et al., *I-MT enhances potency of tumor cell lysate-pulsed dendritic cells against pancreatic adenocarcinoma by downregulating the percentage of Tregs*. J Huazhong Univ Sci Technolog Med Sci, 2010. **30**(3): p. 344-8.
320. Casibang, M. and T.W. Moody, *AH6809 antagonizes non-small cell lung cancer prostaglandin receptors*. Lung Cancer, 2002. **36**(1): p. 33-42.
321. Kufe, D.W., *MUC1-C oncoprotein as a target in breast cancer: activation of signaling pathways and therapeutic approaches*. Oncogene, 2012.
322. Joshi, M.D., et al., *MUC1 oncoprotein is a druggable target in human prostate cancer cells*. Mol Cancer Ther, 2009. **8**(11): p. 3056-65.
323. Ahmad, R., et al., *MUC1-C oncoprotein functions as a direct activator of the nuclear factor-kappaB p65 transcription factor*. Cancer Res, 2009. **69**(17): p. 7013-21.
324. Moerdyk-Schauwecker, M., et al., *Resistance of pancreatic cancer cells to oncolytic vesicular stomatitis virus: Role of type I interferon signaling*. Virology, 2013. **436**(1): p. 221-34.